2017-01-11

Role of Energy Metabolism in the Thermogenic Gene Program

Minwoo Nam
University of Massachusetts Medical School

ROLE OF ENERGY METABOLISM IN THE THERMOGENIC GENE PROGRAM

A Dissertation Presented

By

Minwoo Nam

Submitted to the Faculty of the

University of Massachusetts Graduate School of Biomedical Sciences, Worcester

in partial fulfillment of the requirements for the degree of

DOCTOR OF PHILOSOPHY

JAN 11, 2017

INTERDISCIPLINARY GRADUATE PROGRAM

ROLE OF ENERGY METABOLISM IN THE THERMOGENIC GENE PROGRAM

A Dissertation Presented
By

Minwoo Nam

Dissertation Defense Committee GSBS Members

Michael P. Czech, PhD

Interdisciplinary Graduate Program

Thomas G. Fazzio, PhD

Interdisciplinary Graduate Program

Anthony N. Imbalzano, PhD

Cell Biology

Chair of the Dissertation Committee

Yong-Xu Wang, PhD

Interdisciplinary Graduate Program

External Dissertation Committee Member

Zhen Y. Jiang, MD, PhD

Associate Professor, Boston University

Thesis Advisor

John F. Keaney, Jr, MD

Interdisciplinary Graduate Program

Student Program

Interdisciplinary Graduate Program

JAN 11, 2017

ACKNOWLEDGEMENTS

Thrilled by the riddles of nature, scientists invest huge efforts to unearth her secrets. In so doing, science, on occasion, advances our understanding of human disease. Fascinated by this, I sought to broaden my research experience by attending graduate school. During the six and a half years, I learned many things from many good people who I owe my successful completion to.

I would like to begin by thanking my former thesis advisor, Dr. Marcus Cooper. He was an admirably dedicated scientist and mentor. He showed me his strong enthusiasm for science by having daily discussions with me, helping me troubleshoot the problems that I faced everyday and challenging my thoughts by asking many questions, all of which fostered a rigorous and rich environment for my journey to become an independent researcher. His mentorship also played critical roles when I prepared my AHA predoctoral fellowship and review article. What I learned from him is certainly one of the most valuable assets that I earned during my time at UMMS and will remain helpful as I continue to pursue my research career.

I also thank the members of the Cooper lab. My fellow MD/PhD student Thomas Akie willingly shared his thoughts on my project with me, which was greatly helpful improving my critical thinking and project. We also worked together on research grant application for the lab and I was impressed by the positive attitude that he showed during those intense moments. Our postdoctoral fellow Lijun Liu provided technical assistance and helpful comments in many aspects and I am grateful for her. Another postdoctoral fellow Masato Sanosaka initially set up the breeding of LRPPRC FKO mice that was

central to my project. Thanks to him, I was able to start my thesis project immediately after I joined the lab.

I would like to thank my current thesis mentor, Dr. John Keaney, Jr. When Dr. Cooper was suddenly no longer available to supervise me, Dr. Keaney willingly stepped in to be my mentor and provided all resources that I needed to complete my project. I want to thank Siobhan Craige and Shashi Kant, senior postdoctoral fellows in the Keaney lab. They generously volunteered to assist me, committing both time and effort to support my project and career advancement.

I would like to thank my thesis committee members, chair Dr. Yong-Xu Wang, Dr. Michael Czech and Dr. Thomas Fazzio not only for their advice regarding my project but also for their support in my pursuit of postdoctoral positions. I also thank Dr. Anthony Imbalzano and Dr. Zhen Jiang for serving on my dissertation defense committee. I am grateful for Dr. Mary Ellen Lane for her support during my transition to the Keaney lab.

I thank Milka, Patti and Lauren in the Division of Cardiovascular Medicine for their support during my difficult transition. I also thank all of my fellow Korean graduate students. Especially, Sungwook has been very thoughtful and supportive throughout my years at UMMS.

I am deeply grateful for my dear Sunyoung. She was always there for me. Without her love and support, I could not have gone through hard times that I encountered during my years at UMMS.

Finally, my deepest gratitude goes to my family. My father, mother and brother Jangwoo always support me in every area of my life. Their encouragement and endless support were the most powerful driving force in my doctoral training.

ABSTRACT

In murine and human brown adipose tissue (BAT), mitochondria are powerful generators of heat. Emerging evidence has suggested that the actions of mitochondria extend beyond this conventional biochemical role. In mouse BAT and cultured brown adipocytes, impaired mitochondrial respiratory capacity is accompanied by attenuated expression of *Ucp1*, a key thermogenic gene, implying a mitochondrial retrograde signaling. However, few have investigated this association in the context of mitochondria-nucleus communication.

Using mice with adipose-specific ablation of LRPPRC, a regulator of respiratory capacity, we show that respiration-dependent retrograde signaling from mitochondria to nucleus contributes to transcriptional and metabolic reprogramming of BAT. Impaired respiratory capacity triggers down-regulation of thermogenic and oxidative genes, promoting a storage phenotype in BAT. This retrograde regulation functions by interfering with promoter-specific recruitment of PPARγ. In addition, cytosolic calcium may mediate the retrograde signal from mitochondria to nucleus. These data are consistent with a model whereby BAT connects its respiratory capacity to thermogenic gene expression, which in turn contributes to determining its metabolic commitment.

Additionally, we find that augmented respiratory capacity activates the thermogenic gene program in inguinal (subcutaneous) white adipose tissue (IWAT) from adipose-specific LRPPRC transgenic mice. When fed a high-fat diet at thermoneutrality, these mice exhibit metabolic improvements as shown by reduced fat mass and improved insulin sensitivity. Furthermore, there is increased recruitment of brown-like adipocytes

in IWAT and thus energy expenditure is significantly increased, providing a potential explanation for protection from obesity. These data suggest that augmented respiratory capacity promotes ‘browning’ of IWAT, which has beneficial effects on obesity and diabetes.

TABLE OF CONTENTS

Reviewer Page ii
Acknowledgements iii
Abstract vi
Table of Contents viii
List of Tables xi
List of Figures xii
List of Abbreviations xv
Preface xviii

CHAPTER I: INTRODUCTION 1
1.1. Brown adipose tissue (BAT) 1
1.2. Features of brown fat mitochondria 6
1.2.1. Morphological features 7
1.2.2. Biochemical features 9
1.2.3. Proteomical features 10
1.3. Mitochondria-nucleus communication in BAT 12
1.3.1. Mitochondrial retrograde signaling 13
1.3.2. Genetic manipulation of respiratory capacity and its effect on thermogenic gene expression 15
1.3.2.1. *COX7RP (cytochrome c oxidase subunit VIIa polypeptide 2 like)* 17
1.3.2.2. *TFAM (transcription factor A, mitochondrial)* 17
1.3.2.3. *CRIF1* (*CR6-interacting factor 1)* 19
1.3.2.4. *LSD1 (Lysine-specific demethylase 1)* 20
1.3.2.5. *LRPPRC (Leucine-rich pentatricopeptide repeat containing motif; also called LRP130: leucine-rich protein 130kD)* 21
1.4. Thesis overview 23
1.4.1. Specific Aim 1 23

1.4.2. Specific Aim 2 25

CHAPTER II: MITOCHONDRIAL RETROGRADE SIGNALING CONNECTS RESPIRATORY CAPACITY TO THERMOGENIC GENE EXPRESSION 26

Summary 26

Introduction 28

Materials and Methods 31

Results 39

LRPPRC fat-specific knockout (FKO) mice exhibit impaired respiratory capacity in BAT 39

Impaired respiratory capacity attenuates thermogenic gene expression 42

Impaired respiratory capacity interferes with the recruitment of PPARγ to thermogenic gene promoters 47

Cytosolic calcium may mediate retrograde signals from mitochondria to nucleus 49

Augmented respiratory capacity induces the thermogenic gene program in subcutaneous adipose tissue 54

The browning of subcutaneous adipose tissue protects against diet-induced obesity in LRPPRC FTg mice 56

Discussion 61

CHAPTER III: PERSPECTIVES AND FUTURE DIRECTIONS 69

3.1. Brown fat-specific mitochondrial retrograde signaling 69

3.2. Mitochondrial respiration and calcium 70

3.3. Other potential mediators of mitochondrial retrograde signaling in brown fat 72

3.4. Mitochondrial respiration-independent effects of LRPPRC ablation and Antimycin A (AA) treatment 75

3.5. Quantitative determination of the contribution of PPARγ to the attenuation of thermogenic gene expression 76

3.6. How is the recruitment of PPARγ to the thermogenic enhancers/promoters reduced? 77
3.7. What is the potential link between cytosolic Ca^{2+} and PPARγ? 78
3.8. Therapeutic implications 79
3.9. Is augmented respiratory capacity a universal mechanism to trigger browning of adipose tissue? 82
3.10. Bidirectional communication between thermogenic capacity and respiratory capacity in brown fat 83

APPENDIX: NUTRIENT SENSING BY THE MITOCHONDRIAL TRANSCRIPTION MACHINERY DICTATES OXIDATIVE PHOSPHORYLATION 84
Author contribution 85
Summary 86
Introduction 87
Materials and Methods 90
Results 106
Discussion 131

BIBLIOGRAPHY 158

LIST OF TABLES

Table 1.1: Effects of manipulating the mitochondrial biogenesis pathway on the brown fat gene program 16
Table 1.2: Effects of manipulating mitochondrial respiratory capacity on the brown fat gene program 18
Table 2.1: Mouse primers used for RT-qPCR 67
Table 2.2: Mouse primers used for ChIP assays 68
Table A.S1: Mass spectrometry intensities for lysines in murine LRP130 sensitive to deacetylation by SIRT3 153
Table A.S2: Mouse primers used for RT-qPCR 156
Table A.S3: Human primers used for RT-qPCR 157

LIST OF FIGURES

Figure 1.1: Brown fat-mediated thermogenesis 3
Figure 1.2: Electron microscopic image showing ultrastructure of brown fat mitochondria 8
Figure 1.3: Diverse mitochondrial insults and their outcomes 14
Figure 1.4: Mitochondrial-encoded respiratory subunits 22
Figure 1.5: The central hypothesis 24
Figure 2.1: Respiratory capacity is impaired in BAT from LRPPRC fat-specific knockout (FKO) mice 40
Figure 2.2: Impaired respiratory capacity attenuates thermogenic and oxidative gene expression in BAT from LRPPRC FKO mice living at 22 ℃ 43
Figure 2.3: Impaired respiratory capacity attenuates thermogenic and oxidative gene expression in BAT from LRPPRC FKO mice living at 30 ℃ 45
Figure 2.4: β-adrenergic signaling is intact in BAT from LRPPRC FKO mice 46
Figure 2.5: Impaired respiratory capacity influences the recruitment of PPARγ in a promoter-specific manner 48
Figure 2.6: Pharmacological inhibition of respiratory complex mimics LRPPRC ablation in cultured brown adipocytes 50
Figure 2.7: Cytosolic Ca^{2+} serve as a signaling mediator between BAT mitochondria and nucleus 52
Figure 2.8: *Lrpprc* and mitochondrially encoded genes are induced in IWAT of LRPPRC fat-specific transgenic (FTg) mice 55
Figure 2.9: Mice with the LRPPRC transgene are metabolically similar to WT littermates upon HFD feeding 57
Figure 2.10: LRPPRC FTg mice exhibit improved metabolic phenotypes in diet-induced obesity 59
Figure 3.1: Mitochondrial Ca^{2+} uptake 71

Figure A.1: Fasting coordinately induces mitochondrially encoded transcripts and OXPHOS in liver 107
Figure A.2: Glucagon induces mitochondrially encoded genes and proteins.....109
Figure A.3: Glucagon-mediated induction of mitochondrially encoded genes requires SIRT3.....111
Figure A.4: In liver, SIRT3 is necessary and sufficient for fasting-mediated induction of mitochondrial encoded transcripts and OXPHOS 115
Figure A.5: SIRT3 induces mitochondrially encoded genes by stimulating mitochondrial transcription 118
Figure A.6: SIRT3-mediated induction of mitochondrial transcription requires LRP130 120
Figure A.7: During the fasted response, SIRT3 deacetylates LRP130 in liver mitochondria 124
Figure A.8: LRP130-7KR stimulates mitochondrial transcription and promotes OXPHOS 127
Figure A.9: In fasted liver, the transcription machinery of mitochondria sense nutrient deprivation via SIRT3, culminating in enhanced energy metabolism.....130
Figure A.S1. cAMP signaling mediates induction of mitochondrially encoded genes, Pgc-1α is not required for induction of mitochondrially encoded gene expression but NAD^+-dependent pathways are required.....136
Figure A.S2. Fasting induces mitochondrially encoded genes in 129S mice.....138
Figure A.S3. Effect of fasting in Sirtuin 3 knockout mouse liver (S3KO) on a 129S mice background.....139
Figure A.S4. In liver, knockdown of Sirt3 in C57BL6 mouse liver impairs fasting-mediated induction of mitochondrially encoded genes and OXPHOS.....140
Figure A.S5. Ectopic expression of SIRT3 in mouse liver and primary hepatocytes induces mitochondrially encoded transcripts.....142
Figure A.S6. Respiration and mitochondrial content in H2.35 hepatoma cells with ectopic expression of Sirt3 144

Figure A.S7. Effect of LRP130 protein level on the basal transcription machinery and a schematic of the LRP130 floxed allele 146
Figure A.S8: Effect of ectopic expression of SIRT3 in LRP130 deficient cells 147
Figure A.S9. Comparison of acetylated lysines in LRP130 (LRPPRC) across various studies 148
Figure A.S10. Mapping of the interaction between POLRMT and LRP130.....149
Figure A.S11. Knock-down of human LRP130 in 293T cells and reconstitution with mouse wild-type LRP130 or the LRP130 7KR mutant 150
Figure A.S12. Knock-down of human LRP130 in 293T cells and reconstitution with mouse wild-type LRP130 or the LRP130 7KQ mutant 151

LIST OF ABBREVIATIONS

ADP	adenosine diphosphate
ATP	adenosine triphosphate
BAT	brown adipose tissue
cAMP	cyclic adenosine monophosphate
CD36	cluster of differentiation 36 (also known as fatty acid translocase)
C/EBP	CCAAT-enhancer-binding protein
ChIP	chromatin immunoprecipitation
CIDEA	cell death-inducing DFFA-like effector A
CPT1B	carnitine palmitoyltransferase 1B
CRIF1	CR6-interacting factor 1
CS	citrate synthase
CtBP	C-terminal binding protein
DIO2	iodothyronine deiodinase 2
DNA	deoxyribonucleic acid
EBF2	early B cell factor 2
ELOVL3	elongation of very long chain fatty acid elongase 3
ERRα	estrogen-related receptor alpha
ETC	electron transport chain
EWAT	epididymal white adipose tissue (visceral depot)
FAD	flavin adenine dinucleotide
FAO	fatty acid oxidation
FFA	free fatty acid
^{18}F-FDG	2-deoxy-2-[fluorine-18]fluoro- D-glucose
FKO	fat-specific knockout
FTg	fat-specific transgenic
GDP	guanosine diphosphate

GTP	guanosine triphosphate
HFD	high fat diet
IMM	inner mitochondrial membrane
IWAT	inguinal white adipose tissue (subcutaneous depot)
LCFA	long chain fatty acid
LPL	lipoprotein lipase
LRPPRC	leucine rich pentatricopeptide repeat containing protein
LSD1	lysine-specific demethylase 1
mtDNA	mitochondrial DNA
Myf5	myogenic factor 5
mRNA	messenger ribonucleic acid
NAD	nicotinamide adenine dinucleotide (NADH: the reduced NAD)
NRF-1	nuclear respiratory factor 1
OMM	outer mitochondrial membrane
OXPHOS	oxidative phosphorylation
PARP	poly ADP ribose polymerase
PDC	pyruvate dehydrogenase complex
PDK	pyruvate dehydrogenase kinase
PDP	pyruvate dehydrogenase phosphatase
PET/CT	positron emission tomography–computed tomography
PGC-1	peroxisome proliferator-activated receptor gamma coactivator
PKA	protein kinase A
POLRMT	RNA polymerase, mitochondrial
PPARγ	peroxisome proliferator-activated receptor gamma
RNAi	RNA interference
PRDM16	PR domain containing 16
SCS	succinyl-CoA synthetase

shRNA	short hairpin RNA
SIRT1	sirtuin 1
SIRT3	sirtuin 3
SRC-1/3	steroid receptor coactivator 1 and 3
TCA	tricarboxylic acid
TFAM	transcription factor A, mitochondrial
TFB2M	transcription factor B2, mitochondrial
UCP1	uncoupling protein 1
UPR	unfolded protein response
VDAC	voltage-dependent anion channel

PREFACE

Portions of this dissertation have appeared in:

Nam M. and Cooper, M.P. Role of Energy Metabolism in the Brown Fat Gene Program. *Front Endocrinol (Lausanne)*. **6**:104. (2015).

Nam, M., Akie, T.E., Sanosaka, M., Craige, S.M., Kant, S, Keaney, J.F. Jr., and Cooper, M.P. Mitochondrial Retrograde Signaling Connects Respiratory Capacity to Thermogenic Gene Expression. *Sci. Rep.* Under revision. (2016)

CHAPTER I

INTRODUCTION

1.1. Brown adipose tissue (BAT)

Brown fat is mainly composed of thermogenic adipocytes that convert chemical energy to heat. Found in homeothermic animals such as mammals, brown fat protects against cold stress. In neonates and hibernating mammals, brown fat plays a critical role in thermoregulation. The first description of brown fat was made by Swiss researcher Gessner who wrote a report regarding the anatomy of the Alpine marmot (*Marmota marmot*) in 1551. In this report, he described interscapular brown fat as being 'neither fat nor flesh' (nec pinguitudo, nec caro) (1). In the early 1900s, although brown fat was commonly termed as 'hibernating gland' due to its presence in nearly all hibernating mammals and resemblance of its appearance to a gland, researchers believed that it was a type of adipose tissue (2). It was mid-1900s that the mysterious gland-like adipose tissue was found to function as a heat-producing (thermogenic) organ (3).

There are two types of thermogenic adipocytes: classical brown adipocytes and beige/brite adipocytes. Classical brown adipocytes exhibit constitutive thermogenic capacity with large numbers of mitochondria. Developmentally programmed brown fat such as the rodent interscapular depot consists of these cells. Another type of thermogenic adipocytes is found in white fat, especially in the rodent subcutaneous depot. These cells are recruited by thermogenic stimuli and in turn display comparable

thermogenic capacity to classical brown adipocytes (4-7). Due to these properties, they have been named beige/brite (brown-in-white) adipocytes (8, 9). Although these two forms of adipocytes share thermogenic function, they are distinguished from each other in some ways. This distinction is clearly exemplified in their gene signatures. *Zic1*, *Eva1* and *Epsti1* are highly expressed in classical brown adipocytes whereas *Tbx1, Cd137* and *Tmem26* are enriched in beige adipocytes (10-12). Given different patterns of gene expression in various depots of adipose tissue (13), this is not surprising and likely reflects different regulatory pathways and distinct developmental origins. Indeed, although exceptions exist, classical brown adipocytes are shown to largely originate from $Myf5^+$ precursor cells that are shared with skeletal muscle whereas beige adipocytes are differentiated from $Myf5^-$ precursor cells (14).

The heat-generating process mediated by brown fat is often termed non-shivering thermogenesis that involves dissipation of chemical energy as heat (Figure 1.1). The thermogenic capacity of brown fat is attributed to abundant mitochondria in which heat is generated via uncoupled respiration (9). For this purpose, brown fat uniquely expresses protonophoric protein, uncoupling protein 1 (UCP1). Localized to the inner membrane of mitochondria, activated UCP1 provides an alternative route for proton to flow back into the matrix, a process that uncouples respiration from ATP synthesis, resulting in conversion of energy stored in proton gradient to heat in stimulated brown fat. High sympathetic innervation of brown fat ensures swift activation of the tissue and cold defense (15, 16). Brown fat is also intensively vascularized to support blood warming and prompt delivery of warmed blood to the periphery as well as to meet high demands for

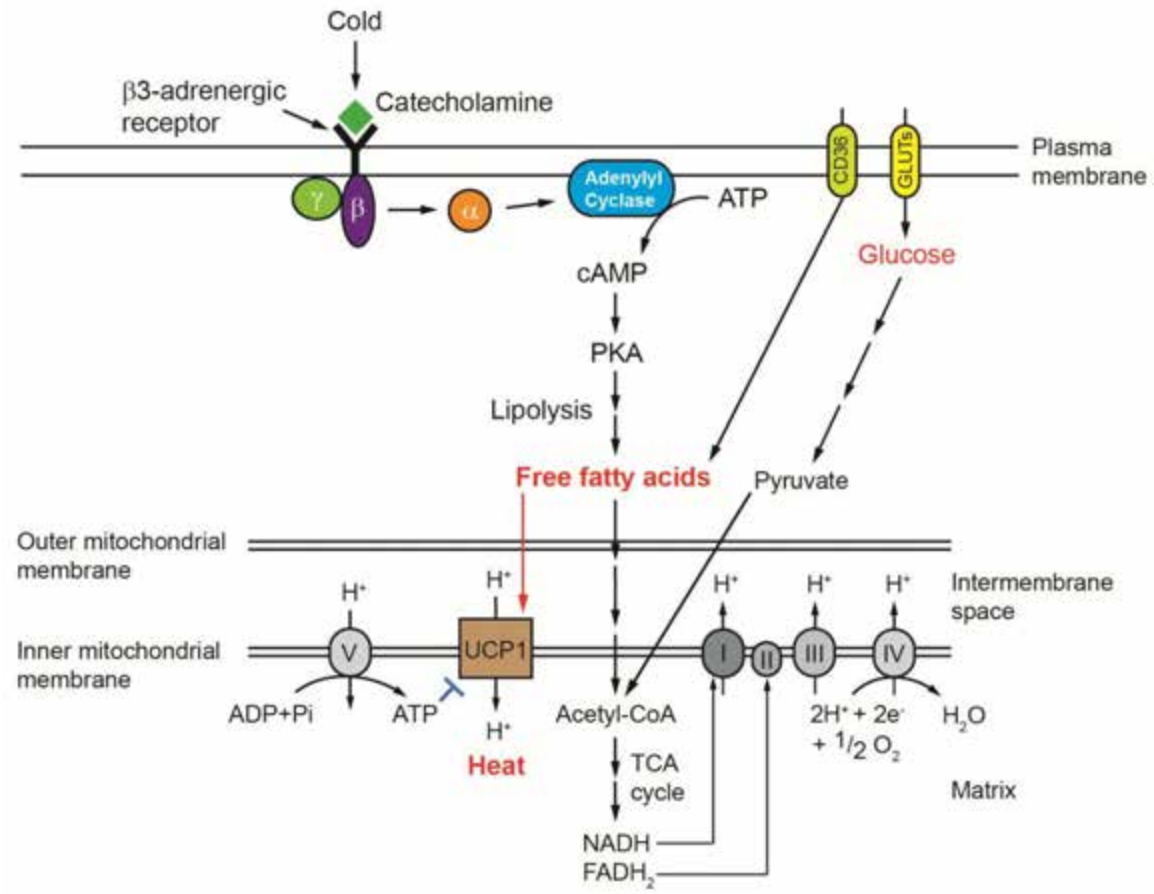

Figure 1.1. Brown fat-mediated thermogenesis. Brown fat mitochondria are generators of heat. In the normal state, they produce ATPs as mitochondria in other tissues do. ATP inhibits UCP1 to block futile proton cycle, which ensures coupled respiration. When exposed to cold, BAT-connected sympathetic nerve system releases catecholamines such as norepinephrine. Norepinephrine in turn activates G protein-coupled β3-adrenergic receptor signaling through cAMP-PKA pathway. This pathway promotes lipolysis and released free fatty acids are oxidized in mitochondria to create proton gradient via electron transport chain (ETC). Glucose and free fatty acids from extracellular sources are also taken up via their transporters and utilized. In addition to their role as fuel, fatty acids are required to overcome ATP-mediated inhibition of UCP1. Activated UCP1 then uncouples respiration from ATP synthesis, which dissipates the energy stored in proton gradient as heat. BAT contains a large number of these heat-producing mitochondria to provide defense against cold.

oxygen supply during uncoupled respiration (17). Calculations have suggested that fully activated brown fat dissipates about 300-400 W/kg of energy as heat compared to 1 W/kg in other tissues (18-20). This high thermogenic capability necessitates robust fuel oxidation. Two major carbon sources—glucose and fatty acids—are used by brown fat for uncoupled respiration. During cold exposure, the uptake of glucose and free fatty acids (FFAs) and lipolysis are greatly increased (21-23). The uptake rate of each substrate is greater than that of skeletal muscle (22, 23), which potentially makes brown fat an important metabolic sink. With its energy-burning property and ability to clear excess nutrients, brown fat thus holds promise as a target to treat various metabolic diseases such as obesity, diabetes and hyperlipidemia (22, 24-26).

Over the last few decades, the transcriptional network that drives adipocyte differentiation (adipogenesis) has been revealed. Using a white adipogenic cell line, 3T3-L1 preadipocytes, researchers have identified key transcription factors of adipogenesis including CCAAT/enhancer binding protein (C/EBP) alpha, beta and delta and peroxisome proliferator-activated receptor (PPAR) gamma (27-30). Importantly, C/EBPα and PPARγ coordinately acts to induce adipocyte-specific genes, resulting in terminally differentiated adipocytes (28, 31, 32). Brown adipocytes also share these major regulators for their development. However, for their thermogenic profile, several additional factors must be involved. A well-known example is PPARγ coactivator 1 (PGC-1) family. PGC-1α was first identified as a cold-inducible interacting partner of PPARγ, which was responsible for cold-induced expression of UCP1 (33). PGC-1α is also well established as a major driver of mitochondrial biogenesis (34). Another family member PGC-1β was

later identified (35), and both family members are required to activate thermogenic and oxidative gene program in brown adipocytes (36). A continuing search for transcriptional regulators that control brown fat-specific gene program identified PR Domain-containing protein 16 (PRDM16). PRDM16 is a nuclear protein containing zinc-finger domains (37). Despite its potential DNA-binding ability, PRDM16 turned out to control brown fat-selective genes by interacting with and co-activating transcription factors C/EBPβ and PPARγ (14, 38). Additionally, PRDM16 plays a role in maintaining brown fat identity by repressing white fat-specific genes. This is achieved by forming a transcriptional repressor complex with CtBP1 and CtBP2 (39). Early B-Cell Factor 2 (EBF2) is an example of playing a dual role in brown fat development. Enriched in brown preadipocytes, EBF2 recruits PPARγ to brown fat-specific genes to induce brown fat phenotype during differentiation (40). Furthermore, EBF2 has a central role in brown preadipocyte commitment by regulating genes enriched in brown preadipose cells (41). These combinatorial transcriptional pathways allow for unique gene signatures that support thermogenic function. UCP1, a key thermogenic protein, is exclusively expressed in brown fat. Cell death-inducing DFFA-like effector a (CIDEA), a modulator of UCP1, and Type II iodothyronine deiodinase (DIO2), an enzyme that converts T4 to active T3 within the tissue locally, are among major thermogenic genes (42-44). Fatty acid oxidation (FAO) genes and electron transport chain (ETC) subunit genes are also enriched (45, 46).

Humans have brown fat as well. In humans, brown fat can be found in the interscapular region in infants, and interscapular, supraclavicular, axillary, neck and

suprarenal regions in children and adolescents (47, 48). In adults, however, brown fat has long been thought to regress with exceptions of those who live in extreme cold and patients with pheochromocytoma characterized by hypersecretion of catecholamines (49-52). Although non-shivering thermogenesis (brown fat-mediated) is critical in infants due to their limited shivering capacity and rapid heat loss caused by larger surface-to-volume ratio, human lifestyles (clothing, shelter, etc), smaller surface-to-volume ratio and enhanced ability to shiver may direct disappearance of brown fat with age. However, with the advent of ^{18}F-FDG PET/CT imaging in oncology, researchers coincidentally detected high glucose uptake around supraclavicular region (53-56). Tissue biopsy confirmed multilocular and UCP1^{+} cells, indicating the existence of functional brown fat in healthy human adults. Several follow-up studies show that the types of thermogenic adipocytes vary depending on anatomical sites. Two reports suggest that supraclavicular human brown fat has molecular features identical to brite/beige fat (10, 57). Another group reported molecular signatures of deep neck fat are virtually identical to 'classical' brown fat of mice while beige-like cells exist in more superficial neck depot (58). Still another group reported molecular signatures intermediate between brown and beige fat (59). The discovery of active brown fat in adults has opened a new era of brown fat research and rekindled an old interest in brown fat as a potential target to treat metabolic diseases.

1.2. Features of brown fat mitochondria

In murine and human brown fat, mitochondria are powerful generators of heat that safely metabolize fat, a feature that has great promise in the fight against obesity and diabetes. Brown fat mitochondria fulfill their duty as cellular powerhouses in the non-stimulated state. In sympathetically stimulated brown fat, UCP1 is rapidly activated and uncouples electron transit and ATP production. Instead, the chemical energy stored in the proton gradient is dissipated as heat. To conduct this specialized task, brown fat mitochondria possess numerous distinct features. The sections below discuss the current knowledge of brown fat mitochondria.

1.2.1. Morphological features

Brown fat mitochondria are dynamic organelles that meet the thermogenic needs of the organism by regulating their number and networking as well as their biochemical and ultrastructural profile. Acute cold exposure (or activation with norepinephrine) immediately promotes mitochondrial fission, an event that precedes and augments thermogenesis (60). Brown fat mitochondria exhibit unique morphological features (Figure 1.2). Notably, brown fat mitochondria are enlarged and densely packed with respiratory units, resulting in dense cristae (61). The morphological features of brown fat also differ across gender with females having larger mitochondria and denser cristae (62). The density of brown fat mitochondria is among the highest of any tissue (63). Even so, chronic cold exposure increases mitochondrial mass even further. This is mediated by catecholamines via β-adrenergic signaling, which increases PGC-1α, a transcriptional coactivator that induces ERRα and NRF-1, culminating in increased mitochondrial mass

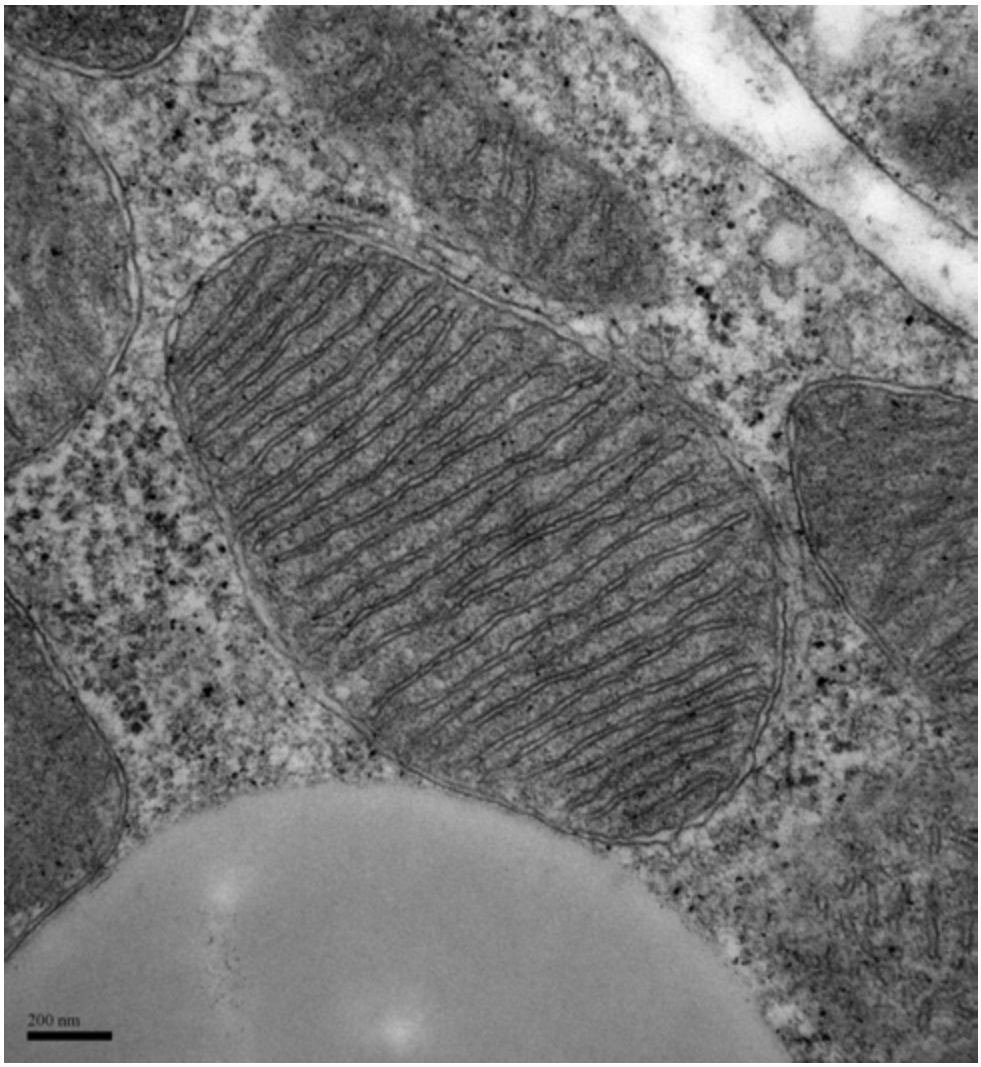

Figure 1.2. Electron microscopic image showing ultrastructure of brown fat mitochondria. Shown are tightly packed lamellar cristae where high density of the electron transport chain resides. Magnification, 43,000x. Scale bar, 200μm.

(33, 34, 64).

1.2.2. Biochemical features

Early biochemical and functional studies on brown fat mitochondria in rodents revealed high cellular respiration but low ATP synthase activity (65). This implied that pathway involving proton leakage must underlie the basis of thermogenesis. Biochemical studies identified that UCP1 constitutes the molecular basis for enhanced proton leak (66). Interestingly, in larger mammals such as lambs the abundance of ATP synthase is higher (67), presumably because larger animals are less dependent on non-shivering thermogenesis due to their smaller surface-to-volume ratio and due to their increased capacity for shivering.

Long chain free fatty acids (LCFAs) activate UCP1, while purine nucleotides inhibit UCP1 (68, 69). Intuitively, mobilization of free fatty acids via β-adrenergic activation is coupled to UCP1 activation and heat production. Fedorenko *et al* reported that UCP1 does not exhibit constitutive proton transport activity (70). Instead, there is obligatory binding of LCFAs to UCP1, a process that transfers protons associated with LCFA into the matrix via a conformational change of UCP1. LCFAs can also overcome inhibition by purine nucleotides. This is important because in the basal state there is no robust lipolysis and inhibition of UCP1 by purine nucleotides will promote coupled ATP-generating respiration.

In theory, uncoupling should de-energize brown fat mitochondria, culminating in an ATP crisis. ATP, however, is required for activation of fatty acids during uncoupling.

Brown fat mitochondria circumvent this by increasing glycolysis as well as the TCA cycle. Arsenite, an inhibitor of pyruvate dehydrogenase complex (PDC) and α-ketoglutarate dehydrogenase, depleted ATP in norepinephrine-stimulated brown adipocytes, implying that the TCA cycle is critical for maintaining ATP during thermogenesis (71). Although succinyl-CoA synthetase primarily generates GTP, this TCA enzyme complex can also generate ATP, a process which may explain how the TCA cycle is critical for maintaining ATP in brown fat (discussed further in 1.2.3). Glycolysis is an important source of ATP as well. Notably, hexokinase activity increases 4-fold in cold acclimated rats, achieving glycolytic activity similar to liver (72).

1.2.3. Proteomical features

Mass spectrometric analysis of mitochondria in mouse brown fat has revealed striking proteomic difference compared with white fat mitochondria (45). In fact, the proteomic profile of brown fat mitochondria was most similar to that of skeletal muscle. Compared with white fat mitochondria, there was an enrichment of catabolic pathways including electron transport chain, TCA cycle and fatty acid metabolism in brown fat mitochondria. Complexes I-IV are present at higher levels, whereas complex V is present at lower levels, a pattern favorable for thermogenesis. There is robust expression of enzymes involved in the TCA cycle—ADP-forming succinyl-CoA synthetase β subunit (A-SCS-β), pyruvate dehydrogenase kinase 4 (PDK4) and pyruvate dehydrogenase phosphatase regulatory subunit (PDPr). SCS converts succinyl-CoA to succinate. This reaction is coupled to the formation of ATP or GTP, which is determined by two different

β subunits, ADP-forming and GDP-forming. In mouse, rat, and human, metabolically active tissues such as brain and heart express high levels of ADP-forming subunits compared with GDP-forming subunits (73). Likewise, brown fat mitochondria may preferentially use A-SCS-β to supply ATP, a feature that matches a role of substrate-level phosphorylation in stimulated brown adipocytes. During cold exposure, lipid uptake and lipogenesis replenish fat stores that have been oxidized (74). Control of lipogenesis during cold exposure is complex and partly regulated by pyruvate metabolism (74, 75). Pyruvate can be targeted for complete oxidation by converting it into acetyl-CoA via the enzymatic action of PDC (76). Alternatively, inhibition of PDC by PDK4 diverts pyruvate into glycerol, which is the backbone for FFA esterification (76). An enzymatic complex consisting of PDPr counteracts the action of PDK4, and thus, targets pyruvate for complete oxidation (77, 78). In summary, opposing regulation by PDK4 and PDP may play a critical role in whether or not the brown adipocyte uses pyruvate for lipogenesis (PDK4-mediated) or complete oxidation (PDPr-mediated).

Fatty acids serve as major substrates for thermogenesis and they activate UCP1 (79). In brown fat, there is high expression of enzymes involved in fatty acid oxidation, including short-, medium-, long-chain acyl-CoA dehydrogenases and 3-ketoacyl-CoA thiolase (45). Long-chain fatty acids require a carnitine palmitoyltransferase 1B (CPT1B)-mediated carnitine shuttle for oxidation in mitochondria. Supporting a role for robust oxidative capacity in brown fat, CPT1B is 50-fold higher in brown fat compared with white fat (45). Brown fat may also exhibit metabolic flexibility in fuel utilization. Highly expressed in brown fat, acetyl-CoA synthetase 2-like (ACSS1) permits oxidation

of ketone bodies during starvation (45, 80, 81). Indeed, activity of ketone body oxidizing enzymes in brown fat parallels that of the heart (82).

A comparative proteomic analysis of human neck brown fat vs. neighboring subcutaneous white fat reveals a similar enrichment of mitochondrial oxidative metabolism pathway to mouse brown fat (83). An interesting finding is that mitochondrial creatine kinases are abundantly expressed in neck brown fat compared with subcutaneous white fat (83). This enzyme converts creatine to phospho-creatine at the expense of ATP, thus yielding ADP. The mitochondrial creatine kinases also plays a central role in forming the 'mitochondrial interactosome' by connecting voltage-dependent anion channel (VDAC) in the outer mitochondrial membrane with adenine nucleotide translocase, phosphate transporter, phosphate transporter and ATP synthase (Complex V) in the inner mitochondrial membrane (84). The role of this energy unit is to ensure a high efficiency of ATP synthesis by concentrating molecules necessary for the process. Indeed, the components of this coupled respiration machinery are highly expressed as well in human neck brown fat, which runs contrary to mouse brown fat (83). Although it remains elusive, abundance of this ATP-generating supercomplex in human brown fat may be in parallel with the dependence of mouse beige adipocytes on a creatine-driven substrate cycle for energy expenditure and thermogenesis (85).

1.3. Mitochondria-nucleus communication in BAT

The endosymbiotic theory suggests that eukaryotic mitochondria are derived from prokaryotes engulfed in others about 1.5 billion years ago. Since then, mitochondria have

evolved to serve as energy-producing organelle with components encoded in their own DNA and nuclear DNA (86, 87). Many metabolic intermediates that are formed from biochemical reactions such as the tricarboxylic acid (TCA) cycle inside mitochondria also play fundamental roles in building essential biological molecules (88). From a signaling perspective, mitochondria are important units participating in several cellular responses. Notably, mitochondrial apoptosis pathway is initiated by release of cytochrome c and other pro-apoptotic molecules from the organelle in the presence of its respective stress (89). Additionally, mitochondrial dysfunction can evoke adaptive cellular responses, many of which are mediated by transcriptional responses in nucleus, suggesting communication between mitochondria and nucleus (90, 91). In the following sections, the mitochondria-nucleus communication will be discussed with particular emphasis on its potential link to thermogenic gene expression in brown fat.

1.3.1. Mitochondrial retrograde signaling

The mitochondria-nucleus crosstalk is a pathway of interorganelle communication, which is generally termed as mitochondrial retrograde signaling. As suggested by the term, information flows from mitochondria to the nucleus, which is contrary to the typical anterograde regulation involving transmission of signals from nucleus to mitochondria. This retrograde signaling represents diverse adaptive cellular responses elicited by various mitochondrial stresses (Figure 1.3). Initially, the retrograde signaling was described in the mitochondrial DNA-depleted strain of *Saccharomyces cerevisiae* (ρ° petites). The most prominent in these respiration-defective ρ° cells is metabolic

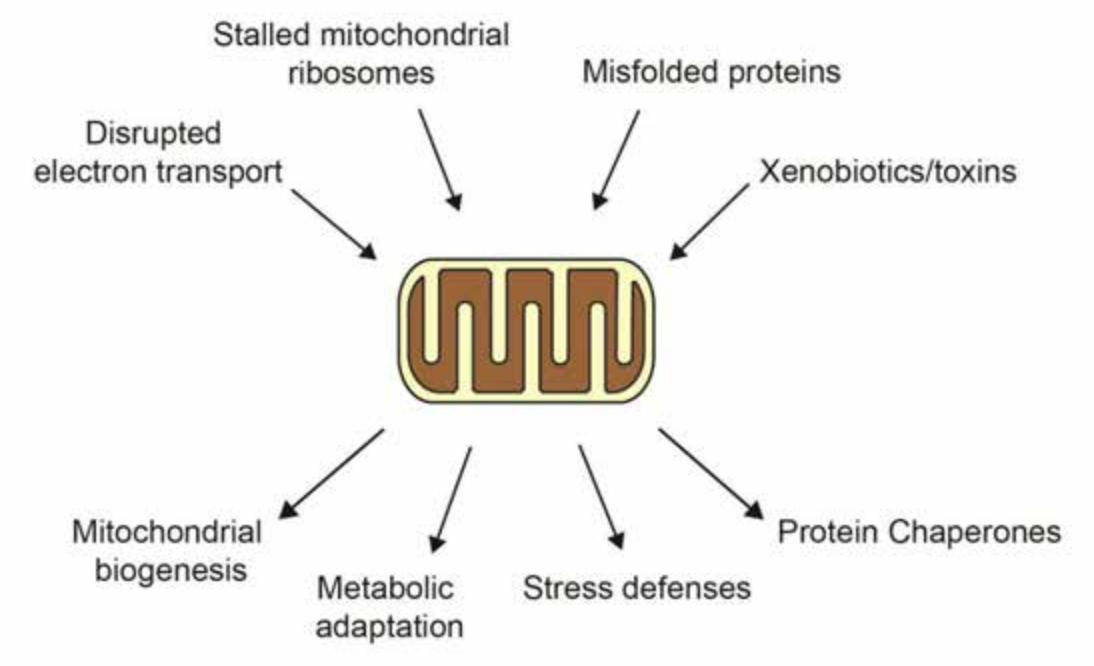

Figure 1.3. Diverse mitochondrial insults and their outcomes. (Adapted and modified from Yun and Finkel, *Cell Metab.* 2014;19(5):757-66)

remodeling to ensure proper supply of glutamate (92). This is important because the TCA cycle cannot operate as a full cycle in a respiration-deficient state and this eventually results in depletion of α-ketoglutarate, a precursor of glutamate. To overcome the metabolically detrimental state, respiration-deficient cells engages peroxisomal biogenesis that leads to increases in fatty acid oxidation and glyoxylate cycle activity, which can supply TCA cycle intermediates acetyl-CoA and citrate, respectively (92). This metabolic reprogramming was also accompanied by supportive transcriptional changes; genes encoding transporters for transfer of key metabolites into mitochondria, genes encoding TCA cycle enzymes responsible for production of α-ketoglutarate and genes encoding peroxisomal proteins were up-regulated (92, 93). To withstand an ATP

crisis, glycolytic genes are also up-regulated (94). Similarly, in mammalian cells, disruption of oxidative phosphorylation activates PGC-1α-driven mitochondrial biogenesis to resolve a crisis in cellular energetics (95).

In addition to mitochondrial respiratory defects, a distinct form of mitochondrial stress can induce a corresponding adaptive response. When misfolded proteins are accumulated in mitochondria, an ER stress response-like pathway is activated, which is also known as the mitochondrial unfolded protein response (UPR^{mt}) (96-99). This pathway promotes the expression of a set of mitochondrial chaperones and proteases to reestablish protein quality control. Well characterized in *Caenorhabditis elegans*, activating transcription factor associated with stress-1 (ATFS-1) plays a crucial role in upregulating the respective genes (98, 99). Although paradoxical, this mitochondrial stress response appears to yield a beneficial effect. Several lines of evidence suggest that activation of the UPR^{mt} is required for an increased lifespan in certain experimental conditions in worms (100, 101). In contrast, the mitochondria-driven signal is also known to play a critical role in various pathological conditions including cancer, neurodegeneration and cardiovascular diseases (102-104), reinforcing the idea that mitochondrial retrograde signaling elicits context-dependent and tissue-specific responses.

1.3.2. Genetic manipulation of respiratory capacity and its effect on thermogenic gene expression

Intuitively, it makes sense that in brown fat, a highly specialized tissue for thermogenesis, such mitochondria-nucleus communication may be crucial in matching

functional and metabolic capacity to genetic programs that influence them. Since respiratory capacity is directly correlated with the number of mitochondria, manipulating factors controlling mitochondrial biogenesis may be feasible to explore the role of mitochondria in the regulation of brown fat-specific thermogenic genes. As summarized in Table 1.1, however, deletion of well-characterized drivers of mitochondrial biogenesis did not necessarily abrogate the mitochondrial mass in brown fat, implying the existence of redundant pathways and/or complementary roles of each regulator (105-111). Furthermore, in some models, targeting the same factor did not produce similar effects on thermogenic genes, making it challenging to delineate a direct relationship between respiratory capacity and the thermogenic gene program *per se*.

Table 1.1. Effects of manipulating the mitochondrial biogenesis pathway on the brown fat gene program

Model	Mitochondrial mass	Brown fat morphology	Brown fat genes	Other
PGC-1α KO	No obvious changes	Increased lipid deposition	Intact *Ucp1 and Dio2*	↓ *Ucp1* and *Dio2* upon cold exposure
PGC-1α KO	Intact mitochondrial ultrastructure	No difference in lipid content	Intact *Ucp1*	No effect on induction of *Ucp1* upon cold
PGC-1α FKO (Adipoq-Cre)	n/a	No difference in lipid content	Intact *Ucp1*, *Cidea and Dio2*	↓ ETC genes ↓ *Cpt1b*
PGC-1β KO	No difference in mitochondrial volume	No difference in lipid content	↑ *Ucp1* ↑ *Pgc1a*	
PGC-1β FKO (Fabp4-Cre)	↓ CS activity Intact mtDNA content	Increased lipid deposition	↓*Ucp1* ↓ *Cidea*	↓ ETC genes and C*pt1b* no effect on *Pgc1a*
ERRα KO	↓ Mitochondrial mass	Increased lipid deposition	Slightly reduced *Ucp1*	↓ *Pgc1a* ↓ ETC and FAO genes
ERRα KO	n/a	n/a	↑ *Ucp1*	

↓ Decrease; ↑Increase; KO, knockout; FKO, fat-specific KO; ETC, electron transport chain; CS, citrate synthase FAO, fatty acid oxidation; n/a, not assessed

The sections below review approaches to directly manipulate mitochondrial respiratory capacity and the attendant effects on the thermogenic genes which are summarized in Table 1.2.

1.3.2.1. COX7RP (cytochrome c oxidase subunit VIIa polypeptide 2 like)

Recent work using COX7RP knockout mice provides direct evidence for the role of respiratory capacity in the brown fat gene program (112). In this study, COX7RP was identified as a novel assembly factor for respiratory chain supercomplexes in mitochondria. ETC complexes are known to form supercomplexes, consisting mainly of complex I, III and IV (so-called respirasome), which enhances respiratory activity (113). With reduced oxygen consumption at a whole-body level, COX7RP KO mice revealed hypertrophic and pale brown fat, generally indicative of defective brown fat. More importantly, *Ucp1* was severely reduced in this dysmorphic brown fat. Microarray analysis also showed a downregulation of several brown fat-enriched genes including *Dio2* and *Elovl3*. Expression of PGC-1 coactivators was decreased but their downstream targets such as *Erra, Nrf1*, and *Tfam* were unaltered, implying no significant impact on the PGC-1 coactivator network. All together, this study strongly suggests that respiratory capacity dictates a retrograde signaling from mitochondria to the nucleus regulating the thermogenic gene program.

1.3.2.2. TFAM (transcription factor A, mitochondrial)

Table 1.2. Effects of manipulating mitochondrial respiratory capacity on the brown fat gene program

	Model	Respiratory capacity	Mitochondrial mass	Brown fat morphology	Brown fat genes	Other
Mouse	COX7RP KO	↓ 10-20% in O_2 consumption	n/a	Hypertrophic, pale	↓ 75% in *Ucp1* ↓ *Dio2, Elovl3*	Normal *Erra, Nrf1, Tfam*
	TFAM FKO (Fabp4-Cre)	↓ 40-60% in complex I and IV; ↑ 70% in complex II (BAT) ↑ 30% in O2 consumption (BAT) ↑ 80% in state3 OCR (BAT mt)	↑ 20% in citrate synthase activity	Normal	Normal	↓ DIO ↓ Insulin resistance
	TFAM FKO (Adipoq-Cre)	↓ 40-80% in complex I and IV (BAT)	↑ 80% in citrate synthase activity	Whitening	Normal	↓ DIO ↑ Insulin resistance Lipodystrophy & inflammation in WAT
	CRIF1 FKO (Fabp4-Cre)	↓ OXPHOS subunits protein	↓ Mitochondrial abundance ↑ Mitochondrial size	Smaller size	Unaltered UCP1	Defective WAT Postnatal death at week 3
	LSD1 Tg (IWAT)	↑ *Nrf1, Cpt1b, Cox8b* ↑ Complex II and IV	↑ Mitochondrial abundance	↑ Beige/brite adipocytes in IWAT	↑ *Prdm16,* ↑ *Ppargc1a, Ucp1*	↓ DIO ↓ Insulin resistance
Cell	LRPPRC KD in brown adipocytes	↓ 20% in O_2 consumption			↓ 40-75% in *Ucp1, Cidea, Cox7a1*	

↓ Decrease; ↑ Increase; KO, knockout; Tg, transgenic; FKO, fat-specific KO; KD, knockdown; mt, mitochondria; OCR, oxygen consumption rate
BAT, brown adipose tissue; IWAT, inguinal white adipose tissue; DIO, diet-induced obesity; n/a, not assessed

One approach to genetically manipulate respiratory capacity is to target components of the basal transcriptional machinery of mitochondrial DNA (mtDNA). Among them is TFAM, a key player in mtDNA transcription and maintenance (114). Fabp4-Cre-driven loss of TFAM led to diminished respiratory activity and a drop in mtDNA copy number in brown and white fat (115). Paradoxically, in those mice, brown fat showed enhanced respiratory capacity as evidenced by increased oxygen consumption, fatty acid oxidation, and citrate synthase activity. Although reduced in weight, this brown fat had normal expression of brown fat genes. Similarly, brown fat markers were intact in brown fat with Adipoq-Cre-driven loss of TFAM, which was accompanied by increased citrate synthase activity (116). Therefore, it is likely that the unaltered brown fat gene program in TFAM deficient fat is ascribed to a compensatory increase in respiratory capacity. Although not decisive, observations from adipose-specific TFAM knockout mice imply that whole-cell respiratory capacity is monitored by an innate sensor to dictate the thermogenic gene program.

1.3.2.3. CRIF1 (CR6-interacting factor 1)

CRIF1 is a mitochondrial protein that controls the translation and insertion of mitochondrially encoded respiratory subunits into the inner membrane (117). The activities of Complexes I, III and IV are abrogated by CRIF1 deficiency in mouse embryonic fibroblasts (117). The severity of impaired respiratory capacity by ablation of CRIF1 is evident in brain-specific and cardiac muscle-specific knockout mice in which severe neurodegeneration and premature death develop, respectively (117, 118). Adipose-

specific CRIF1 knockout mice (driven by Fabp4-Cre) show a developmental defect in white fat, reduced body weight and post-natal death at week 3 (119). Brown fat in these mice is smaller in size, however, histology is unremarkable and UCP1 expression is normal. Because mice die by 3 weeks of age, it was not possible to assess the chronic effect of respiratory defects in brown fat. Although mice with Adipoq-Cre-driven deletion of CRIF1 were viable, data regarding the brown fat genes were not shown (119). Even so, these data could suggest that impaired mitochondrial function does not influence brown adipocyte development. Future studies will be necessary to address if mitochondrial function is critical for the maintenance of the brown fat program. Finally, similar to TFAM, the method by which cellular respiration is disrupted may have differential effects on mitochondrial signaling and subsequent transcriptional events in the nucleus.

1.3.2.4. LSD1 (Lysine-specific demethylase 1)

LSD1 demethylates mono- and di-methylated lysines (particularly lysine 4 and 9 of histone H3) via the cofactor flavin adenosine dinucleotide (FAD) (120). Ubiquitously expressed, LSD1 is essential for embryogenesis and tissue-specific differentiation (121). In the study by Duteil *et al*, LSD1 was newly identified as a cold-, and β3-adrenergic signaling-inducible protein in mouse white fat (122). Ectopic expression of LSD1 further revealed that it was sufficient to induce respiratory capacity through nuclear respiratory factor 1(NRF1) in white adipose cell lines. In addition, there was an activation of the brown fat gene program including *Prdm16*, *Ppargc1a*, and *Ucp1* in LSD1-overexpressing

white adipocytes. LSD1 transgenic mice confirmed these *in vitro* findings. Interestingly, this browning effect was more robust in subcutaneous white fat where beige adipocytes reside. However, in brown fat of LSD1 transgenic mice, respiratory activity was modestly increased and there were no significant changes in the brown fat markers. These data suggest that augmented respiratory capacity may promote browning by stimulating beige adipocytes.

1.3.2.5. LRPPRC (Leucine-rich pentatricopeptide repeat containing motif; also called LRP130: leucine-rich protein 130kD)

A potential role of mitochondrial respiratory capacity in the brown fat gene program was reported in a study using LRPPRC-deficient brown adipocytes (123). LRPPRC was originally identified as a causal protein in a rare neurological and metabolic disorder called Leigh Syndrome French Canadian variant (124). Initial studies using human fibroblasts identified defects in cytochrome c oxidase deficiency; however, later studies using mouse models revealed that LRPPRC affected the expression of all mitochondrially encoded subunits of the ETC (13 subunits) (Figure 1.4), which has differential effects on respiratory complex activity related to cell type (125-128). Especially, our lab has demonstrated that LRPPRC is a strong coactivator for basal mitochondrial transcription machinery consisting of POLRMT and TFB2M (126, 129). LRPPRC directly regulates respiratory capacity by controlling the availability of mitochondrial-encoded ETC subunits, which further affects oxidative metabolism such as fatty acid oxidation (126). Since manipulating LRPPRC has no significant impact on

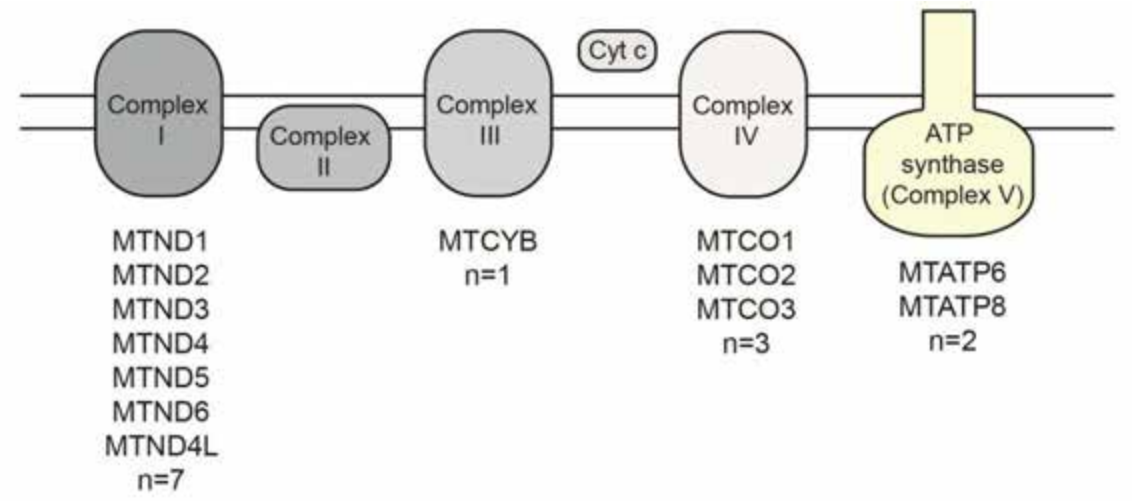

Figure 1.4. Mitochondrial-encoded respiratory subunits. The subunits encoded in mitochondrial genome are shown below each respiratory complex.

mitochondrial biogenesis (126), specific alteration of mitochondrial respiratory capacity in the desired tissue could be achieved by targeting LRPPRC in a tissue-specific manner, which makes it a useful tool to study the effects of mitochondrial respiration on diverse cellular processes.

Brown adipocytes with shRNA-driven depletion of LRPPRC were notable for impaired oxygen consumption but intact mitochondrial density and PGC-1 coactivators, indicating a specific impairment of respiratory capacity without altering mitochondrial biogenesis (123). LRPPRC-deficient brown adipocytes had a marked reduction in brown fat-selective genes, including *Ucp1* and *Cidea*, suggesting a link between respiratory capacity and a basal expression of certain brown fat genes (123).

While LRRPRC is weakly expressed in the nucleus, recent data show that the majority of LRPPRC is localized to mitochondria and regulates mtDNA-encoded

transcripts across various species, suggesting that a nuclear role of LRPPRC in the regulation of brown fat genes may be modest and that the predominant effect is mediated by impaired cellular respiration (126, 130-132). In addition, cAMP-mediated induction of *Ucp1* was unaffected in LRPPRC-deficient brown adipocytes (123). Given that PGC-1α is responsible for this cAMP effect, it is less likely that LRPPRC is an essential part of PGC-1α coactivator complexes necessary for *Ucp1* expression. Furthermore, in human fibroblasts, deficiency of LRPPRC did not affect expression of PGC-1α target genes (133), implying that signals are generated by impaired cellular respiration rather than reduced nuclear expression of LRPPRC.

1.4. Thesis overview

The goal of my thesis research is to understand the role of mitochondrial respiratory capacity in the regulation of thermogenic gene expression in brown fat. Based on the previous studies by our lab and others, I have formulated the central hypothesis that the status of mitochondrial respiratory capacity dictates the thermogenic gene program, which in turn critically determines the metabolic commitment of the tissue (Figure 1.5). To test this hypothesis, I investigated two specific aims using LRPPRC as a model system.

1.4.1. Specific Aim 1: Characterize the effect of impaired respiratory capacity on the thermogenic gene program and determine how the mitochondria signal dictates thermogenic gene expression

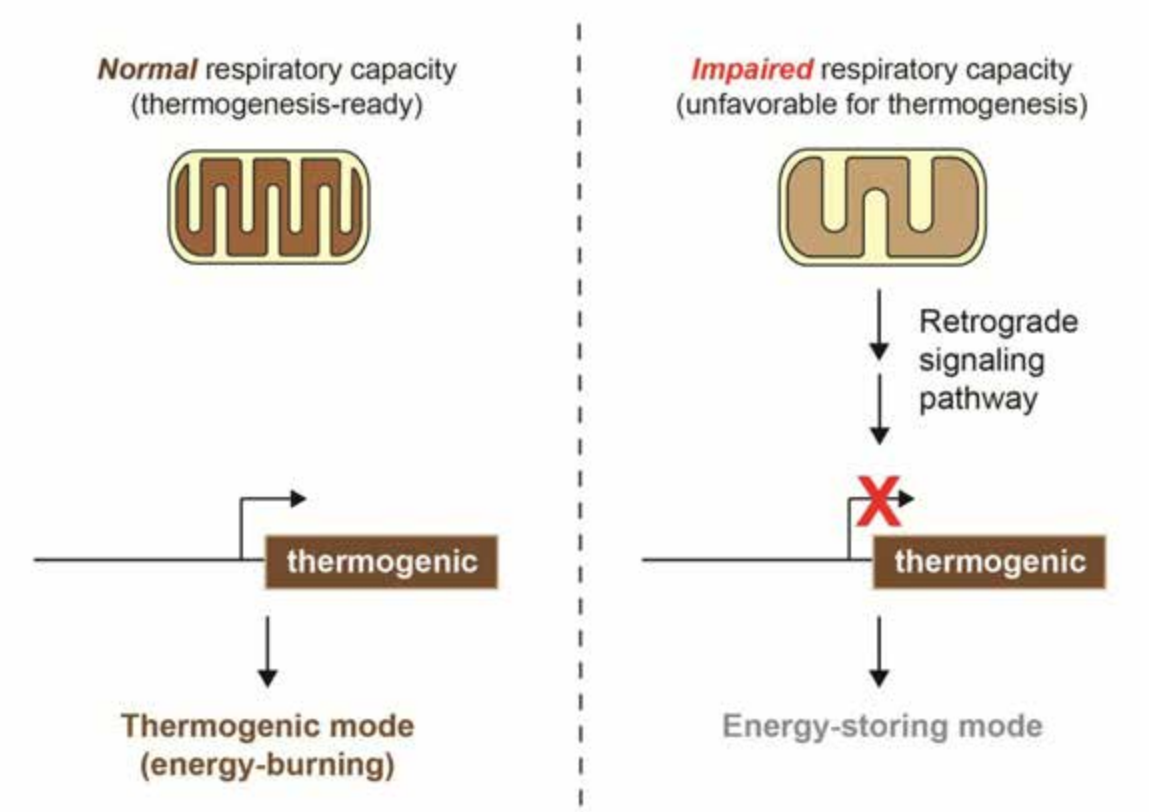

Figure 1.5. The central hypothesis. Thermogenesis relies on mitochondrial respiration; thus brown fat with normal respiratory capacity are ready for thermogenesis and thermogenic genes are normally expressed, both of which support thermogenic function of brown fat. On the other hand, impaired respiratory capacity, which is an unfavorable condition for thermogenesis, activates a retrograde signaling pathway to attenuate thermogenic gene expression. Reduced mitochondrial respiration and reduced thermogenic gene expression eventually directs brown fat to an energy-storing mode. In other words, brown fat coordinates its respiratory capacity with thermogenic gene expression. This contributes to determining which metabolic state brown fat adopts.

Recent studies suggest that the actions of mitochondria extend beyond their conventional role as generators of heat. There is mounting evidence that impaired mitochondrial respiratory capacity is accompanied by attenuated expression of *Ucp1*. This implies a mitochondrial retrograde signaling that negatively influences the thermogenic gene program, culminating in a storage phenotype. In this aim, I used

genetic (LRPPRC fat-specific knockout) and pharmacological (respiratory inhibitor) approaches to model impaired respiratory capacity in mouse brown fat and cultured brown adipocytes, respectively. I observed the attenuation of a group of thermogenic and oxidative genes. I also identified PPARγ as the key transcription factor that are influenced by the respiratory defect and calcium as the signal that mitochondrial respiration uses to control nuclear transcription.

1.4.2. Specific Aim 2: Evaluate if augmented respiratory capacity induces the thermogenic gene program in adipose tissue and protects against obesity

This aim tested a therapeutic aspect of manipulating adipose respiratory capacity in the setting of diet-induced obesity. I generated LRPPRC fat-specific transgenic mice and observed an induction of the thermogenic genes in inguinal (subcutaneous) white fat. In addition, I discovered that such induction was beneficial for fighting obesity and diabetes largely through increased whole-body energy expenditure.

CHAPTER II

MITOCHONDRIAL RETROGRADE SIGNALING CONNECTS RESPIRATORY CAPACITY TO THERMOGENIC GENE EXPRESSION

Summary

Mitochondrial respiration plays a crucial role in determining the metabolic state of brown adipose tissue (BAT), due to its direct roles in thermogenesis, as well as through additional mechanisms. Here, we show that respiration-dependent retrograde signaling from mitochondria to nucleus contributes to genetic and metabolic reprogramming of BAT. In mouse BAT, ablation of LRPPRC (LRP130), a potent regulator of mitochondrial transcription and respiratory capacity, triggers down-regulation of thermogenic genes, promoting a storage phenotype in BAT. This retrograde regulation functions by inhibiting the recruitment of PPARγ to the regulatory elements of thermogenic genes. Chelating cytosolic Ca^{2+} reverses the attenuation of thermogenic genes in brown adipocytes with impaired respiratory capacity, while induction of cytosolic Ca^{2+} phenocopies the attenuation program, indicating that cytosolic Ca^{2+} mediates mitochondria-nucleus crosstalk. Our findings suggest that respiratory capacity governs thermogenic gene expression and BAT function via mitochondria-nucleus communication, which in turn leads to either a thermogenic or storage mode.

Conversely, augmented respiratory capacity induces thermogenic gene expression

in subcutaneous white adipose tissue. Consequently, mice are protected against diet-induced obesity through increased energy expenditure. These data suggest that augmenting respiratory capacity in adipose tissue provides new avenue for fighting obesity and diabetes.

Introduction

Brown adipose tissue (BAT) generates heat to combat cold stress (11). When activated by cold or β-agonists, BAT oxidizes glucose and lipids (in the form of fatty acids) to fuel uncoupling protein 1 (UCP1)-mediated uncoupled respiration, which drives non-shivering thermogenesis (79). Due to this unique energy-burning property, BAT has the potential to mitigate obesity (134, 135). Since functional BAT exists in adult human subjects (11) and likewise has the potential to mitigate obesity, there is great interest in understanding the molecular and cellular pathways that dictate its development, recruitment and maintenance.

Thermogenesis from BAT relies on abundant mitochondria in the tissue (79). This makes BAT capable of higher levels of respiration than any other tissues (136). It is thus readily anticipated that the metabolic state of BAT is influenced by mitochondrial respiration. Any circumstance where respiratory activity is low leads to reduced substrate oxidation, and will drive lipid accumulation in brown adipocytes like white adipocytes specialized for storing excess energy as lipids. On the other hand, high respiratory activity entails elevated substrate oxidation, thereby resulting in an energy-burning state in which stored lipids as well as uptaken glucose and lipids are oxidized. These two metabolic fates of BAT are also supported by two distinct gene programs. Lipogenic genes are enriched in both white and brown adipocytes, controlling fatty acid synthesis and esterification of glycerol with fatty acids. Thermogenic genes are uniquely expressed in BAT and oxidative genes are also highly present to enable high rates of fuel oxidation and respiration required for thermogenesis.

Previous studies have suggested that BAT senses its respiratory capacity and coordinates the expression of thermogenic genes to determine which metabolic states BAT adopts. Mice deficient for COX7RP, a factor that ensures proper function of mitochondrial respiratory complexes, exhibit increased lipid deposition in BAT (112). Interestingly, expression of several thermogenic genes including *Ucp1, Dio2* and *Elovl3* is concurrently decreased. This suggests that mitochondria with impaired respiratory capacity communicate with the nucleus to attenuate expression of certain thermogenic genes. A similar mitochondria-nucleus communication has been described in brown adipocytes deficient for LRPPRC (123). *Lrpprc* is the causative gene of the French-Canadian type of Leigh Syndrome, a rare metabolic and neurological disorder (124). LRPPRC is a mitochondrial protein and has been shown to regulate mitochondrial-encoded electron transport chain (ETC) subunits and thus respiratory capacity by our laboratory and others (126, 132, 133, 137). LRPPRC knockdown causes a reduction in mitochondrial respiratory capacity and decreased expression of thermogenic genes including *Ucp1* and *Cidea* (123). However, gene expression profiling in BAT with impaired respiratory capacity is incomplete and the molecular mechanism by which mitochondria exert transcriptional control over those nuclear genes remains to be addressed.

In the present study, we explored the role of respiratory capacity in thermogenic gene expression by manipulating LRPPRC in an adipose-specific manner and by treating brown adipocytes with an inhibitor of mitochondrial respiration. We find that impaired respiratory capacity triggers a retrograde signaling pathway that represses thermogenic

and oxidative genes, favoring decreased fuel oxidation and energy storage. Furthermore, we provide evidence that this information is transmitted via Ca^{2+}-mediated mitochondrial retrograde signaling, which ultimately controls whether BAT participates in thermogenesis or energy storage. Additionally, we tested whether augmenting respiratory capacity by force expressing LRPPRC promotes thermogenic gene expression in adipose tissue. We show that augmented respiratory capacity activates the thermogenic gene program in inguinal (subcutaneous) white adipose tissue (IWAT), which protects mice from diet-induced obesity through increased energy expenditure.

Materials and Methods

Animals

Lrpprc$^{flox/flox}$ mice were generated as previously described (129). To ablate *Lrpprc* in a fat-specific manner, *Lrpprc*$^{flox/flox}$ mice were crossed to *Adipoq-Cre* mice. The resultant *Lrpprc*$^{flox/+}$;*Adipoq-cre/0* mice were then crossed to *Lrp130*$^{flox/flox}$ mice to produce *Lrpprc*$^{flox/flox}$;*Adipoq-cre/0* mice (termed LRPPRC FKO). Our final breeding strategy was to cross *Lrpprc*$^{flox/flox}$ mice to LRPPRC FKO mice, resulting in *Lrpprc*$^{flox/flox}$:LRPPRC FKO=1:1. Because there was no metabolic or genetic differences between WT, *flox/flox* mice or *Adipoq-Cre/0* mice, comparisons between control (flox/flox) and *Lrpprc*$^{flox/flox}$;*Adipoq-cre/0* mice were use for this study. *Lrpprc*$^{flox/flox}$ mice and *Adipoq-Cre* mice are on a C57BL6/J background.

Mice with ectopic transgenic expression of LRPPRC were generated by constructing an inducible floxed LRPPRC cassette. Mouse *Lrpprc* with Myc and His fused at its C-terminus was inserted into the Cre-activable pCAG-CAT-EGFP construct (a gift from Dr. Junichi Miyazaki at Osaka University) in place of EGFP cDNA. Microinjection into C57BL/6J eggs was performed by UMMS Transgenic animal core facility using the linearized construct. Transgenic founders were identified by a quantitative PCR and bred to produce offsprings. Mice hemizygous for the transgene (*Lrpprc*$^{Tg/0}$) were crossed to *Adipoq-Cre* mice to yield WT: *Lrpprc*$^{Tg/0}$:*Adipoq-cre/0*: *Lrpprc*$^{Tg/0}$;*Adipoq-cre/0* (termed LRPPRC FTg)= 1:1:1:1. For high-fat diet feeding, mice were fed a 55% kcal from fat diet (Harlan Teklad TD-93075) for 16 weeks before metabolic phenotyping. Mice were maintained in 12-hour light/12-hour dark cycle. In all

experiments, LRPPRC FKO and FTg mice had appropriate littermate control mice with the same age. All animal experiments were performed in accordance with protocols approved by UMMS IACUC (Docket number 2085).

Cold exposure

Mice were acclimatized at 30 ℃ for 4 weeks. The mice were then housed individually and acutely exposed to cold (4 ℃). Rectal temperature was measured hourly using a digital thermometer (MicroTherma 2T, Thermoworks) and a rectal probe (RET-3, Physitemp) for up to 8 hours. The end point was a 10 ℃ drop in core temperature (approximately 27 ℃) and mice were immediately euthanized.

Histology

For hematoxylin and eosin (H&E) staining, brown adipose tissue was collected, washed in ice-cold PBS and fixed in 4% paraformaldehyde with gentle shaking at 4℃ overnight. Subsequent procedures were performed by UMMS morphology core facility.

Transmission electron microscopy (TEM)

BAT was dissected and chopped finely in PBS, followed by overnight fixation in 0.1M cacodylate buffer (pH 7.2) containing 2.5 M glutaraldehyde. Sample preparation and image acquisition were performed by UMMS core electron microscopy facility using FEI Tecnai Spirit 12 TEM.

Metabolic phenotyping

Composition of fat and lean mass was measured using 1H-MRS (Echo Medical System) and analysis of food/water intake, physical activity and energy expenditure was performed by the UMMS Mouse Metabolic Phenotyping Core using metabolic cages (TSE Systems).

Glucose and Insulin Tolerance Testing (GTT/ITT)

Glucose and insulin tolerance testing was performed at 14 weeks of HFD feeding as previously described (138).

Reverse transcription-quantitative PCR (RT-qPCR)

Total RNA was isolated from cell culture using Trizol according to the manufacturer instructions (Invitrogen). For mouse adipose tissue, the aqueous phase prepared from Trizol extraction was subject to acidic phenol extraction (pH 4.4) to remove residual lipid, followed by purification using RNeasy (Qiagen) or GeneJET RNA columns (Thermo Scientific). cDNA was synthesized from 0.5-1 μg RNA, using MultiScribe reverse transcriptase (Applied Biosystems). Quantitative PCR was performed using Fast SYBR Green Master Mix (Applied Biosystems) on a 7500 FAST Real-Time PCR system (Applied Biosystems). For a normalization purpose, several widely used internal control genes were tested in all experimental groups and the most stable one was selected. Relative gene expression was calculated by the comparative C_T

method. Coefficient of variation for the reference genes was less than 1% across samples. Primers are listed in Table. 2.1.

Quantification of mitochondrial DNA (mtDNA) content

Approximately 5-10 mg of frozen brown fat were lysed in 300 μL tissue lysis buffer (50 mM Tris-Cl pH 7.5, 50 mM EDTA pH 8.0, 100 mM NaCl, 1% Triton X-100, 5 mM DTT and 100 mg/ml proteinase K) at 56 ℃ for 6 hours. DNA isolation and quantitative PCR were performed as previously described (129).

Immunoblotting

Approximately 10 mg of frozen brown fat or 50 mg of frozen inguinal white fat were placed in ice-cold RIPA buffer supplemented with protease inhibitor cocktail (Sigma), phosphatase inhibitor cocktail (Sigma) and sodium β-glycerophosphate. The tissue was then homogenized using a bead mill homogenizer (Qiagen TissueLyzer). The lysates were vortexed vigorously for 5 seconds, incubated on ice for 10 minutes and cleared by centrifuging at 13200 rpm for 15 minutes at 4 ℃. Preparation of lysates from cell culture was performed as above without using TissueLyser. Protein concentration was determined using a BCA kit (Pierce). Indicated amounts of proteins were separated on a polyacrylamide gel and blotted onto a PVDF membrane. The membrane was blocked in 5% non-fat milk in TBS-tween, followed by incubation with primary antibodies directed against proteins of interest and HRP-conjugated secondary antibodies. The protein signals were visualized with Amersham ECL kit (GE Healthcare) or

WestPico ECL kit (Thermo Scientific) and digitally recorded using Amersham Imager 600 (GE Healthcare). The antibodies used are as follows: LRPPRC (produced in-house using mice); UCP1 (U6382, Sigma); PPARγ (sc-7273, Santa Cruz); COXI (ab14705, Abcam); COXVa (ab110262, Abcam); NDUFS3 (ab110246, Abcam); Citrate Synthase (GTX110624, GeneTex); VDAC (4866, Cell Signaling); ATP2A2 (sc-8095, Santa Cruz); ATP2A3 (sc-81759, Santa Cruz); GAPDH (sc-25778, Santa Cruz).

Lactate measurement

Lactate levels were measured in homogenates prepared from approximately 5-10 mg of BAT using Lactate Assay kit II (Biovision). For AA-treated cells, lactate secretion was measured in culture medium using the same kit.

Complex activity and citrate synthase activity

Complex activity and citrate synthase activity were measured in BAT homogenates as previously described (129, 139).

Chromatin immunoprecipitation (ChIP)

Interscapular brown fat was collected, washed with ice-cold PBS and finely minced. Minced tissue was cross-linked in 10 volume of PBS containing 1% paraformaldehyde for 10 minutes at room temperature on a rotator. Cross-linking was quenched by adding a final concentration of 125 mM glycine. The samples were then dounced on ice 10 times, washed twice with ice-cold PBS. Disaggregated tissue was

placed in 1ml of RSB buffer (3 mM MgCl2, 10 mM NaCl, 10 mM Tris-Cl pH 7.4, 0.1% NP-40 and protease inhibitor cocktail [Sigma]), dounced on ice 30 times, incubated on ice 5 minutes and filtered through 100 μM cell strainer. The homogenate was centrifuged and the pellet was resuspended in nuclei lysis buffer (1% SDS, 10mM EDTA, 50 mM Tris-Cl pH 8.1 and protease inhibitor cocktail). The chromatin was subject to three sonication cycles (a cycle of 10 minutes with a duty of 30 seconds on / 30 seconds off) using Diagenode Bioruptor. The samples were cleared by centrifugation, diluted in ChIP dilution buffer (1 % Triton-X100, 2 mM EDTA, 150 mM NaCl, 20mM Tric-Cl pH 8.0 and protease inhibitor cocktail) and incubated overnight at 4 ℃ with 2 μg of anti-PPARγ antibody (sc-7196, Santa Cruz). Immunocomplexes were recovered with protein A/G beads (Pierce) and eluted DNA was further purified using the QIAquick gel extraction kit (Qiagen). Quantitative real-time PCR was performed using specific primers for the indicated gene promoters. The primers are designed based on the previously identified PPREs (Ucp1 (140); Cpt1b (141); Pank1 and Pdk4 (142); Fabp4 (143); Lpl (144); Cd36 (145); Plin1 (146)) and listed in Table. 2.2.

Cell culture

Primary stromal vascular fraction containing preadipocytes was isolated from interscapular depot of P0-P2 newborn swiss webster mice (Taconic Biosciences) as previously described (123). Primary brown adipocytes were grown to >90% confluence in DMEM (Corning) containing 20% FBS, 20 mM HEPES and 1 mM sodium pyruvate. Immortalized brown preadipocytes were grown in the same condition except 10% FBS.

For adipocyte differentiation, confluent cells were exposed to DMEM containing 0.5 μM dexamethasone, 125 μM indomethacin, 0.5 mM isobutylmethylxanthine, 20 nM insulin, 1 nM T3 and 10% FBS for 2 days, after which medium was switched to DMEM containing 20 nM insulin, 1 nM T3 and 10% FBS, and replenished every 2 days. On day 6 post differentiation, cells were treated as indicated. At least three independent experiments were performed.

Lentiviral transduction

ATP2A2 shRNA oligomers were annealed and cloned into pLKO.1-hygro lentiviral vector as described in the protocol available from Addgene. 21 bp sense sequences for shATP2A2 are as follows: shATP2A2 #1: 5'-GGCGAGAGTTTGATGAATTAA-3'; shATP2A2 #2: 5'-TGACTCTGCTTTGGATTATAA-3'; shScr (negative control, Addgene #1864). To produce lentiviruses, HEK-293T cells were transfected with the pLKO.1-hygro construct, psPAX2 and pMD2.G using lipofectamine 2000 (Invitrogen) according to the manufacturer instructions. Medium was replaced after 16-20 hours of incubation with the DNA:lipofectamine mixture. At 48 hours post transfection, medium was harvested and passed through 0.45 μm filter (Thermo Scientific). The medium was diluted 2-fold in fresh medium and added to subconfluent immortalized brown preadipocytes plated in 12-well plate with 4 μg/ml polybrene. After overnight incubation, cells were replenished with fresh medium and incubated for additional 24-30 hours. Cells were then trypsinized and seeded in 100 mm dish in the

presence of 400 μg/ml hygromycin, after which medium was replaced every 48 hours. At day 5-6 post selection, hygromycin was removed and cells were used for differentiation.

Calcium measurement

Preadipocytes were plated and differentiated in a 96-well clear bottom black plate (Costar). Fully differentiated cells (day 6) were washed with 150 ul HBSS (Gibco 14175-095) supplemented with 1.8 mM CaCl2, 0.8 mM MgSO4, 1 nM T3 and 20 nM insulin. Cells were then loaded with 4 μM Fluo 4-AM (Invitrogen) in 100 ul HBSS for 1 hour at 37 ℃ (30 ℃ for ATP2A2-deficient cells), followed by two washes with 150 ul HBSS. Fluorescence was measured at 485/520 nm in 100 ul HBSS using a microplate reader (POLARstar Omega, BMG LABTECH). Three independent experiments were performed and each experiment included biological duplicates.

Statistics

Statistical analyses were performed using GraphPad Prism 6 (ver. 6.07). The statistical tests used were specified in the figure legends. Statistical significance was defined as P <0.05. The cutoff for a not-significant (ns) P-value to show the exact number is 0.07.

Results

LRPPRC fat-specific knockout (FKO) mice exhibit impaired respiratory capacity in BAT

To examine whether respiratory capacity controls BAT gene expression *in vivo*, we generated fat-specific LRPPRC knockout mice (hereafter, FKO mice) by crossing LRPPRC floxed mice with Adiponectin-Cre mice. mRNA and protein levels of LRPPRC was reduced by >90% in BAT from FKO mice (Figure 2.1A and C). Compared to WT mice (LRPPRC fl/fl), expression of mitochondrial-encoded ETC genes were globally reduced and COXI protein levels were also decreased (Figure 2.1B and C). Interestingly, several nuclear-encoded subunits were also reduced at both mRNA and protein level (Figure 2.1C and D). Abrogated expression of the ETC subunits resulted in impaired activities of respiratory complexes (Figure 2.1E). Electron microscopy and image analysis revealed that WT mitochondria exhibited tightly packed lamellar cristae whereas FKO mitochondria displayed dysmorphic cristae architecture alongside reduced number of cristae (Figure 2.1F and G). This is in agreement with the previous observation that heart-specific loss of LRPPRC leads to disorganized cristae (128). Deficits in respiratory capacity were unlikely due to large changes in mitochondrial biogenesis, since markers of mitochondrial mass (VDAC, citrate synthase and mtDNA) were unchanged (Figure 2.1C, E and H). Furthermore, lactate levels were increased 1.8-fold in FKO mice (Figure 2.1I), consistent with previous studies demonstrating that pharmacological inhibition of the ETC causes increased lactate production due to increased glycolysis (147).

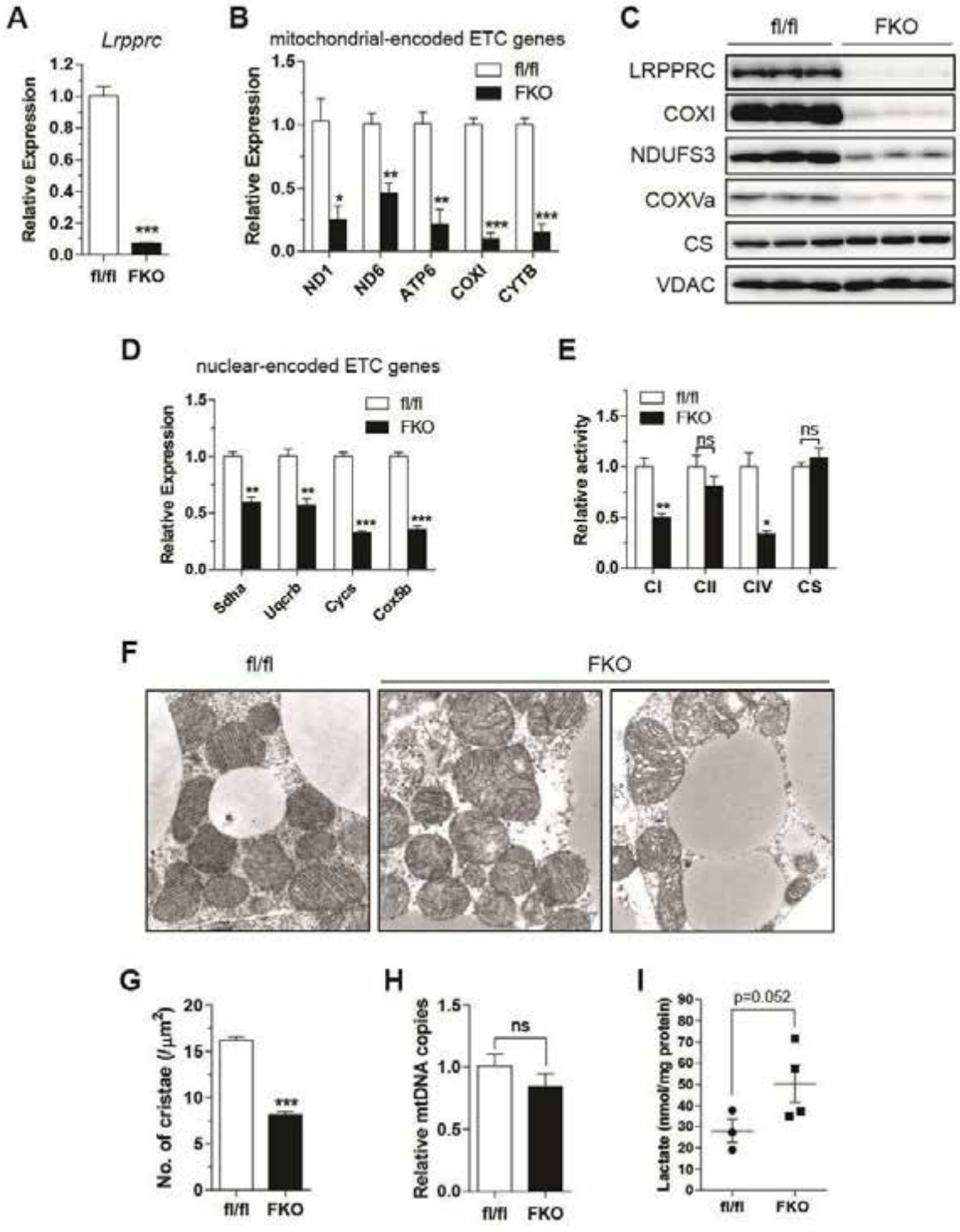
A
Lrpprc
Relative Expression
fl/fl
FKO
B
mitochondrial-encoded ETC genes
Relative Expression
fl/fl
FKO
ND1
ND6
ATP6
COXI
CYTB
C
fl/fl
FKO
LRPPRC
COXI
NDUFS3
COXVa
CS
VDAC
D
nuclear-encoded ETC genes
Relative Expression
fl/fl
FKO
Sdha
Uqcrb
Cycs
Cox5b
E
Relative activity
fl/fl
FKO
ns
ns
CI
CII
CIV
CS
F
fl/fl
FKO
G
No. of cristae (/μm²)
fl/fl
FKO
H
Relative mtDNA copies
ns
fl/fl
FKO
I
p=0.052
Lactate (nmol/mg protein)
fl/fl
FKO

Figure 2.1. Respiratory capacity is impaired in BAT from LRPPRC fat-specific knockout (FKO) mice. (A-B) mRNA levels of *Lrpprc* (A) and mitochondrial-encoded ETC genes (B) in BAT from WT mice (fl/fl) and FKO mice. (C) Immunoblot of LRPPRC, COXI, NDUFS3, COXVa, VDAC, citrate synthase (CS) and GAPDH (loading control) in BAT. (D) mRNA levels of nuclear-encoded ETC genes in BAT. (E) Complex activity in BAT. (F) Transmission electron microscopy (TEM) images of mitochondria in BAT (16,500X). (G) Number of cristae per μm^2 of mitochondrion. 6-10 fields per mouse were analyzed (n=3; total 174 mitochondria for fl/fl and 120 for FKO). (H) mitochondrial DNA (mtDNA) content in BAT. (I) Lactate levels in BAT. (A-E, H): 11-12 week-old male, n=3-5. (F,G): 14 week-old male, n=3. Data are mean ± SEM. **P* < 0.05, ***P* < 0.01, ****P* < 0.001, one-tailed (I) and two-tailed unpaired Student's *t*-test (A-B, D-E, G-H).

Impaired respiratory capacity attenuates thermogenic gene expression

Having established a model of deficient respiratory capacity in BAT, we assessed BAT function and gene expression. On gross examination, BAT from FKO mice housed at room temperature (22 ℃ at our facility) was pale and enlarged (Figure 2.2A, upper panel). Increased lipid deposition with unilocular droplets was apparent in histological sections, an appearance associated with reduced respiratory activity (Figure 2.2A, lower panel). Although *Ucp1* mRNA levels were decreased, we observed that UCP1 protein was stabilized in FKO mice housed at room temperature (Figure 2.2B and C). 22 ℃ is a mild cold stressor to mice and such stabilization of UCP1 protein in cooler environments has been reported (148). Upon acute cold exposure, these mice were not cold sensitive in spite of impaired respiratory capacity (Figure 2.2D). Although not formally assessed, augmented shivering thermogenesis due to housing under mild cold stress may compensate for UCP1-mediated non-shivering thermogenesis, enabling effective defense against cold. Cold also stimulates β-adrenergic signaling (134). Since β-adrenergic signaling is a key regulator of both thermogenic and respiratory programs (149, 150), we sought to determine whether impaired respiratory capacity *per se* affects BAT function and gene expression under circumstances devoid of β-adrenergic stimulation. To do so, mice were acclimated at thermoneutrality (30 ℃) for 4 weeks, a timeframe that is sufficient to offset the impacts of thermal stress. Even at thermoneutrality, FKO mice maintained larger lipid droplets in BAT (Figure 2.3A). Like FKO mice housed at room temperature, thermoneutral-acclimated FKO mice displayed robust depletion of LRPPRC and severe reduction in levels of COXI and nuclear-encoded respiratory subunits

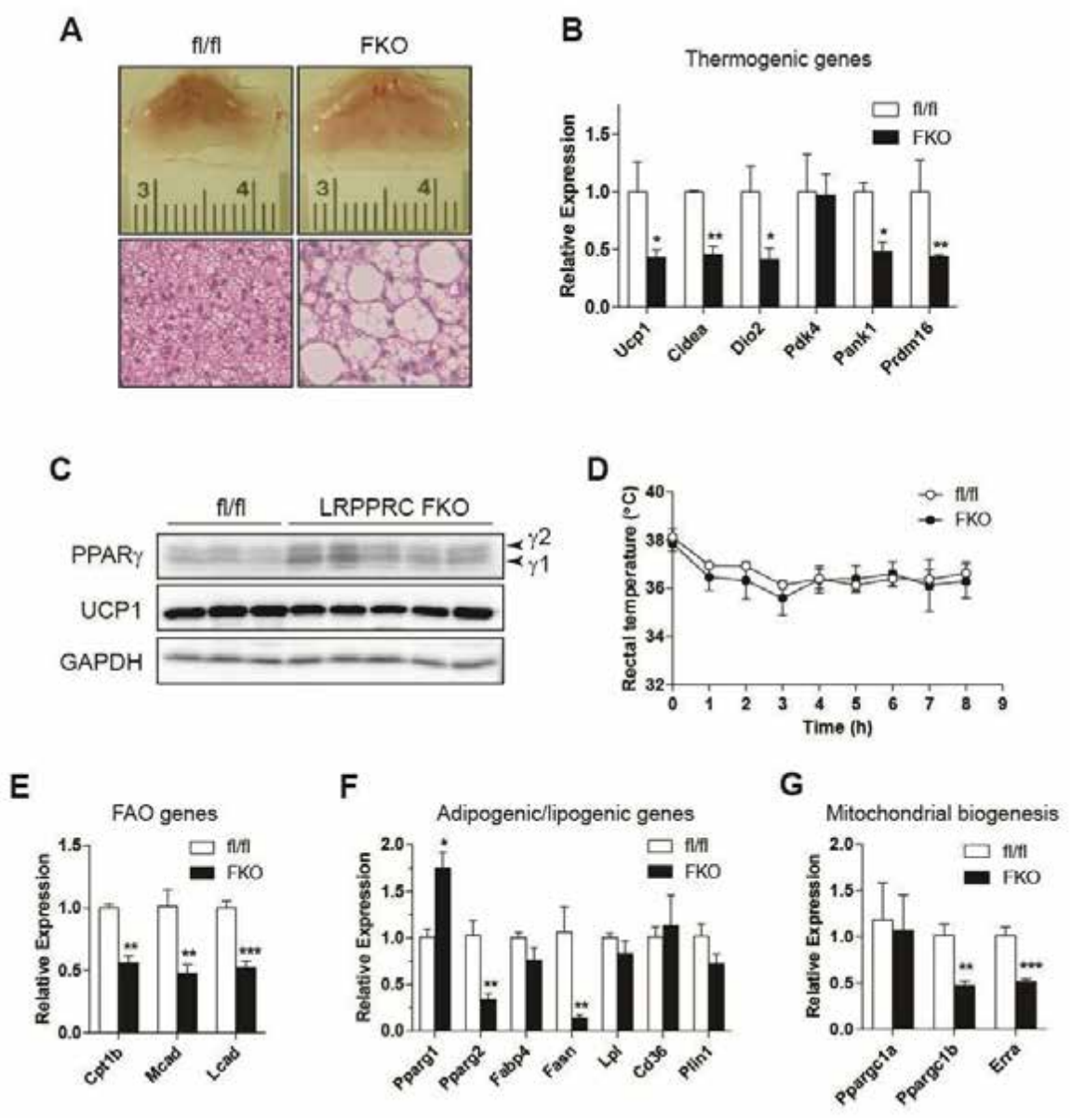

Figure 2.2. Impaired respiratory capacity attenuates thermogenic and oxidative gene expression in BAT from LRPPRC FKO mice living at 22 °C. (A) Representative images (upper) and H&E staining (lower) of BAT. (B) mRNA levels of thermogenic genes in BAT. (C) Immunoblot of PPARγ, UCP1 and GAPDH (loading control) in BAT. (D) Core temperature of control and LRPPRC FKO mice during acute cold exposure at 4 °C. (E-G) mRNA levels of FAO genes (E), adipogenic/lipogenic gene (F), and mitochondrial biogenesis genes (G) in BAT. (A-D): 9 week-old male mice, n=3-5. Data are mean ± SEM. **P*<0.05, ***P*<0.01, ****P*<0.001, two-tailed unpaired Student's t-test (B,E-G).

while VDAC was unchanged and CS was slightly reduced (Figure 2.3B). In these mice, expression of thermogenic genes was severely decreased (Figure 2.3C). Notably, both *Ucp1* mRNA and protein levels were severely reduced (Figure 2.3C and D), and mice were exquisitely sensitive to cold stress (Figure 2.3E).

We next assessed expression of genes that regulate fatty acid oxidation (FAO), adipogenesis, lipogenesis and mitochondrial biogenesis. Interestingly, FAO genes were globally reduced (Figure 2.3F). Alongside decreased nuclear-encoded ETC genes, down-regulation of the FAO genes may favor transitioning of BAT into an energy-storing mode. In contrast, *Pparg*, a master regulator of adipogenesis, and its target lipogenic genes were unaltered or upregulated (Figure 2.3G). *Ppargc1b* and *Erra* (*Esrra*) mRNA levels were reduced but not *Ppargc1a* mRNA (Figure 2.3H). Although these genes are involved in mitochondrial biogenesis, as stated earlier, markers of mitochondrial mass were unchanged, suggesting alterations in various gene programs were not simply the result of reduced mitochondrial biogenesis. Mice housed at room temperature showed almost identical expression patterns of the aforementioned genes (Figure 2.2B and E-G), suggesting that mitochondrial retrograde signaling acts independent of β-adrenergic signaling. Furthermore, in support of normal β-adrenergic signaling in FKO mice living at thermoneutrality, the relative fold change for induction of *Ppargc1a* and *Ucp1* was comparable to control mice, following a cold stress (Figure 2.4A and B). If some brown adipocytes still contained residual LRPPRC, possibly due to inefficient recombination, one would predict a normal fold change of gene induction, following cold exposure. To exclude this possibility, we measured phosphorylated PKA, which is activated by

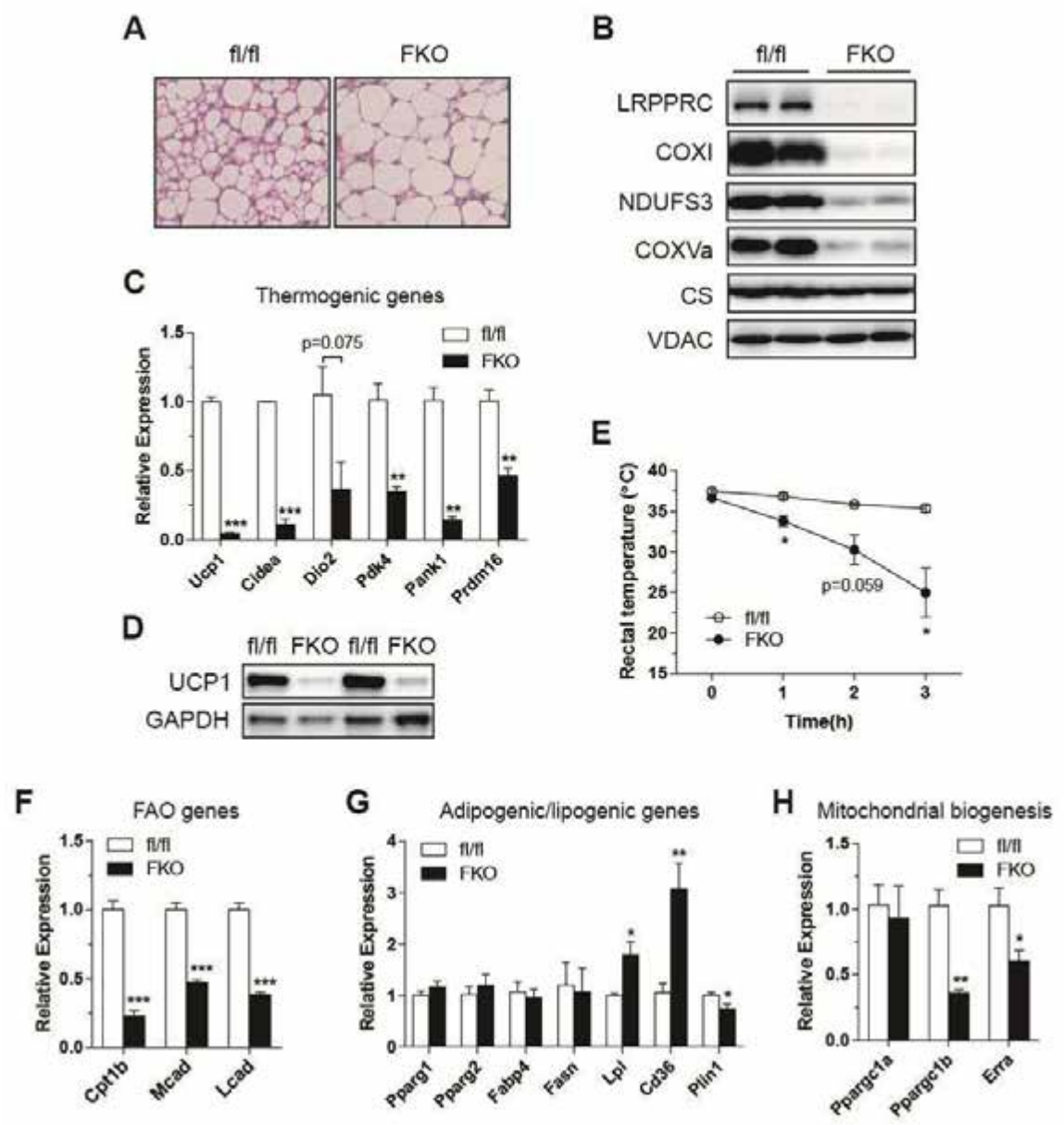

Figure 2.3. Impaired respiratory capacity attenuates thermogenic and oxidative gene expression in BAT from LRPPRC FKO mice living at 30 ℃. (A) H&E staining of BAT. (B) Immunoblot of LRPPRC, COXI, NDUFS3, COXVa, CS and VDAC in BAT. (C) mRNA levels of thermogenic genes in BAT. (D) Immunoblot of UCP1 and GAPDH (loading control) in BAT. (E) Core temperature of control and LRPPRC FKO mice during acute cold exposure at 4 ℃. (F-H) mRNA levels of FAO genes (F), adipogenic/lipogenic genes (G) and mitochondrial biogenesis genes (H) in BAT. 12-14 week-old male were used, n=3-4. Data are mean ± SEM. **P* < 0.05, ***P* < 0.01, ****P* < 0.001, two-tailed unpaired Student's *t*-test (C, E-H).

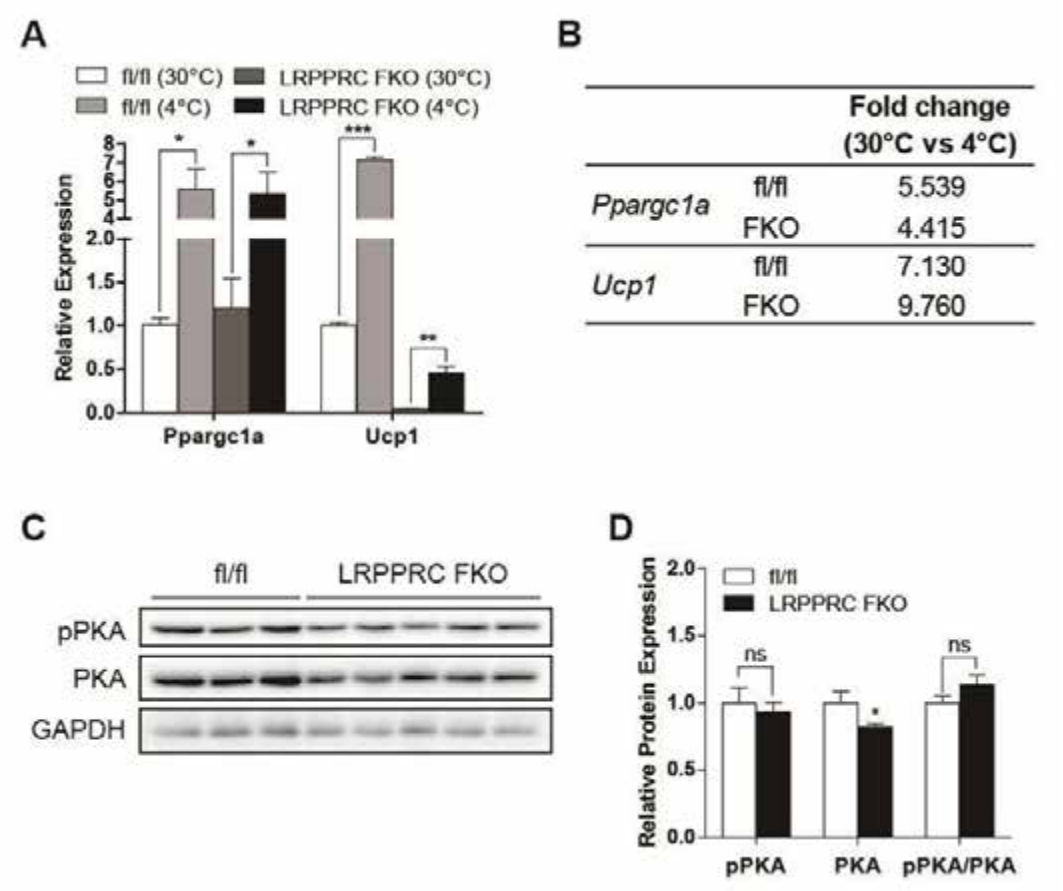

Figure 2.4. β-adrenergic signaling is intact in BAT from LRPPRC FKO mice. (A) mRNA levels of cold-responsive genes in BAT of thermoneutral-acclimated (30 ℃) or cold-exposed (4 ℃) mice. (B) Table showing fold change for 30 ℃ vs. 4 ℃ for the genes from (A). (C) Immunoblot of phosphorylated PKA (pPKA Thr197), total PKA and GAPDH (loading control). (D) Quantification of pPKA and total PKA relative to GAPDH. (a): 12-14 week-old male, n=3-5. (C-D): 12 week-old male mice, n=3-5. Data are mean ± SEM. **P*<0.05, ***P*<0.01, ****P*<0.001, two-tailed unpaired Student's t-test (A,D).

β-adrenergic signaling. In BAT, pPKA was unchanged in FKO mice living at room temperature (Figure 2.4C and D), further supporting that the β-adrenergic signaling pathway was not altered.

In summary, these data indicate that impaired respiratory capacity triggers a retrograde signaling pathway that represses thermogenic and oxidative genes, favoring decreased fuel oxidation and thus energy storage. This may explain why lipid accumulation was increased in LRPPRC-deficient BAT.

Impaired respiratory capacity interferes with the recruitment of PPARγ to thermogenic gene promoters

We were interested in the transcriptional basis by which deficits in respiratory capacity affects thermogenic gene expression. PPARγ governs many aspects of brown fat development and maintenance (151, 152). Protein levels of PPARγ and coactivators including SRC1 and PGC-1α, however, were unchanged in LRPPRC FKO mice (Figure 2.5A). Even so, PPARγ has been shown to exhibit promoter specificity under certain metabolic conditions (153). We, therefore, queried whether or not the recruitment of PPARγ to various transcriptional regulatory units was altered using ChIP assays (Figure 2.5B). As shown in Figure 2.5C, the recruitment of PPARγ to the enhancer region of *Ucp1* and the promoters of other thermogenic genes was reduced. Because PPARγ is required for the expression of these genes (142, 154), reduced recruitment to these regulatory regions might explain their reduced transcription. Interestingly, recruitment of

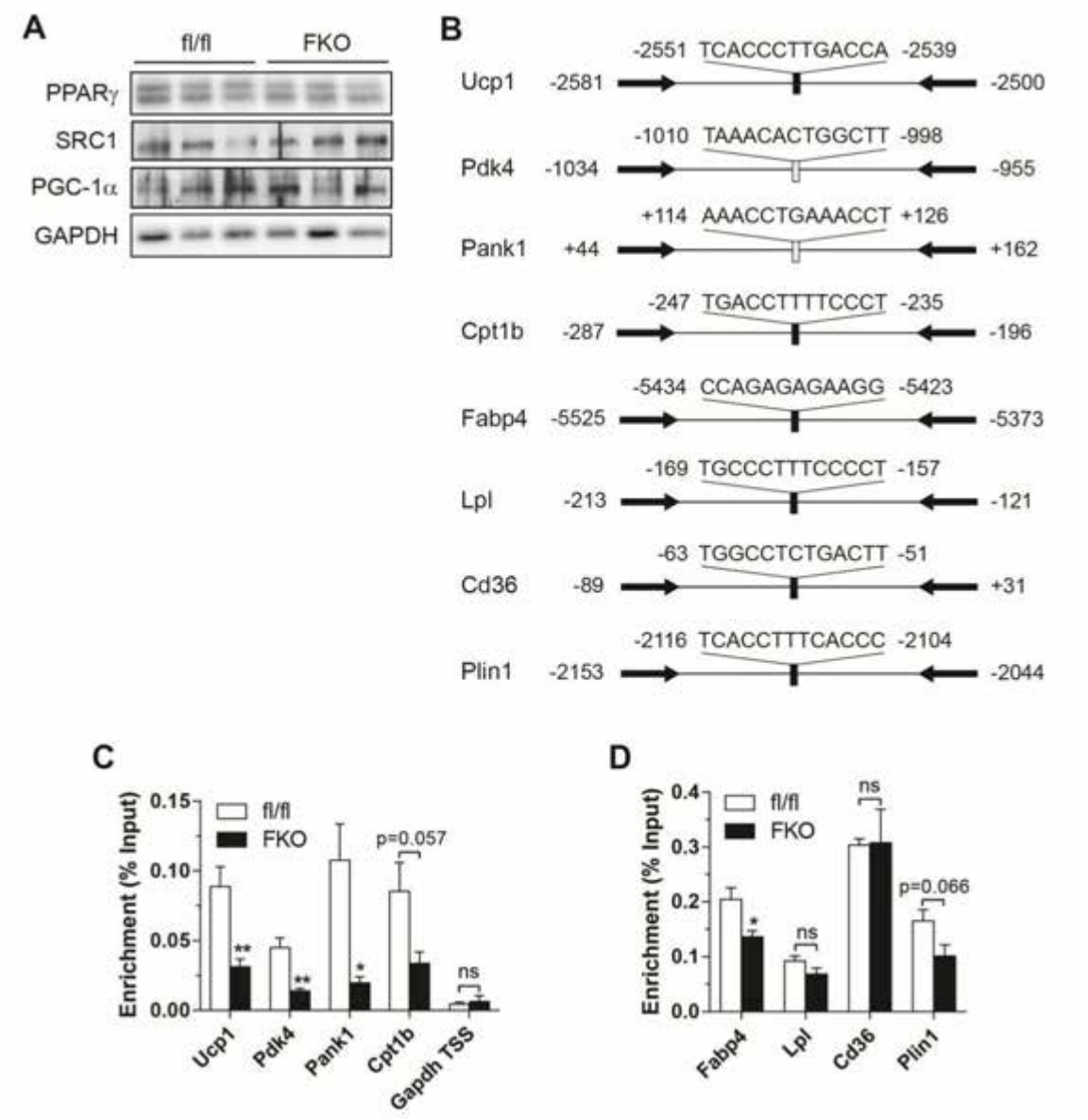

Figure 2.5. Impaired respiratory capacity influences the recruitment of PPARγ in a promoter-specific manner. (A) Immunoblot of PPARγ, SRC1, PGC-1α and GAPDH (loading control) in BAT. (B) Schematic diagram depicting the positions of primers used for ChIP and the positions/sequences of PPREs of the genes assessed by ChIP assays. Filled bar: previously identified PPRE; Open bar: putative PPRE. The arrows indicate the positions of primers. (C-D) PPARγ ChIP assay of thermogenic and oxidative gene enhancer/promoters (C) and lipogenic gene promoters (D) in BAT. 12-14 week-old male at 30 ℃. (C-D): n=4-5. Data are mean ± SEM. **P* < 0.05, ***P* < 0.01, two-tailed unpaired Student's *t*-test (C,D).

PPARγ to the promoters of lipogenic genes was unchanged with some minimally affected (Figure 2.5D), a finding consistent with intact lipogenic gene expression in LRPPRC FKO mice (Figure 2.3G). These data suggest that mitochondrial retrograde signaling influences promoter specific recruitment of PPARγ, a metabolic switch that governs whether or not BAT adopts a thermogenic or storage phenotype.

Cytosolic calcium may mediate retrograde signals from mitochondria to nucleus

Next, we tested whether pharmacological inhibition of respiratory complex can recapitulate the findings from genetic model of impaired respiratory capacity (LRPPRC FKO mice). Since electrons entered from complexes I and II converge at complex III, inhibiting complex III will block the entire electron transit, which impairs respiratory capacity. Thus we treated primary cultured brown adipocytes with antimycin A (AA), an inhibitor of complex III. As in BAT from LRPPRC FKO mice, lactate levels were increased in AA-treated brown adipocytes (Figure 2.6A). Notably, AA treatment resulted in the reduced expression of several thermogenic genes such as *Ucp1* and *Cidea* and minimally affected adipogenic and lipogenic genes (Figure 2.6.B and C). UCP1 protein was also reduced whereas PPARγ and its coactivators SRC1 and PGC-1α were unaltered (Figure 2.6D). Overall, inhibiting ETC in cell culture recapitulates the findings from LRPPRC FKO mice, providing an *in vitro* model to study downstream signaling pathway. These data also suggest that the effects of impaired respiratory capacity on thermogenic gene expression are cell autonomous.

Several studies have shown that ETC dysfunction leads to increased cytosolic

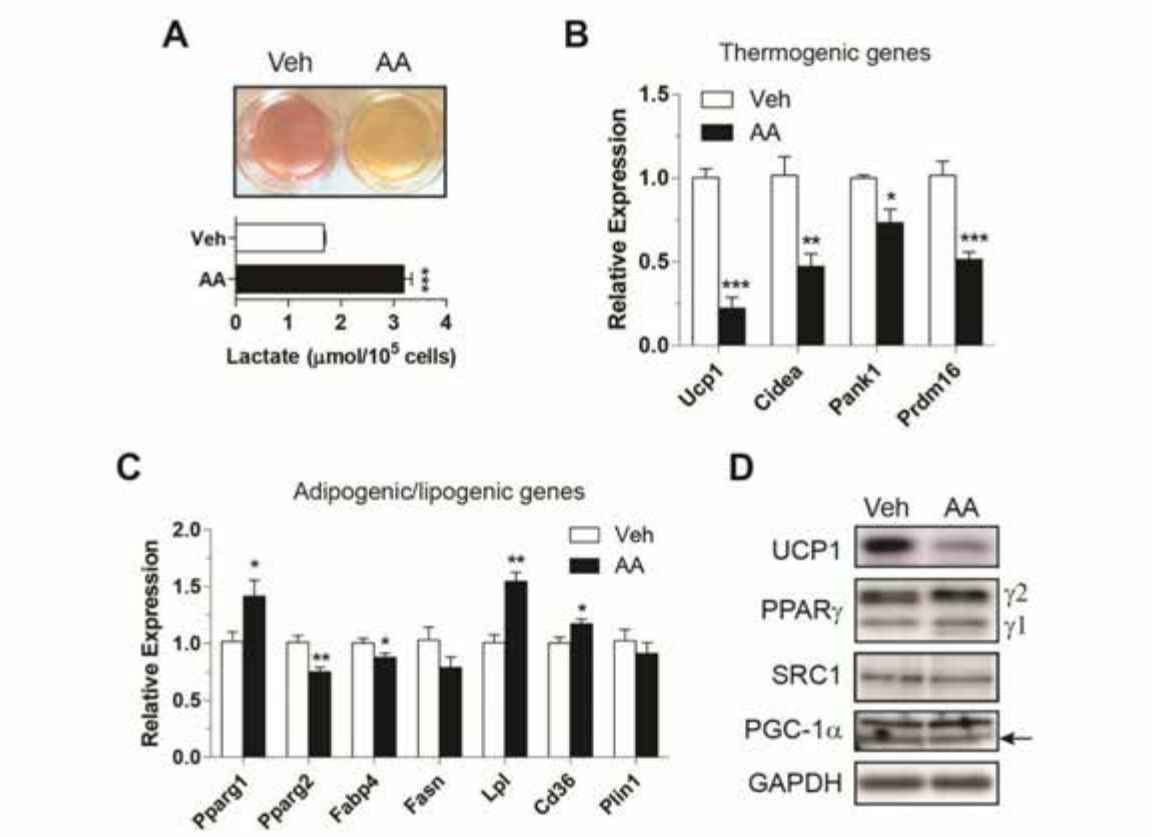

Figure 2.6. Pharmacological inhibition of respiratory complex mimics LRPPRC ablation in cultured brown adipocytes. (A) Representative image of acidic media (upper) and lactate production (lower) in primary brown adipocytes treated with 10 nM AA for 18 hr. (B-C) Thermogenic gene expression (B) and adipogenic/lipogenic gene expression (C) in cells from (A). (D) Immunoblot of UCP1, PPARγ, SRC1, PGC-1α and GAPDH (loading control). Data are mean ± SEM. **P* < 0.05, ***P* < 0.01, ****P* < 0.001, two-tailed unpaired Student's *t*-test (A-C).

Ca^{2+} levels (155-157). These studies demonstrated that Cathepsin L (*Ctsl*) was induced in a Ca^{2+}-dependent manner. First, as an indirect measure of altered cytosolic Ca^{2+} levels, we quantified *Ctsl* mRNA in BAT from LRPPRC FKO mice and AA-treated brown adipocytes. *Ctsl* gene expression was induced in FKO mice housed at 22 ℃ and 30 ℃ and AA-treated cells, indicating elevated levels of cytosolic Ca^{2+} (Figure 2.7A and B). Next, we quantified steady-state levels of cytosolic Ca^{2+}, and observed a 20% increase in AA-treated brown adipocytes (Figure 2.7C). We then examined if reduction of free cytosolic Ca^{2+} levels can rescue AA-mediated repression of thermogenic genes using BAPTA-AM, a cell-permeable Ca^{2+} chelator. BAPTA partially rescued AA-mediated decreases in thermogenic genes but had no effect on lipogenic genes (Figure 2.7D and E). BAPTA was also able to reverse AA-dependent induction of *Ctsl* (Figure 2.7D), indicating that BAPTA effectively blocked Ca^{2+}-dependent alterations in gene expression. In summary, these data support a model in which Ca^{2+} serves as a signaling mediator for the attenuation of thermogenic genes under impaired respiratory capacity.

Finally, we tested whether increasing cytosolic Ca^{2+} mimics the effects of impaired respiratory capacity by silencing sarco/endoplasmic reticulum (SR/ER) Ca^{2+}-ATPase (SERCA) in brown adipocytes. Since SERCA transports Ca^{2+} from cytosol into SR/ER at the expense of ATP, cytosolic Ca^{2+} is expected to be increased in SERCA-deficient cells. Although three paralogous genes encode SERCA (*Atp2a1*, *Atp2a2* and *Atp2a3*), mouse brown adipocytes only express *Atp2a2* and *Atp2a3* with the latter being induced upon differentiation (data not shown). Immunoblot analysis confirmed protein expression of ATP2A2 (SERCA2) in cultured brown adipocytes but ATP2A3 (SERCA3)

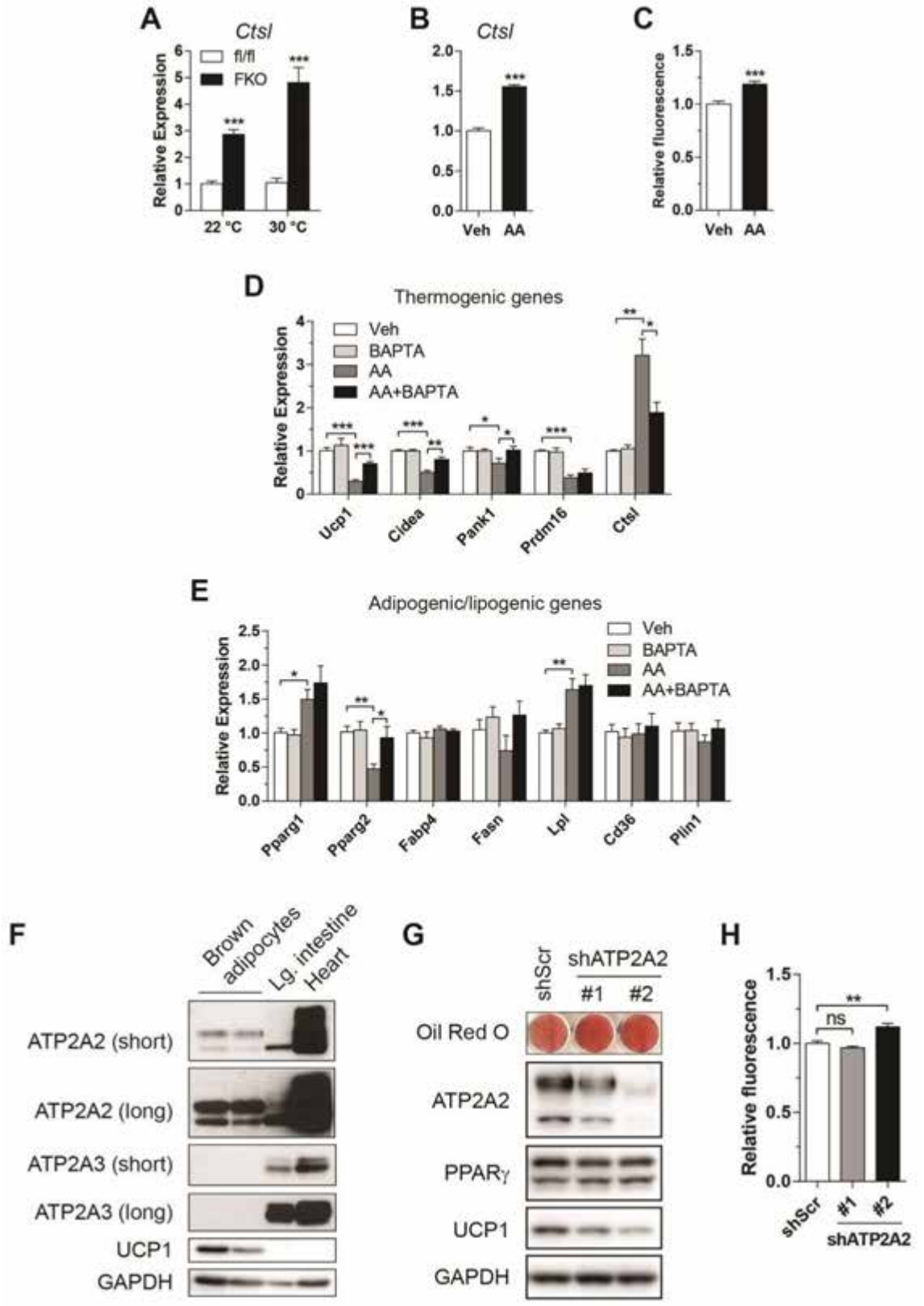
A
Ctsl
fl/fl
FKO
Relative Expression
22 °C
30 °C
B
Ctsl
Veh
AA
C
Relative fluorescence
Veh
AA
D
Thermogenic genes
Veh
BAPTA
AA
AA+BAPTA
Relative Expression
Ucp1
Cidea
Pank1
Prdm16
Ctsl
E
Adipogenic/lipogenic genes
Veh
BAPTA
AA
AA+BAPTA
Relative Expression
Pparg1
Pparg2
Fabp4
Fasn
Lpl
Cd36
Plin1
F
Brown adipocytes
Lg. intestine
Heart
ATP2A2 (short)
ATP2A2 (long)
ATP2A3 (short)
ATP2A3 (long)
UCP1
GAPDH
G
shScr
shATP2A2
#1
#2
Oil Red O
ATP2A2
PPARγ
UCP1
GAPDH
H
Relative fluorescence
ns
shScr
#1
#2
shATP2A2

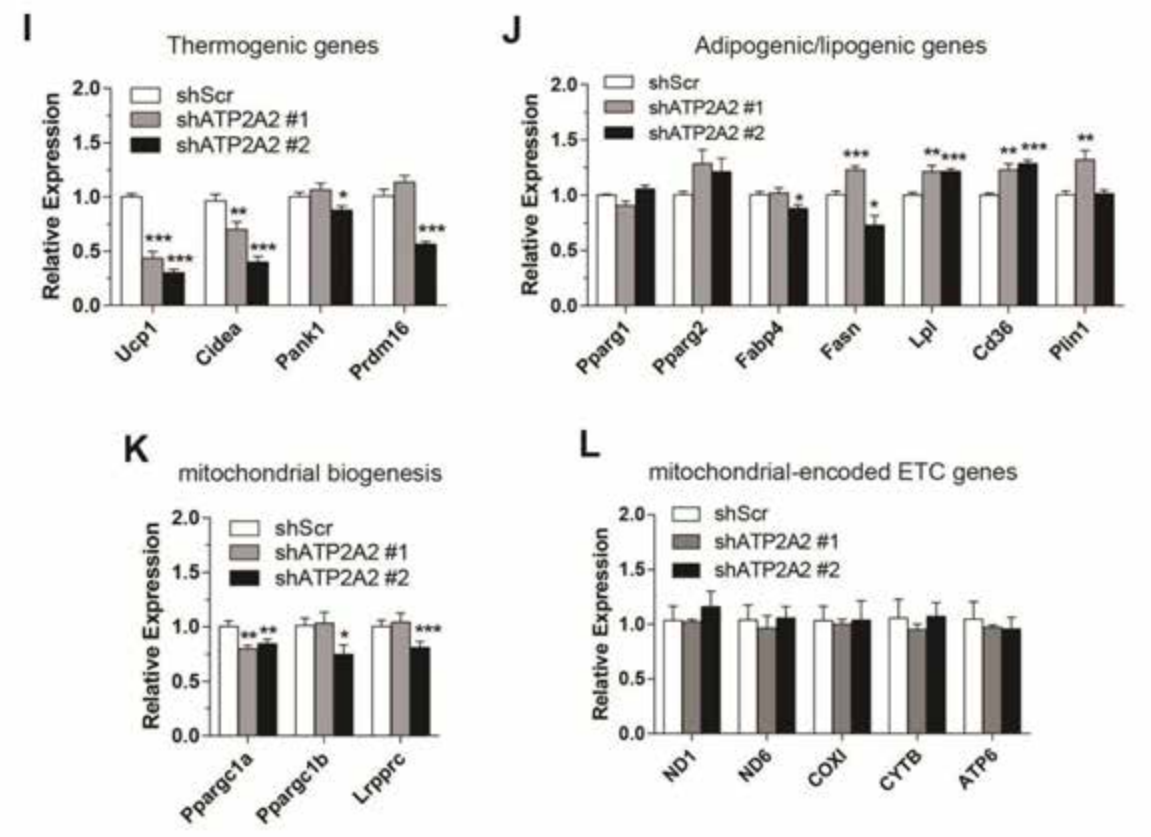

Figure 2.7. Cytosolic Ca^{2+} serves as a signaling mediator between BAT mitochondria and nucleus. (A-B) mRNA levels of *Ctsl* in BAT (A) and primary brown adipocytes (B). (C) Measurement of cytosolic Ca^{2+} in immortalized primary brown adipocytes using a Ca^{2+}-specific fluorescent indicator, Fluo4-AM. (D-E) mRNA levels of thermogenic genes (D) and adipogenic/lipogenic genes (E) in immortalized primary brown adipocytes co-treated with AA and BAPTA. 40 μM BAPTA-AM was loaded into cells for 1 hr, followed by treatment with 20 nM AA for 18 hr. (F) Immunoblot of ATP2A2, ATP2A3, UCP1 and GAPDH (loading control). Short: short exposure; Long: long exposure; Lg: large. Heart was used as a positive control for ATP2A2 and ATP2A3. Lg. intestine was used as a positive control for ATP2A3. (G) Oil red O staining of immortalized primary brown adipocytes stably transduced with ATP2A2 shRNA and immunoblot of ATP2A2, UCP1, PPARγ and GAPDH (loading control). (H) Measurement of cytosolic Ca^{2+} in immortalized primary brown adipocytes stably expressing shATP2A2. (I-L) mRNA levels of thermogenic genes (I), adipogenic/lipogenic genes (J), mitochondrial biogenesis genes (K) and mitochondrial-encoded ETC genes (L). (A): n=3-5. Data are mean ± SEM. **P* < 0.05, ***P* < 0.01, ****P* < 0.001, two-tailed unpaired Student's *t*-test (A-E, H-L).

was undetectable with our immunoblotting methods in the same cells (Figure 2.7F). Even though low levels of ATP2A3 protein are expressed, ATP2A3 has unusually low Ca^{2+} affinity, rendering it essentially inactive at normal intracellular Ca^{2+} concentration ($\leq$0.1μM) (158). Therefore, we chose to silence a single isoform: ATP2A2. Two different sequences of ATP2A2 shRNA yielded moderate to severe silencing (Figure 2.7G). Oil red O staining and unaltered PPARγ protein indicated no apparent effect of ATP2A2 knockdown on differentiation (Figure 2.7G). Cytosolic Ca^{2+} was increased in cells with severe knockdown but not with modest knockdown (Figure 2.7H); we speculate that any change that may be caused by moderate knockdown of ATP2A2 appears to be outside the detection range of the method. Nonetheless, *Ucp1* mRNA and protein were reduced in proportion to the extent of ATP2A2 knockdown (Figure 2.7G and I). Other thermogenic genes were also similarly repressed (Figure 2.7I) whereas lipogenic genes were unaffected with some slightly induced (Figure 2.7J) and genes regulating mitochondrial biogenesis exhibited minimal changes (Figure 2.7K). Finally, *Lrpprc* and mitochondrial-encoded respiratory genes were unaltered, indicating that SERCA knockdown affects Ca^{2+} trafficking through a distinct mechanism (Figure 2.7K and L). Together, these data support that cytosolic Ca^{2+} may be a second messenger for the mitochondrial retrograde signaling in brown adipocytes.

Augmented respiratory capacity induces the thermogenic gene program in subcutaneous adipose tissue

Data from FKO mice motivated the hypothesis that augmented respiratory

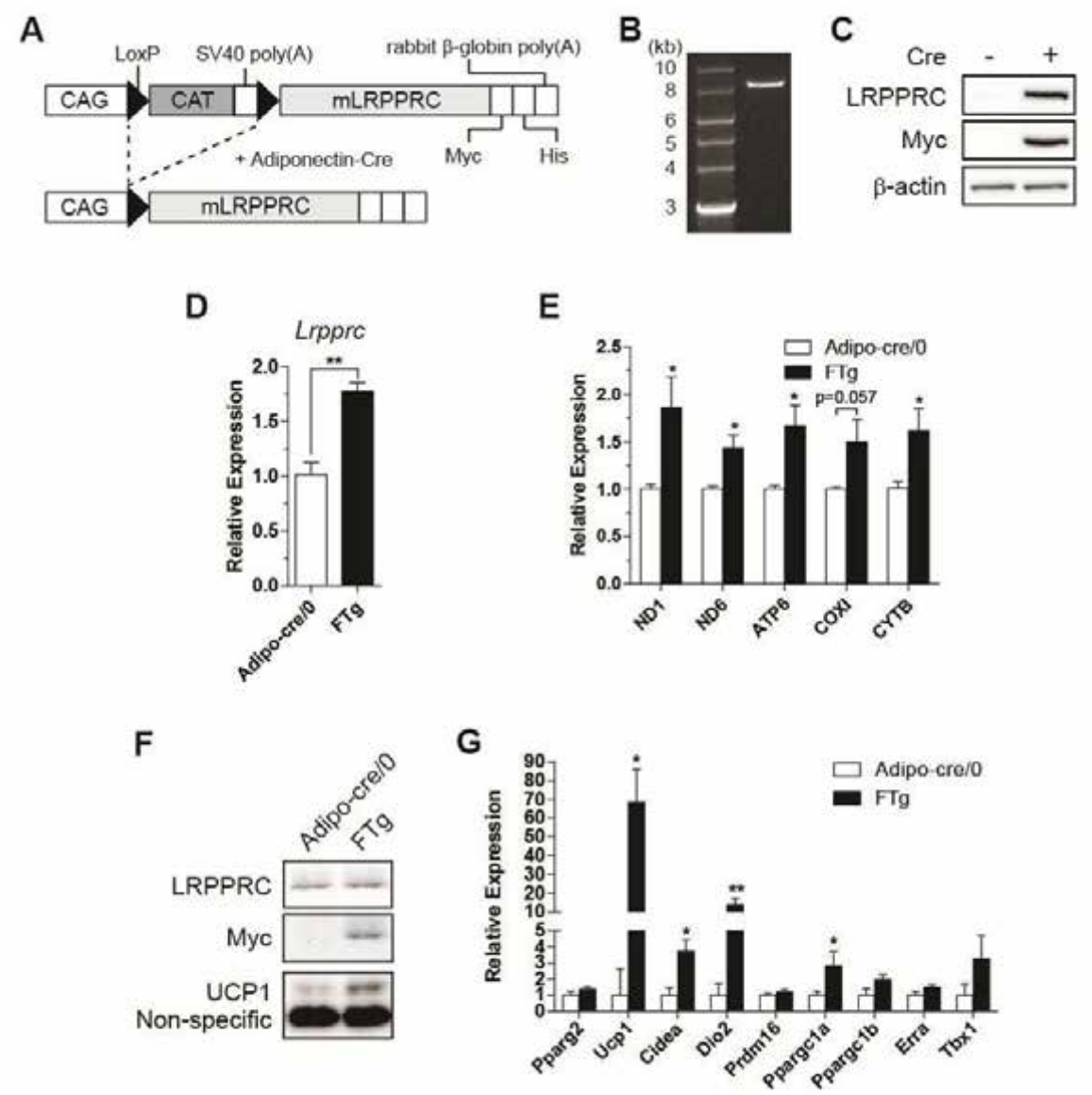

Figure 2.8. *Lrpprc* and mitochondrially encoded genes are induced in IWAT of LRPPRC fat-specific transgenic (FTg) mice. (A) Schematic diagram of a construct allowing fat-specific expression of LRPPRC. (B) *KpnI*/*PmeI*-digested 8.1kb transgene construct used for microinjection. (C) Immunoblot of LRPPRC, Myc-tag and β-actin (loading control) in HEK293T cells transfected with the construct and Cre recombinase (Cre)-carrying plasmid. (D) mRNA levels of Lrpprc in inguinal white adipose tissue (IWAT) from LRPPRC FTg mice. (E) mRNA levels of mitochondrial-encoded ETC genes in IWAT. (**E**) Immunoblot of LRPPRC, Myc-tag and UCP1 in IWAT. (**F**) Gene expression in IWAT. 12-14 week-old male mice at 22 ℃, n=3-4. Data are mean ± SEM. **P*<0.05, ***P*<0.01, two-tailed unpaired Student's t test (D,E,G). CAG: chicken β-actin promoter; CAT: chloramphenicol acetyltransferase; mLRPPRC: mouse LRPPRC.

capacity activates the thermogenic gene program in adipose tissue. To test this hypothesis, we generated mice with ectopic expression of Myc-tagged LRPPRC in adipose tissue (LRPPRC FTg) (Figure 2.8A and B). The transgene encoding LRPPRC was activated only in the presence of Cre recombinase (Figure 2.8C). In BAT, the transgene was not sufficient to influence total endogenous *Lrpprc* gene expression presumably because LRPPRC levels are very high. In IWAT, however, ectopic expression of LRPPRC increased LRPPRC protein and mRNA as wells as its target genes (Figure 2.8D-F). We suspect that the modest expression of LRPPRC may be due to dilutional effects of the presence of non-adipocytic cells. *Ucp1* mRNA and protein were induced and the levels of several BAT-specific genes including *Cidea* and *Dio2* were also increased (Figures 2.8F and G). Overall, the collective data suggest augmenting respiratory capacity is sufficient for 'browning' of subcutaneous white adipose tissue.

The browning of subcutaneous adipose tissue protects against diet-induced obesity in LRPPRC FTg mice

Browning of IWAT enhances energy expenditure, leading to metabolic improvements in mice fed a high fat diet (HFD) (122, 159). We tested whether LRPPRC FTg mice could benefit from browning of IWAT under metabolic stress. To avoid any confounding effects of thermal stress on the whole body metabolism at 22 ℃, animals were acclimated to thermoneutral conditions for 4 weeks upon weaning, followed by 16 weeks of HFD feeding. We first assessed mice carrying the transgene (Flox/0) alone after HFD feeding to rule out any unintended impacts from insertion of the transgene. Flox/0

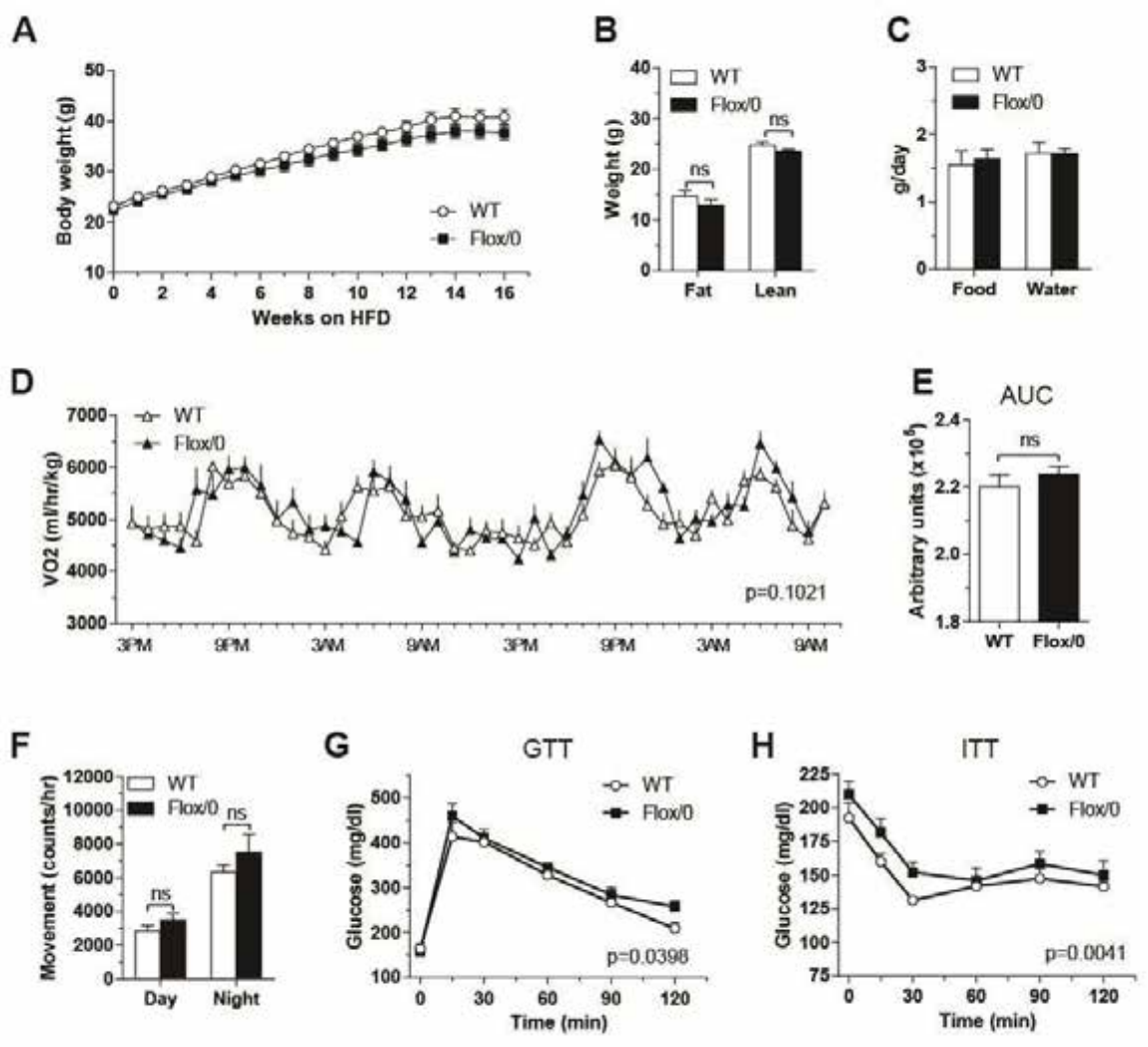

Figure 2.9. Mice with the LRPPRC transgene are metabolically similar to WT littermates upon HFD feeding. (A) Body weight, (B) Body composition, (C) Food and water intake, (D) Whole body oxygen consumption (VO2), (E) Area under curve of (D), (F) Physical activity, and (G) Glucose and (H) Insulin tolerance test (GTT/ITT) in wildtype (WT) littermates and transgene-carrying mice (Flox/0) fed a HFD. (A-H): n=5-7. Data are mean ± SEM. Multiple *t* tests using the Bonferroni correction (A); Two-tailed unpaired (B,C,E,F) Student's *t* test; two-way ANOVA (D,G,H).

mice were similar to WT littermates in terms of their body weight, fat/lean mass and food intake (Figure 2.9A-C). In addition, oxygen consumption and physical activity did not differ significantly between WT and Flox/0 mice (Figure 2.9D-F). Finally, Flox/0 mice were only slightly more insulin-resistant than WT mice (Figure 2.9G and H). Overall, we concluded that the LRPPRC transgene *per se* had minimal effect on whole body metabolism. We next measured the same metabolic parameters in HFD-fed LRPPRC FTg mice. FTg mice gained less weight (~15%) than their littermate controls (Adipo-cre/0) (Figure 2.10A), consistent with a reduction in fat mass observed in these animals (Figure 2.10B). Given no significant difference in food intake (Figure 2.10C), it is likely that alterations in energy expenditure explain the lower fat accumulation in FTg mice. Indeed, we observed that oxygen consumption was increased in these mice (Figure 2.10D and E). Although diurnal physical activity was similar, FTg mice showed a tendency for increased nocturnal physical activity, which may be due to their lower body weight and may contribute to higher energy expenditure during the night cycle (Figure 2.10F). In addition, as reported by others, reduced body weight and increased energy expenditure was associated with improved whole-body insulin sensitivity in FTg mice (Figure 2.10G and H). Notably, these mice exhibited brown-like adipocytes bearing multilocular lipid droplets in IWAT, while similar cells were rarely seen in IWAT from control mice (Figure 2.10I). Collectively, these data demonstrate that browning by augmented respiratory capacity in adipose tissue promotes resistance to diet-induced obesity primarily via increased energy expenditure.

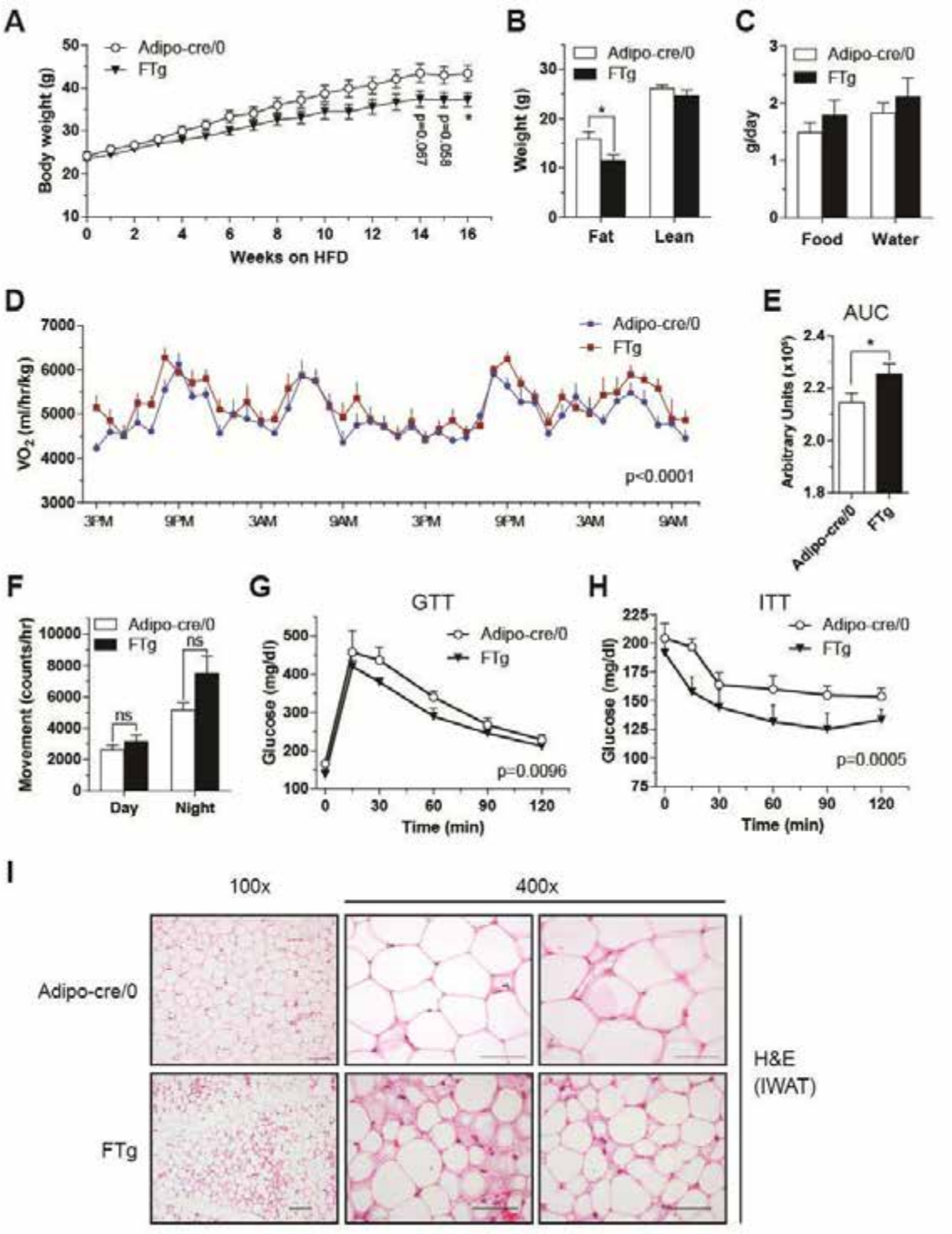
A
Adipo-cre/0
FTg
Body weight (g)
Weeks on HFD
p=0.059
p=0.067
B
Adipo-cre/0
FTg
Weight (g)
Fat
Lean
C
Adipo-cre/0
FTg
g/day
Food
Water
D
Adipo-cre/0
FTg
VO2 (ml/hr/kg)
p<0.0001
3PM
9PM
3AM
9AM
E
AUC
Arbitrary Units (x10⁶)
Adipo-cre/0
FTg
F
Adipo-cre/0
FTg
Movement (counts/hr)
ns
Day
Night
G
GTT
Adipo-cre/0
FTg
Glucose (mg/dl)
p=0.0096
Time (min)
H
ITT
Adipo-cre/0
FTg
Glucose (mg/dl)
p=0.0005
Time (min)
I
100x
400x
Adipo-cre/0
FTg
H&E
(IWAT)

Figure 2.10. LRPPRC FTg mice exhibit improved metabolic phenotypes in diet-induced obesity. (A) Body weight, (B) Body composition, (C) Food and water intake, (D) Whole body oxygen consumption (VO_2), (E) Area under curve (AUC) of (D), (F) Physical activity, (G) Glucose and (H) Insulin tolerance test (GTT/ITT), and (I) Representative H&E staining images of IWAT in Adipo-cre/0 (control) and LRPPRC FTg mice fed a high-fat diet (HFD). Scale bar: 100μm (100x); 50μm (400x). (A-I): n=5-6. Data are mean ± SEM. **P* < 0.05, ***P* < 0.01, ****P* < 0.001, multiple *t* tests using the Bonferroni correction (A); one-tailed unpaired (E) and two-tailed unpaired (B,C,F) Student's *t* test; two-way ANOVA (D,G,H).

Discussion

In this study, we tested whether reducing respiratory capacity in mouse BAT affects thermogenic gene expression and BAT function. We modeled impaired respiratory capacity by ablating LRPPRC in an adipose-specific manner. Impaired respiratory capacity activated retrograde signaling pathway to attenuate thermogenic and oxidative gene expression. The transcriptional basis for this repression was the reduced recruitment of PPARγ to the promoters of those genes. Using an inhibitor of respiratory complex and shRNAs against SERCA pump in cultured brown adipocytes, and conversely the chelation of Ca^{2+} under respiration-impaired conditions, we also showed that Ca^{2+} mediates the crosstalk between mitochondria and nucleus. Conversely, augmenting respiratory capacity in mouse IWAT was sufficient to increase thermogenic gene expression. Overall, our work illustrates an adaptive coordination of respiratory capacity with the expression of thermogenic genes.

Mitochondrial retrograde signaling is triggered by various mitochondrial stresses (90, 91, 103). This signaling pathway affects nuclear gene expression, resulting in a multitude of cellular adaptive responses (90, 91, 103). Our data highlight an adaptive response of brown adipocytes to impaired respiratory capacity, which is an unfavorable condition for thermogenesis. In contrast, adipose-specific loss of TFAM, an activator of mitochondrial transcription and positive regulator of mtDNA replication, had no such defects in BAT(115, 116). Despite the reduced expression of mitochondrial-encoded ETC genes, however, oxygen consumption, FAO, and citrate synthase activity were paradoxically increased in TFAM-deficient BAT(115, 116), which confounds

interpretation. Importantly, the phenotypic similarities between LRPPRC ablation and pharmacological inhibition of respiratory complex exclude pleiotropic effects of LRPPRC loss. Moreover, impaired respiratory capacity was associated with remodeling of oxidative program in BAT. In LRPPRC FKO mice, gene programs involved in mitochondrial respiration (nuclear-encoded) and fatty acid oxidation were impaired. Some of the changes might be explained by reduced expression of *Ppargc1b* and *Erra* (*Esrra*), both of which govern mitochondrial biogenesis and fatty acid oxidation and (150). It is noteworthy that LRPPRC depletion in hepatocytes had no overt effect on the oxidative gene program (160). This differential gene regulation suggests tissue specificity of mitochondrial retrograde signaling. Attenuated expression of genes involved in fatty acid oxidation was not simply due to decreased mitochondrial content. Interestingly, impaired respiratory capacity in BAT was not associated with a compensatory increase in mitochondrial content. This is in contrast to inhibition of oxidative phosphorylation (OXPHOS) in skeletal muscle where induction of PGC-1 coactivators promotes mitochondrial biogenesis to presumably compensate for OXPHOS deficits (95). This dichotomy is interesting as it indicates the status of respiratory capacity in BAT globally determines adipocyte function: storage versus heat dissipation. With normal respiratory capacity, BAT is committed to function as a thermogenic organ and thermogenic and oxidative gene expression is maintained. However, upon impaired respiratory capacity, a condition unfavorable for thermogenesis, thermogenic and oxidative gene expression is suppressed. Concurrently, glycolysis is increased, which can supplement ATP and enhance *de novo* lipogenesis (161). These mechanisms converge to reprogram BAT into

a storage mode.

While we have shown that reduced recruitment of PPARγ to the promoters of thermogenic genes may be responsible for their attenuated expression, precisely how PPARγ is dislodged from those promoters remains unknown. A coactivator complex consisting of PGC-1α, SRC-1/3 and other general coactivators is necessary for PPARγ-dependent thermogenic gene expression but is dispensable for expression of lipogenic genes (36, 162). Based on our findings of attenuated (coactivator-dependent) thermogenic gene expression but intact (coactivator-independent) lipogenic gene expression, disrupted coactivator complex may be a potential mechanism. More importantly, SRC-1 and SRC-3 are jointly required for recruitment of PPARγ to a PPRE site on the *Ucp1* enhancer in BAT but not to lipogenic gene promoters (162). One possibility is that impaired respiratory capacity interferes with the function of SRC family as a PPARγ coactivator, leading to diminished docking of PPARγ on the thermogenic promoters. In addition, given a model in which binding of PGC-1α to PPARγ promotes recruitment of SRC-1 and CBP/p300 (163), abrogation of physical interaction between PPARγ and PGC-1α could indirectly hinder PPARγ docking by sequestering SRC-1 and possibly SRC-3 from PPARγ coactivator complexes.

We provide evidence of cytosolic Ca^{2+} as a signal that may mediate mitochondria-nucleus crosstalk triggered by impaired respiratory capacity in BAT. It has been reported that cytosolic Ca^{2+} was increased by certain mitochondrial stresses including depletion of mtDNA and inhibition of the respiratory chain in various cell types, which ultimately

affected nuclear gene expression (102, 155, 157, 164). In brown adipocytes treated with an inhibitor of respiratory complex, increased cytosolic Ca^{2+} was responsible for repressed thermogenic genes. To our knowledge, this is a first report describing Ca^{2+}-mediated mitochondrial retrograde signaling in BAT. In contrast, Ca^{2+} is also known to positively regulate BAT thermogenesis. β3-adrenergic stimulation of brown adipocytes led to a rise in intracellular Ca^{2+} evoked from mitochondria, ER and entry across plasma membrane (165). It has been suggested that Ca^{2+} influx mediated by TRPV2, a Ca^{2+}-permeable non-selective cation channel, was required for isoproterenol-induced expression of *Ppargc1a* and *Ucp1* in brown adipocytes (166). Moreover, activation of TRPM8, a cold-sensing non-selective cation channel, induced UCP1 expression through Ca^{2+}-mediated PKA phosphorylation in brown adipocytes (167). This discrepancy suggests that mitochondrial retrograde signaling involves a Ca^{2+} signaling pathway that is distinct from the one in stimulated brown adipocytes. Although unclear at present, investigating how Ca^{2+} influences PPARγ and possibly its coactivator complex may help elucidate the distinct mechanism, which could prove of therapeutic utility. Defective respiratory chain function is associated with deranged mitochondrial Ca^{2+} handling (168, 169). We speculate that impaired respiratory capacity may impair Ca^{2+} buffering by mitochondria, leading to increased cytosolic Ca^{2+}.

Interestingly, our gain-of-function model (LRPPRC FTg) suggests that augmented respiratory capacity serves as a transcriptional trigger to promote a BAT-like gene signature in certain WAT. The trigger is functional in IWAT, the only depot in which LRPPRC was overexpressed. This may be due to limitations in our transgenic

approach that involves random insertion. Indeed, it has been shown that retrovirally expressed human LRPPRC successfully increased thermogenic genes including *Ucp1*, *Cidea* and *Dio2* in classic white adipose cell line 3T3-F442A (123). We also do not exclude the occurrence of brown-like cells in other white adipose depots such as mesenteric depot in LRPPRC FTg mice. It would be interesting to determine whether increasing respiratory capacity is a universal mechanism to activate the thermogenic gene program in WAT. Under thermoneutral conditions, these FTg mice displayed resistance to diet-induced obesity and improved insulin sensitivity as whole-body energy expenditure was significantly increased. As stated in the above, we do not exclude a possibility that other depots such as mesenteric depot can undergo browning and contribute to the metabolic improvements in FTg mice. The limited weight gain could potentially affect energy expenditure by altering physical activity. Further analyses are needed to determine what portions of increased energy expenditure in FTg mice derive from the browning of IWAT. Supporting our data, it has been documented that browning of IWAT resulted in similar metabolic improvements in HFD-fed mice via increased energy expenditure (122, 159). Importantly, unlike these studies, our work was performed at thermoneutrality. Several lines of evidence have demonstrated that housing temperature may have confounding impacts on modeling of metabolic diseases in rodents (134, 170). Given that humans live predominantly under thermoneutral conditions, our work indicate that ‘browning’ of white adipose tissue may be a physiologically plausible strategy to fight obesity and diabetes in humans.

In summary, our study demonstrates that BAT coordinates its respiratory status

with the expression of thermogenic and oxidative genes through retrograde signaling to determine its metabolic commitment. When respiratory capacity is impaired, BAT adopts a storage phenotype by turning off thermogenic genes and down-regulating genes involved in fuel oxidation. Furthermore, functioning as a transcriptional trigger, augmented respiratory capacity induces thermogenic gene expression in IWAT, which increases energy expenditure and protects mice from diet-induced obesity. Our work may provide the important framework for future research on mitochondrial control of thermogenic gene pathway and energy dissipation.

Table 2.1. Mouse primers used for RT-qPCR

Primer	Forward (5' -> 3')	Reverse (5' -> 3')
Cd36	TCTTCCAGCCAATGCCTTTG	TGGAGATTACTTTTTCAGTGCAGAA
Cidea	TGCTCTTCTGTATCGCCCAGT	GCCGTGTTAAGGAATCTGCTG
Cox5b	GCTGCATCTGTGAAGAGGACAAC	CAGCTTGTAATGGGTTCCACAGT
Cpt1b	TTATTAAGAACACAAATGTGCAAGCA	TTGCGGCGATACATGATCA
Ctsl	TCTGTTGCTATGGACGCAAG	ATAGCCATAGCCCACCAACA
Cycs	GCAAGCATAAGACTGGACCAAA	TTGTTGGCATCTGTGTAAGAGAATC
Dio2	CAGTGTGGTGCACGTCTCCAATC	TGAACCAAAGTTGACCACCAG
Erra (Esrra)	GCAGGGCAGTGGGAAGCTA	CCTCTTGAAGAAGGCTTTGCA
Fabp4	ACAGCTCCTCCTCGAAGGTTT	AAGCCCACTCCCACTTCTTTC
Fasn	GAAAGGACCTGCCCAATCTCT	AAGGACCACACAGCCTCGTAA
Lcad	GGCTGGTTAAGTGATCTCGTGAT	ATGGGCAGGCGATCGA
Lpl	CTCGCTCTCAGATGCCCTAC	CCATCCTCAGTCCCAGAAAA
Lrpprc	GACTTCCTGGCAAAGATGGA	ACCTTCAATGTCCCCAACAT
Mcad	AACACTTACTATGCCTCGATTGCA	CCATAGCCTCCGAAAATCTGAA
Pank1	GTCAGCATCCTGGCAGTGTA	CTAGGAATGTCCCACCTCCA
Pdk4	CCGCTTAGTGAACACTCCTTC	TCTACAAACTCTGACAGGGCTTT
Plin	CTCTGGGAAGCATCGAGAAG	AAGGGGCTGACTCCTTGTCT
Pparg1	CGGGCTGAGAAGTCACGTTC	GAATATCAGTGGTTCACCGCTTC
Pparg2	GCATGGTGCCTTCGCTGA	TGGCATCTCTGTGTCAACCATG
Ppargc1a	AATGCAGCGGTCTTAGCACT	TTGTGGCTTTTGCTGTTGAC
Ppargc1b	GCCTCTCCAGGCAGGTTCA	TAGAGAACTCAGTCCAGAAGGCTTT
Prdm16	TCTCCGAGATCCGAAACTTCA	GATCTCAGGCCGTTTGTCCAT
Sdha	GCTGGTGTGGATGTCACTAAGG	CCCACCCATGTTGTAATGCA
Ucp1	ACTGCCACACCTCCAGTCATT	CTTTGCCTCACTCAGGATTGG
Uqcrb	CGGGCCGATCTGCTGTT	ACCACTTTCGAAAACCATCCA
Tbp	ACCCTTCACCAATGACTCCTATG	TGACTGCAGCAAATCGCTTGG
36b4	TGCAGATCGGGTACCCAACT	ACGCGCTTGTACCCATTGA
18S	AGTCCCTGCCCTTTGTACACA	CGATCCGAGGGCCTCACTA
ND1	CCCCTTCGACCTGACAGAAG	GGGCCGGCTGCGTATT
ND6	ACAAAGATCACCCAGCTACTACCAT	TTGATGATGTTGGAGTTATGTTGGA
ATP6	AATTACAGGCTTCCGACACAAAC	TGGAATTAGTGAAATTGGAGTTCCT
COXI	TTTTCAGGCTTCACCCTAGATGA	CCTACGAATATGATGGCGAAGTG
CYTB	AGACAACTACATACCAGCTAATCCACTAA	GAATGGCGTATGCAAATAGGAAA

Table 2.2. Mouse primers used for ChIP assays

Primer	Forward (5' -> 3')	Reverse (5' -> 3')
Cd36	GGCTCAAATCAGTTCCGTTG	TTTCTGGTGAAGACCCATCA
Cpt1b	GCCCTGGAATTAGGGAAAAG	GTGAGCATGGTTGCATCAGT
Fabp4	TTCCCAGCAGGAATCAGGTAG	CTGGGAACTCCATTTGCTCTC
Gapdh TSS	GCTCTCTGCTCCTCCCTGTTC	TGGCAACAATCTCCACTTTGC
Lpl	CGGTAGGCAAACTGGAGTCTA	AAACGGTAACGAGGCTCAAC
Plin	ACCCTCGCCCTTAGGATCT	CCTGAAAGCTCTGCTGACAA
Pank1	ACTTTCGTGGGGCGGGGATG	TCGGGAGGAATGCCGGAGGA
Pdk4	GCAACCAAGTCGTTACAGCGTCC	ACCTCTCTCGTCCTCCCGTTC
Ucp1 enhancer	TCACTCCTCTACAGCGTCACAGA	TCTGGCAGGAAGAGTGGAAAG

CHAPTER III

PERSPECTIVES AND FUTURE DIRECTIONS

3.1. Brown fat-specific mitochondrial retrograde signaling

Each cell type is designed to perform a highly specialized function that is primarily governed by their unique transcriptomes. This cell-type or tissue specificity is also reflected in mitochondrial retrograde signaling as manifested by different transcriptomic changes and various outcomes in distinct cell types (102, 103, 156). The differential effects of LRPPRC deficiency on oxidative genes in hepatocytes and brown adipocytes could be explained by the cell type differences. Furthermore, given the complex nature of mitochondrial retrograde signaling, responses elicited by mitochondrial respiratory defect could be differential depending on the approaches used. Although we have seen almost identical changes in key thermogenic genes such as *Ucp1* in brown fat lacking LRPPRC or COX7RP and AA-treated brown adipocytes, it is possible that each method differently alters gene expression. Importantly, in order to obtain a better understanding of brown fat-specific mitochondrial retrograde signaling, whole-transcriptome analysis is critical. Microarray or RNA-seq will be a starting point toward this goal. By comparing the data from three models including LRPPRC, COX7RP and AA, commonly altered genes can be identified. Then, bioinformatical approaches may be able to reveal what functional classes of genes are affected, providing a clue to the nature of brown fat-specific mitochondrial retrograde signaling.

Mitochondrial retrograde signaling can affect the activities and abundance of numerous transcription factors and co-regulators (171). DNA motif analysis may be useful to determine a list of candidate transcriptional factors that mediate transcriptomic changes provoked by mitochondrial retrograde signaling. Aligning the regulatory elements of the genes identified from the comparative transcriptome analysis will allow us to profile transcription factor binding sites shared by the genes within each functional group. The high-scoring DNA motifs would indicate their relevant transcription factor as strong candidates.

3.2. Mitochondrial respiration and calcium

Mitochondria are important buffers of intracellular Ca^{2+} (172). To be accumulated into mitochondria, Ca^{2+} should pass through their outer and inner membranes. Cations such as Ca^{2+} can freely diffuse across the outer mitochondrial membrane (OMM) but not the inner mitochondrial membrane (IMM) (172). The fact that Ca^{2+} can be accumulated into the mitochondrial matrix (173, 174) motivated a search for transporters responsible for mitochondrial Ca^{2+} uptake, and mitochondrial calcium uniporter (MCU) was identified (175-178). MCU is highly Ca^{2+}-specific but has low Ca^{2+} affinity (179). Moreover, Ca^{2+} efflux pathways across the IMM can act against MCU (172). Due to these drawbacks, additional components are obligatory for effective and rapid accumulation of Ca^{2+} into the mitochondrial matrix. VDAC promotes Ca^{2+} transfer across the OMM, resulting in locally high concentrations of Ca^{2+} in the intermembrane space (172). Electrochemical proton gradient also plays a pivotal role. This gradient is created

by the ETC across the IMM and its predominant part electrical potential serves as a large driving force for Ca^{2+} uptake into the matrix (172).

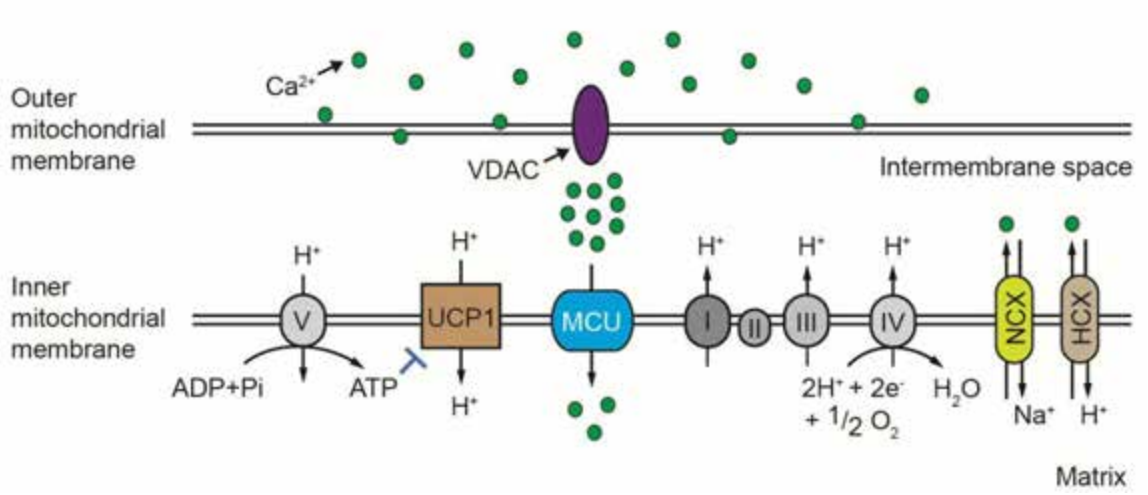

Figure 3.1. Mitochondrial Ca^{2+} uptake. Ca^{2+} accumulation into mitochondria is mediated by MCU, which requires two additional components, VDAC and ETC. Despite Ca2+ efflux through Na^{+}/Ca^{2+} exchanger (NCX) and H^{+}/Ca^{2+} exchanger (HCX), the combinatorial actions of MCU, VDAC and ETC allow for effective and rapid Ca^{2+} uptake by mitochondria**.** Note that this is an over-simplified cartoon with a focus on mitochondrial components of the process.

In brown fat, LRPPRC ablation abrogated the expression of mitochondrial-encoded ETC subunits and thus complex activities, which collapses the proton gradient, and thereby electrical potential is reduced. Due to insufficient driving force, mitochondria in brown fat lacking LRPPRC have a decreased ability to accumulate Ca^{2+}, leading to increased cytosolic Ca^{2+}. In IWAT of LRPPRC FTg mice, despite the augmented respiratory capacity, paradoxically cytosolic Ca^{2+} could be increased, which argues against the induction of thermogenic genes such as *Ucp1*. This seemingly inconsistent situation arises due to UCP1 function. Since UCP1 lowers the proton gradient and thus weakens driving force for Ca2+ accumulation, increased UCP1 in IWAT of LRPPRC

FTg mice can results in increased cytosolic Ca^{2+}. However, this is less likely based on the following reasoning. At standard temperature for mouse housing, UCP1 protein must be modestly active, and thereby its impact on the proton gradient could be also moderate. Under this condition, electrical potential is likely to be sufficient to support normal calcium buffering by mitochondria. Nonetheless, future study is required to explore the effect of augmented respiratory capacity on cytosolic Ca^{2+} and the potential role of cytosolic Ca^{2+} on thermogenic gene expression in IWAT of LRPPRC FTg mice.

3.3. Other potential mediators of mitochondrial retrograde signaling in brown fat

While we identified Ca^{2+} as a signal between brown fat mitochondria and the nucleus, the partial rescue by Ca^{2+} chelation and relatively modest effects of SERCA2 knockdown would suggest that other mediators are perhaps involved. Mitochondrial respiratory defects are often associated with increased mitochondrial reactive oxygen species (ROS), which serves as a downstream signaling molecule (90, 171, 180, 181). Although we did not formally assess mitochondrial ROS production in brown fat lacking LRPPRC and AA-treated brown adipocytes, mitochondrial superoxide production was increased in LRPPRC-deficient HepG2 cells, a human hepatoma cell line (unpublished data). Even though it is assumed that mitochondrial ROS levels are elevated by AA treatment, our preliminary data show that ROS scavengers including N-Acetylcysteine (NAC) and MnTMPyP fail to rescue the effects of AA on thermogenic genes in cultured brown adipocytes, excluding ROS as a signaling mediator. Even so, mitochondrial ROS would be worth further investigation in LRPPRC FKO mice. Additionally, given that

cold exposure increases mitochondrial ROS, an induction that is necessary for thermogenic energy expenditure and UCP1 function (182), brown fat may use ROS as an effector under a defined circumstance. If this is true, it would be quite interesting to identify how brown fat distinguishes the two different ROS-producing contexts.

Mitochondrial respiration directly contributes to the pools of cellular NAD^+ by oxidizing a reducing equivalent NADH to NAD^+ via ETC. NAD+ is recycled in the TCA cycle to generate NADH. In addition, NAD^+ serves as an obligate cofactor of sirtuins and PARPs. In mice with loss of PARP-1, a major cellular NAD^+ consumer (183), NAD^+ levels in brown fat was increased and thus sirtuin 1 (SIRT1) activity was induced (184). Activated SIRT1 deacetylated PGC-1α, which was sufficient to induce many oxidative genes and several thermogenic genes including *Ucp1* and *Dio2* in brown fat (184). However, SIRT1 KO mice showed no significant difference in UCP1 protein expression in brown fat compared to WT mice (185). This would argue against an essential role of SIRT1 in maintaining the key thermogenic program. Similarly, although forced expression of sirtuin 3 (SIRT3), a mitochondrial NAD^+-dependent deacetylase, was sufficient to increase expression of *Ucp1*, *Ppargc1a* and several respiratory genes in brown adipocytes (186), SIRT3 KO mice exhibited normal expression of thermogenic and oxidative genes in brown fat (NCBI Accession number GSE27309, (187)). The role of other NAD^+-dependent surtuins in the thermogenic gene program remain elusive.

Respiratory defects through mtDNA depletion or complex III inhibitors have been shown to inhibit pyrimidine (uridine, cytidine) biosynthesis (188, 189). In particular, protein levels of p53 were elevated in response to complex III inhibitors, which was

rescued not by ROS scavengers but by uridine supplementation. This finding suggests that a certain type of mitochondrial retrograde signal is transmitted via depletion of the pyrimidine pools. It would be interesting to see if supplying exogenous uridine to LRPPRC-deficient cells and AA-treated cells can reverse the decreases in thermogenic gene expression.

A previous study on mice with ectopic expression of glycerol 3-phosphate dehydrogenase (GPDH, encoded by *Gdc-1*) raises a potential connection between accumulation of lipids and certain thermogenic genes such as *Ucp1* in brown fat. GPDH is a cytosolic enzyme that is responsible for conversion of a glycolytic intermediate dihydroxyacetone phosphate to glycerol 3-phosphate, a backbone for triglyceride synthesis. The GPDH transgenic mice exhibited increased lipid deposition in brown fat and liver whereas the lipid contents of subcutaneous and visceral white fat were decreased (190). This discordant lipid metabolism and the observation that GPDH-null mice had normal lipid content (191) suggest that GPDH overexpression promotes lipid redistribution between metabolic tissues but does not enhance lipogenesis. The most interesting finding is a severe reduction in *Ucp1* mRNA levels in brown fat from the transgenic mice. Decreased adrenergic tone is unlikely because *Ucp1* was almost equally induced in WT and the transgenic mice upon cold exposure (190). Based on these data, the following model could arise: As seen in COX7RP KO mice and LRPPRC FKO mice, impaired mitochondrial respiratory capacity promotes lipid accumulation presumably via decreased fatty acid oxidation. The accumulated lipids may in turn activate a pathway that negatively influences the thermogenic genes.

3.4. Mitochondrial respiration-independent effects of LRPPRC ablation and Antimycin A (AA) treatment

We used LRPPRC ablation and AA treatment for genetic and pharmacological impairment of respiratory capacity, respectively. In this section, the potential pitfalls of these approaches and possible solutions will be discussed.

Although controversial, a few studies have suggested that LRPPRC is a dual-targeted protein that can be located in nuclei as well as mitochondria (192, 193). However, as discussed in the introduction (see Chapter 1.3.2.5), it is unlikely that depletion of nuclear LRPPRC underlies the attenuation of thermogenic gene expression in brown fat lacking LRPPRC. Even so, this issue could be addressed by using LRPPRC with mutated nuclear localization signal (NLS). LRPPRC has a weak NLS that is thought to support its nuclear localization (193). When LRPPRC with mutated NLS is introduced into LRPPRC-deficient brown fat, the mutant protein will only localized to mitochondria and this experiment will tell us whether nuclear LRPPRC plays a role in regulating thermogenic gene expression.

Another possibility is that LRPPRC deletion *per se* may have pleiotropic effects that are not mediated by suppressed mitochondrial transcription and impaired mitochondrial respiratory capacity. To exclude this possibility, recovering mitochondrial transcription in a LRPPRC-independent way can be considered. Hypothetically, hyperactive POLRMT mutant could increase the rate of basal mitochondrial transcription in the absence of LRPPRC. Practically, mitochondrial topoisomerase 1 (TOP1MT), a negative regulator of mitochondrial transcription (194), can be a solution. Compared to

LRPPRC single-knockout, double knockout of LRPPRC/TOP1MT will increase the availability of mitochondrial transcripts and thus respiratory capacity to some extent, and this should at least in part rescue attenuated thermogenic gene expression in brown fat.

Like other chemical modulators, AA may exert non-specific effects. Any system that disables AA action on its primary target (complex III) will be useful addressing this issue. Let us assume that there is a mutant subunit of complex III that AA is unable to bind and this mutant does not interfere with the enzyme activity. Deleting WT subunit and introducing the mutant subunit will ensure that AA is no longer able to inhibit complex III. If the effects of AA that we observed are through inhibition of complex III and the resultant impairment of respiratory capacity, mutant complex III should block AA action on thermogenic genes in brown adipocytes. Alternatively, AA-insensitive complex III ortholog from other species will be equally effective. In case of complex I, rotenone (complex I inhibitor)-insensitive NADH–quinone oxidoreductase was identified in yeasts (195). To the best of our knowledge, it is unknown that AA-insensitive enzyme with the same function as complex III exists in other species.

3.5. Quantitative determination of the contribution of PPARγ to the attenuation of thermogenic gene expression

We examined a subset of genes among a broad array of brown fat-selective genes that are known to be regulated by PPARγ (142). To quantitatively determine to what extent the attenuated thermogenic gene expression is explained by PPARγ, further investigation is required using a systematic approach.

Using the data sets obtained from whole-transcriptome analysis outlined in Chapter 3.1, expression profiles of the previously identified brown fat-specific PPARγ target genes can be collected. These data will reveal the number of the PPARγ target genes that are down-regulated in LRPPRC-deficient brown fat. Another quantitative and comparative analysis of PPARγ target gene expression can be performed using PPARγ-deficient brown fat as a reference. Since PPARγ ablation causes embryonic lethality (196) and even adipose-specific loss leads to abnormal development of brown fat (152, 197), PPARγ deletion in mature brown fat using an inducible system such as Cre-ER^{T2} is necessary and this model is available (151). Then, gene expression profiles from LRPPRC-deficient and PPARγ-deficient brown fat can be compared for the brown fat-specific PPARγ target genes. From this comparison, differences in fold changes of each gene between the two conditions can be assessed, leading to estimation of PPARγ effect on the observed changes in LRPPRC-deficient brown fat.

3.6. How is the recruitment of PPARγ to the thermogenic enhancers/promoters reduced?

The specific reduction in occupancy of the thermogenic enhancers/promoters by PPARγ implies that specific factor(s) and/or specific modifications of PPARγ or its coactivators are likely involved. Besides the roles of PPARγ coactivators in its recruitment to thermogenic enhancers/promoters, it has been recently shown that EBF2 is necessary for the binding of PPARγ to those regulatory elements (40), making it a strong

candidate. While our preliminary data shows unaltered mRNA levels of *Ebf2* in brown fat from LRPPRC FKO mice, it is possible that EBF2 proteins are reduced or EBF2 docking on its binding sites near PPARγ binding sites within the thermogenic enhancers/promoters is decreased. Another scenario could be that a post-translational modification of the coactivators interferes with binding to PPARγ, a process that may dislodge PPARγ from the enhancers/promoters. In fact, PGC-1α is known to undergo this type of modification, which separates gluconeogenic and mitochondrial functions (198). Lastly, a study shows that CDK5-mediated phosphorylation of PPARγ at serine 273 only affects a subset of its target genes (153). While this study showed that the binding of phosphorylated PPARγ to those gene promoters was unaltered, a novel posttranslational modification of PPARγ could possibly regulate its thermogenic gene-specific docking.

3.7. What is the potential link between cytosolic Ca^{2+} and PPARγ?

The answer to this question will be most speculative in this chapter because little is known about the Ca^{2+} regulation of PPARγ. As outlined earlier, the key PPARγ coactivators including PGC-1α, SRC-1/3 are required for PPARγ regulation of thermogenic genes but not for adipogenic and lipogenic genes (162, 163). Interestingly, intracellular calcium is known to regulate abundance or activity of certain coactivators. In skeletal muscle, exercise or caffeine treatment, both of which are known to increase cytosolic Ca^2 via ryanodine receptor (RyR)-mediated Ca^{2+} release from the sarcoplasmic reticulum (SR), promote nuclear translocation and expression of PGC-1α, resulting in increased mitochondrial biogenesis (199, 200). The expression of RyRs are largely

restricted to skeletal and cardiac muscle, and Ca^{2+} outflow from the receptors generates so-called 'calcium spark' that is a localized rise in cytosolic Ca^{2+} concentration and underlies excitation-contraction coupling in muscle (201). It may be that the spatiotemporal patterns of cytosolic Ca^{2+} increase are different between contracting muscle and brown fat with impaired respiratory capacity. This may lead to divergence from each other in the regulation of PGC-1α possibly via different calcium signaling pathways. It would be worthwhile to see if the nuclear translocation of PGC-1 family members is decreased in brown fat from LRPPRC FKO mice and SERCA-deficient brown adipocytes.

Ca^{2+} is also known to control gene expression through Ca^{2+}-activated effectors. A well-characterized example is nuclear factor of activated T-cells (NFAT). Increased cytosolic Ca^{2+} activates the serine/threonine phosphatase calcineurin through a Ca^{2+}-sensing protein calmodulin. Activated calcineurin dephosphorylates NFAT, allowing for the nuclear translocation of NFAT to promote target gene expression (202). A similar but converse concept could be applied to PPARγ. With an assumption that PPARγ is phosphorylated at unknown residue(s) and the phospho-PPARγ has a reduced ability to dock on the thermogenic enhancer/promoters, Ca^{2+}-regulated kinases such as protein kinase C (PKC), Ca^{2+}/calmodulin-dependent protein kinases (CaMKs) may serve as a link between cytosolic Ca^{2+} and PPARγ by phosphorylating PPARγ at the residue(s).

3.8. Therapeutic implications

While leveraging uncoupled respiration in brown fat seems a tempting strategy to

fight obesity-related diseases, brown fat is scarce or the activity under cold exposure is low in morbidly obese humans (53, 54, 203-205). As for the former case, transplantation of brown/beige fat derived from patient's own progenitor cells may be promising as immune-deficient mice implanted with capillary-derived human beige adipocytes show metabolic improvements when fed a high-fat diet (HFD) (206). With regards to impaired brown fat function in obesity and diabetes, a similar association has been reported for various animal models including *ob/ob* mice, *db/db* mice, SHR/N-*cp* rats and HFD (containing normal amount of sucrose or high sucrose)-fed mice (207-212). In these murine models of obesity and diabetes, there is 'de-browning' of brown fat, characterized by concomitant reduction in UCP1 protein and respiratory complex activities. Similar to classical brown adipocytes, beige adipocytes exhibit this type of de-browning in mice fed a HFD, implying a shared mechanism for both types of thermogenic adipocytes (213). However, we and others here at UMass Medical School have observed that a well-studied obesity-prone mouse strain C57BL6/J did not show a decrease in UCP1 expression upon HFD feeding. It is probable that the composition of HFD used may have caused this discrepancy in HFD response. Notably, a study describing reduced levels of *Ucp1* mRNA in brown fat of C57BL6/J mice used a HFD supplemented with high sucrose, the western-style diet (208) whereas our lab and others used a HFD with regular amount of sucrose. It has also known that dietary polyunsaturated fatty acids (PUFAs) promote UCP1 expression in mice and rats (214-216); thus combined actions of different nutrients may lead to different responses. Alternatively, strain backgrounds could be an important variable. Two unrelated mouse strains, namely CD-1 (outbred) and AKR/J (inbred)

display the similar de-browning of brown fat in diet-induced obesity (212, 217).

As detailed earlier, several models and systems from us and others have established a causal relationship between mitochondrial respiratory capacity and transcription of genes involved in thermogenesis. Impaired respiration in certain models of obesity and diabetes may explain impaired transcription of the thermogenic genes. An interesting question would be whether the similar crosstalk is present in human obesity. If so, altering respiratory capacity may prove promising in restoring brown fat function in certain forms of obesity and diabetes. Even if there are no effects on transcriptional programs involved in thermogenesis, augmenting respiratory capacity could still effectively protect against obesity and diabetes by way of increased respiratory capacity and/or by promoting browning of certain fat tissues as shown in LRPPRC FTg mice, which in turn would increase thermogenic capacity.

In humans and rodents, cold exposure and β-adrenergic agonists activate brown fat to promote energy expenditure (218-224). Many adrenergic receptor (AR) agonists, including pan-adrenergic (ephedrine) and β3-adrenergic (CL-316,243, etc.) agonists, have been unsuccessful in humans due to either undesirable cardiovascular effects, poor oral availability, or in the case of CL-316,243, weak agonism for the human β3-AR (225). Recently, a clinical study has shown that a new class of β3-AR agonist increases energy expenditure via brown fat-meditated thermogenesis with no significant effect on cardiovascular system (226). Based on my dissertation and other work, a mitochondrial retrograde signaling interdicts transcription of thermogenic and oxidative genes,

contributing to transition to an energy-storing mode. The status of mitochondrial respiratory capacity might reveal unanticipated limitations of β3-agonist therapies being considered for humans, limitations predicted to manifest wherever there is a respiratory defect of brown fat, and altering respiratory capacity may need to be considered as adjunctive therapies to either restore or enhance the thermogenic gene program.

3.9. Is augmented respiratory capacity a universal mechanism to trigger browning of adipose tissue?

An EGFP transgene whose configuration is identical to the LRPPRC transgene successfully induced EGFP in whole body of a mouse that expresses ubiquitous Cre recombinase (Cre) (227). Likewise, LRPPRC in the transgene construct should be expressed to a similar extent in any tissue upon excision of LoxP-flanked chloramphenicol acetyltransferase (CAT) gene by tissue-specific Cre. However, our initial characterization of the LRPPRC conditional transgenic mice through crossing with mice expressing a CMV promoter-driven Cre showed that there was differential expression of ectopic LRPPRC in various tissues. Others also reported that their cyclooxygenase-2 (COX-2) transgene with the equal configuration as the EGFP and LRPPRC transgenes was differentially expressed across tissues (228). It is possible that the transgenes may be landed on a tissue-dependent silent region of chromatin via random insertion. Given the mixed origins of adipose tissue, each depot may have different profiles of silent chromatin. One solution would be to design a targeting vector bearing the transgene so that the construct can be inserted into the ubiquitously expressed

locus such as ROSA26 (R26), which would allow us to avoid the silent chromatin issue. Once these mice are successfully generated, we should be able to determine whether or not augmented respiratory capacity is a universal mechanism to trigger browning of adipose tissue.

3.10. Bidirectional communication between thermogenic capacity and respiratory capacity in brown fat

This dissertation and other work describe a one-way regulation that the status of mitochondrial respiratory capacity dictates thermogenic gene expression. Interestingly, it has been shown that the thermogenic capacity afforded by UCP1 expression also communicate with its partner respiratory capacity in brown fat. In UCP1 KO mice, the expression of respiratory subunits that consist of complexes I and IV is severely reduced, thereby leading to abrogated complex activities (229). Along with these functional defects, brown fat mitochondria from UCP1 KO mice have disorganized and less dense cristae. This is specific to brown fat because there is no such defect in heart. Overall, this intriguing observation indicates that brown fat monitors the status of the mutually connected components of thermogenesis to accordingly modulate its function.

APPENDIX

NUTRIENT SENSING BY THE MITOCHONDRIAL TRANSCRIPTION MACHINERY DICTATES OXIDATIVE PHOSPHORYLATION

The work in this section has appeared in publication in the Journal of Clinical Investigation:

Liu L, Nam M, Fan W, Akie TE, Hoaglin DC, Gao G, Keaney JF Jr, Cooper MP.
J Clin Invest. 2014 Feb;124(2):768-84.

Author contribution

- Breeding, Fasting mice and AAV injection were performed by Lijun Liu and Wei Fan.
- Isolation of liver mitochondria was performed by Lijun Liu, Minwoo Nam and Wei. Fan
- Gene expression (RT-qPCR) analysis and quantification of mtDNA (qPCR) in liver were performed by Minwoo Nam, Lijun Liu and Wei Fan.
- Primary hepatocyte experiment and adenoviral infection were performed by Lijun Liu and Wei Fan.
- Immunoblotting in H2.35 cells was performed by Lijun Liu and Minwoo Nam.
- 4sU labeling assay, gene expression analysis in H2.35 cells, oxygen consumption assay, complex activity assay, PGC-1α knockout liver experiment, construction and characterization of LRP130 KR/KQ mutants were performed by Lijun Liu.
- S35 labeling of mitochondrial proteins, alkaline extraction of mitochondrial proteins, citrate synthase immunoblotting/activity assay and Mitotracker assay were performed by Minwoo Nam.
- Mass spec analysis and acetylation assay were led and performed by Wei Fan
- Palmitate oxidation assay was performed by Thomas E. Akie
- Comparison of acetylated LRP130 sites across studies was performed by David C. Hoaglin.

Summary

Sirtuin 3 (SIRT3), an important regulator of energy metabolism and lipid oxidation, is induced in fasted liver mitochondria and implicated in metabolic syndrome. In fasted liver, SIRT3-mediated increases in substrate flux depend on oxidative phosphorylation (OXPHOS), but precisely how OXPHOS meets the challenge of increased substrate oxidation in fasted liver remains unclear. Here, we show that liver mitochondria in fasting mice adapt to the demand of increased substrate oxidation by increasing their OXPHOS efficiency. In response to cAMP signaling, SIRT3 deacetylated and activated leucine-rich protein 130 (LRP130; official symbol, LRPPRC), promoting a mitochondrial transcriptional program that enhanced hepatic OXPHOS. Using mass spectrometry, we identified SIRT3-regulated lysine residues in LRP130 that generated a lysine-to-arginine (KR) mutant of LRP130 that mimics deacetylated protein. Compared with wild-type LRP130 protein, expression of the KR mutant increased mitochondrial transcription and OXPHOS in vitro. Indeed, even when SIRT3 activity was abolished, activation of mitochondrial transcription and OXPHOS by the KR mutant remained robust, further highlighting the contribution of LRP130 deacetylation to increased OXPHOS in fasted liver. These data establish a link between nutrient sensing and mitochondrial transcription that regulates OXPHOS in fasted liver and may explain how fasted liver adapts to increased substrate oxidation.

Introduction

In normal fasted liver, an increase in ATP-dependent processes (such as gluconeogenesis and ureagenesis) and ketogenesis requires substrate oxidation, specifically β-oxidation of fatty acids. Presumably, oxidative phosphorylation (OXPHOS) must match this increased need for ATP during fasting. Precisely how coordination of this kind occurs in vivo remains an open question. Addressing this question is important, as several studies imply that a mismatch between substrate oxidation and OXPHOS may sustain or exacerbate metabolic disease (230-232). In principle, an increase in mitochondrial content (biogenesis) and/or OXPHOS efficiency (OXPHOS activity per mitochondrion) could accommodate increased ATP requirements in fasted liver. In terms of regulatory control, sirtuin 3 (SIRT3), a mitochondrial sensor of nutrients, is an attractive candidate, since SIRT3 influences both substrate oxidation and OXPHOS.

SIRT3 is a mitochondrial NAD^+-dependent deacetylase that senses nutrient deprivation (233). Upon fasting, SIRT3 protein is induced in liver, where it activates enzyme systems involved in fatty acid oxidation and ketogenesis (234, 235). Both long-chain acyl-CoA dehydrogenase (ACADL; also known as LCAD) and 3-hydroxy-3-methylglutaryl-CoA synthase 2 (HMGCS2) are deacetylated by SIRT3, culminating in enhanced β-oxidation of fatty acids and ketogenesis, respectively (234, 235). In cell culture, SIRT3 influences energy metabolism; however, different mechanisms have been proposed for various cell types (236-239). Nevertheless, whether and how SIRT3 influences energy metabolism in vivo, and under what biological conditions, remains an

open question. Given that SIRT3 is implicated in metabolic syndrome (239, 240), resolving this question might explain how defective mitochondria emerge in metabolic disease.

Mitochondrial transcription potently influences energy metabolism (126). The basal transcription machinery of mitochondria consists of mitochondrial transcription factor B2 (TFB2M) and mitochondrial RNA polymerase (POLRMT) (241-243). The basal machinery is activated by mitochondrial transcription factor A (TFAM), which also participates in mitochondrial DNA (mtDNA) packaging and replication (244-249). Recently, leucine-rich protein 130 (LRP130; official symbol, LRPPRC [leucine-rich PPR motif–containing]), a protein implicated in Leigh syndrome (124, 250), was found to stimulate transcription of the core mitochondrial machinery and induce mitochondrially encoded transcripts (126), including 13 polypeptides that encode core subunits of the electron transport chain (86, 251). Independent of mitochondrial biogenesis, LRP130 induced mitochondrially encoded gene expression, culminating in increased OXPHOS efficiency (i.e., greater OXPHOS per mitochondrion). Additionally, cells and liver replete with LRP130 had greater β-oxidation of fatty acid (126), which implies that increased OXPHOS facilitates greater substrate oxidation. If the transcription machinery of mitochondria is activated by nutrient deprivation to enhance energy metabolism, this might explain how fasted liver increases its substrate oxidation, a process critical for ATP-dependent pathways, such as gluconeogenesis and ureagenesis, as well as for ketogenesis.

Here, we investigated coordination between nutrient deprivation and OXPHOS activity, considering mitochondrial biogenesis and/or OXPHOS efficiency as potential mechanisms. We found that normal fasted liver used mitochondria with greater OXPHOS efficiency, rather than increasing mitochondrial mass. Greater OXPHOS efficiency was achieved by increasing mitochondrial transcription, regulatory control that was dependent on SIRT3 and LRP130. In fasted liver, SIRT3 deacetylated and activated LRP130, which stimulated mitochondrial transcription to promote OXPHOS. This process was triggered by glucagon/cAMP signaling. We propose that the transcription machinery of mitochondria senses nutrients via SIRT3, permitting augmentation of OXPHOS.

Materials and Methods

Cell culture and animal experiments

Stable transduction of H2.35 cells with SIRT3 or LacZ was achieved using pQCXIP vectors (Clontech), as previously described (126). H2.35 cells stably expressing SIRT3 or LacZ were treated with 500 μM NAD^+ 16 hours prior to harvest. Knockdown of murine *Lrp130* was performed as previously described (123, 160). The shRNA sequence targeted against human *LRP130* was 5′-ATGTGAGTCACTATAATGCT-3′. Primary hepatocytes were isolated from mice as previously described (105). Briefly, approximately 400,000 hepatocytes were seeded per well of a 6-well plate and infected with adenovirus encoding the gene of interest. Virus sufficient to produce a multiplicity of infection of 400 in AD-293 cells (Stratagene, catalog no. 240085) was used to infect 400,000 hepatocytes. After 16 hours, virus was removed and replaced with fresh medium. Hepatocytes were further incubated for 20 hours, after which cells were harvested. For transduction of liver, 8×10^9 live adenoviral particles were tail vein injected into C57BL/6 mice on day 0 in 100 μl PBS. On day 5, liver tissue was harvested. Mice were maintained in 12-hour light/12-hour dark cycle.

Lrp130$^{flox/flox}$ mice, which harbor loxP sites flanking exons 3 and 4 of Lrp130, were generated by the University of Massachusetts Medical School Transgenic Animal Modeling Core from KOMP ES cell clone CSD33081. Prior to experimentation, mice were backcrossed for at least 8 generations onto the C57BL/6 background. *Lrp130*$^{flox/flox}$ mice and wild-type controls aged 8–12 weeks were infected with AAV-Cre at 1.0×10^{11} GC/mouse in 100 μl PBS. The vector for liver-specific cre recombinase driven by the

human thyroxine-binding globulin promoter was packaged in adeno-associated virus by the Viral Vector Core of the University of Massachusetts Medical School as previously described (252). 3 weeks after injection, mice were singly housed beginning at 10 AM for exactly 24 hours in a fed or fasted state, after which they were euthanized for protein and genetic studies. *Pgc1a*$^{flox/flox}$ mice (The Jackson Laboratory, stock no. 009666) were injected with AAV-Cre as described above. 3 weeks after infection, primary hepatocytes were isolated for experimentation. All animal experiments were approved by the IACUC of University of Massachusetts Medical School.

Assessment of mitochondrial mass using MitoTracker Green FM

Mitochondrial mass was evaluated by flow cytometric analysis of cells stained with MitoTracker Green FM (Invitrogen). Briefly, cells were stained with Mitotracker Green FM at 100 nM for 30 minutes at 37℃. Cells were rinsed with PBS, trypsinized, and centrifuged at 130 *g* for 4 minutes. Cell pellets were resuspended in PBS containing 1% FBS for FACS. To quantify mitochondrial mass, 20,000 live cell counts were gated. Since MitoTracker Green FM is excited at 490 nm and emits at 516 nm, the FITC channel (excitation at 494 nm, emission at 520 nm) was used to detect signal.

Quantification of transcription and RNA degradation in whole cells

4sU was used to quantify transcription and RNA degradation as previously described (253), with some modifications. For transcription assays, 1.77×10^6 H2.35 cells stably expressing LacZ or SIRT3 were plated in 10-cm dishes and allowed to attach overnight. Cells were treated with 500 μM NAD^+ for 16 hours and labeled with 2 mM

4sU (Sigma-Aldrich, catalog no. T4509) for 15 minutes at 37°C. RNA was isolated from cells using Trizol and Qiagen's RNeasy mini kit. 50 μg RNA was labeled with EZ-link Biotin-HPDP for 1.5 hours at room temperature. Unbound Biotin-HPDP was removed by chloroform/isoamylalcohol (24:1) extraction at 16,000 *g* for 5 minutes. A 1:10 volume of 5 M NaCl and an equal volume of isopropanol were added. Precipitated RNA was pelleted at 16,100 *g* for 20 minutes at 4°C. The pellet was washed with 75% ethanol and again pelleted at 16,100 *g* for 5 minutes at 4°C. The pellet was resuspended in 100 μl TE buffer (10 mM Tris-Cl pH 8.0, 1 mM EDTA). RNA samples were denatured at 65°C for 10 minutes, then rapidly cooled on ice for 5 minutes. Subsequently, denatured biotinylated RNA was captured using Dynabeads M-270 streptavidin (Invitrogen) with rotation at room temperature for 15 minutes. Beads were washed 3 times with 55°C wash buffer (100 mM Tris pH 7.5, 10 mM EDTA, 1 M NaCl, 0.1% Tween-20), followed by 3 washes at room temperature. Biotin-labeled RNA was eluted with 100 mM DTT by rotating at room temperature for 10 minutes. De novo transcripts were cleaned up using Qiagen's RNeasy mini kit. Recovered transcripts were quantified using Ribogreen (Invitrogen). Approximately 120 ng RNA was used for reverse transcription and subsequent qPCR (RT-qPCR). To assess specificity, a reaction containing no 4sU label was performed in parallel. In general, 4sU transcripts were enriched more than 60-fold.

For RNA degradation studies, on day 0 at 9 AM, H2.35 cells stably expressing LacZ or SIRT3 were plated at a density of 2.8×10^5 cells/well of a 6-well plate. On day 1 at 9 AM, cells were labeled with 0.1 mM 4sU, labeling that continued for 24 hours. On day 1 at 5 PM, labeling medium was supplemented with 500 μM NAD^+. The 0-hour time

point was defined as 9 AM on day 2. At the 1- and 2-hour time points, cells were washed with PBS, after which medium containing 20 mM uridine (Sigma-Aldrich, catalog no. U3003) was used to chase the 4sU label. RNA harvesting and processing proceeded as described above.

Immunopurification of acetylated proteins and detection of acetylated LRP130 protein

Acetylated proteins were immunopurified as previously described (254). Briefly, crude mitochondria were extracted from approximately 400 mg of mouse liver, then frozen on liquid nitrogen. The frozen mitochondrial pellet, about 100 μl volume, was lysed in 500 μl FLAG lysis buffer (50 mM Tris-Cl pH 7.8, 137 mM NaCl, 10 mM NaF, 1 mM EDTA, 1% Triton X-100, 0.2% sarkosyl, 10% glycerol) supplemented with 10 μM TSA and 5 mM nicotinamide. The typical lysate yielded a protein concentration of about 5 mg/ml. 2–10 mg mitochondrial lysate was incubated with 30 μl anti–acetylated lysine antibody–conjugated beads (Immunechem, catalog no. ICP0388) at 4°C overnight. The beads were washed with FLAG lysis buffer 4 times, 1 minute per wash, at room temperature. Acetylated protein was eluted with 49 μl freshly prepared glycine (0.1 M, pH 2.5) for 5–10 minutes at room temperature. 1 elution usually proved sufficient, yielding the highest protein concentration. 1 μl saturated Tris, prepared by dissolving Tris base in ddH_2O until saturated, was added to the eluate to achieve a pH of 7.0. To detect acetylated LRP130 protein, immunoenriched acetylated fractions were immunoblotted for LRP130 using anti-LRP130 rabbit polyclonal sera, as previously reported (126).

qPCR of mtDNA content and RT-qPCR

To isolate total DNA, approximately 20 mg frozen liver was lysed in 200 µl tissue lysis buffer (50 mM Tris-Cl pH 7.5, 50 mM EDTA pH 8.0, 100 mM NaCl, 1% Triton X-100, 5 mM DTT, 100 mg/ml proteinase K) at 56℃ overnight. The lysate was extracted once with phenol/chloroform, after which the aqueous phase was precipitated with 0.1 volumes of 3 M sodium acetate (pH 5.2) and 2.5 volumes of 100% ethanol. Total DNA was quantified using Quant-iT Picogreen dsDNA assay kit (Invitrogen). In a qPCR reaction volume of 15 µl, 400 pg total DNA was used to quantify mtDNA content. Showing strong agreement, 4 mtDNA genes — *ND1*, *ND6*, *ATP6*, and *COX1* — were used to quantify mtDNA content. *18S* and *28S* rRNA served as nuclear reference genes (unless otherwise indicated). In addition, *Tbp* served as a reference gene (unless otherwise indicated); however, 10 ng total DNA in a reaction volume of 15 µl was used. For RT-qPCR, total RNA was isolated and processed as previously described (126). See Tables A.S2 and A.S3 for primers.

Citrate synthase activity in whole liver homogenate

Citrate synthase assay was performed as previously described (255), with slight modifications. 30 mg frozen liver was placed in 300 µl RIPA buffer (50 mM Tris-Cl pH 7.4, 150 mM NaCl, 5 mM EDTA pH 8.0, 0.1% SDS, 1% sodium deoxycholate, 1% NP40) supplemented with PMSF and protease inhibitor cocktail (Sigma-Aldrich), followed by homogenization using a bead-mill homogenizer (Qiagen GmbH) at 25 Hz for

120 seconds. The liver homogenate was incubated on ice for 30 minutes, then centrifuged at 16,100 *g* for 10 minutes at 4°C. The protein concentration of the cleared homogenate was determined using a BCA kit (Thermo Scientific). 10 μg protein was loaded in citrate synthase assay buffer (100 mM Tris-Cl pH 8.0, 0.1 mM DTNB, 0.1 mM acetyl-CoA). The reaction was started by adding 0.25 mM freshly prepared oxaloacetate. A blank sample contained all reagents except liver homogenate. The increase in absorbance due to the formation of 5-thio-2-nitrobenzene anion at 412 nm was measured every 30 seconds for 15 minutes at room temperature. The activity of citrate synthase was expressed as the blank-corrected slope of the absorbance versus time plot within the linear range. Activity was presented as absorbance units per second per milligram protein (AU/s•mg protein), obtained by multiplying AU/s•10 μg protein by 1,000 μg/mg protein.

Cloning and construction of LRP130-7KR

Lysine-to-arginine (KR) mutations were made using a Quick Change II XL site-directed mutagenesis kit (Stratagene, catalog no. 200521). First, a 5KR mutant (K1036R, K1059R, K1250R, K1348R, and K1355R) was generated by serially mutating a C-terminal fragment of LRP130 (1,011–1,392 aa) contained in the pET30a vector. After PCR amplification, the mutated fragment was digested with BlpI/PacI and ligated into the BlpI/PacI site of a pQCXIP vector encoding full-length murine LRP130. Second, a 2KR mutant (K225R and K452R) was generated by serially mutating an N-terminal fragment of LRP130 (60–1,010 aa) contained in the pET30a vector. After PCR amplification, the fragment was digested with BspE1 and ligated into the BspE1 site of LRP130-

5KR/pQCXIP, yielding LRP130-7KR (K225R, K452R, K1036R, K1059R, K1250R, K1348R, and K1355R). Confirmation of mutations was assessed using Sanger method sequencing.

Cloning and construction of LRP130-7KQ

Lysine-to-glutamine (KQ) mutations were made using a Quick Change II XL site-directed mutagenesis kit (Stratagene, catalog no. 200521). First, a 2KQ mutant (K1036Q and K1250Q) was generated by serially mutating a C-terminal fragment of LRP130 (1,011–1,392 aa) contained in the pET30a vector. After PCR amplification, the mutated fragment was digested with BlpI/PacI and ligated into the BlpI/PacI site of a pQCXIP vector encoding full-length murine LRP130. Second, we removed a segment of the above LRP130-2KQ/pQCXIP plasmid by digestion with SnaBI, yielding the 7.6-kb truncation product LRP130-2KQ/ΔpQCXIP. Then, 3 additional C-terminal KQ mutations (K1059Q, K1348Q, and K1355Q) were generated by serially mutating the LRP130-2KQ/ΔpQCXIP vector. This mutated fragment was digested with XhoI/PacI and reinserted into a similarly digested, full-length LRP130/pQCXIP vector, producing a 5KQ mutant of LRP130. A third 2KQ mutant (K225Q and K452Q) was generated by serially mutating an N-terminal fragment of LRP130 (60–1,010 aa) contained in the pET30a vector. After PCR amplification, the fragment was digested with BspE1 and ligated into the BspE1 site of LRP130-5KQ/pQCXIP, yielding LRP130-7KQ (K225Q, K452Q, K1036Q, K1059Q, K1250Q, K1348Q, and K1355Q). Confirmation of mutations was assessed using Sanger sequencing.

Purification of recombinant proteins

For purification of LRP130 fragments contained in pET30a, a single colony was cultured in 6 ml kanamycin LB media at 37℃ overnight. 5 ml of overnight culture was transferred into 100 ml of LB media and shaken at 37℃ for 3 hours until OD_{600} was about 0.4. The culture was then induced with 1 mM IPTG for 5 hours at 37℃. Bacteria were harvested by centrifugation at 1,500 *g* for 15 minutes, and the pellet was frozen at –80℃ until further processing. After thawing, the pellet was resuspended in 10 ml lysis buffer (50 mM NaH_2PO_4, 300 mM NaCl, 10 mM imidazole, 0.5 mM PMSF, pH 8.0). 1 mg/ml lysozyme and 100 µl of 10% Triton X-100 was added into the lysis buffer and incubated at 37℃ for 10 minutes. Bacterial DNA was sheared by sonicating (Sonic Dismemberator 60, Fisher, maximum output) twice for 10 seconds. Cell debris was pelleted at 9,300 *g* for 20 minutes at 4°C. 100 µl Ni-NTA beads were added to the supernatant and incubated at 4℃ overnight. The beads were washed 3–4 times with 1 ml wash buffer (50 mM NaH_2PO_4, 300 mM NaCl, 20 mM imidazole, pH 8.0), 1 minute each, at room temperature. His-tagged LRP130 protein was eluted 2 hours at 4℃ with elution buffer (50 mM NaH_2PO_4, 300 mM NaCl, 250 mM imidazole). The buffer was exchanged to BC100 (100 mM NaCl, 20% glycerol, 20 mM Tris-Cl pH 7.9, 0.1% NP-40) using a NucAway spin column (Invitrogen).

For purification of CBP-GST fusion protein, *E. coli* Rosetta (DE3) cells were transformed with plasmid encoding CBP-HAT-GST (pGEX-4T1-CBP-HAT). Bacteria

were cultured in 6 ml LB medium containing carbencillin (100 μg/ml). After overnight culture at 37℃ with vigorous shaking, 1,000 ml fresh LB medium was inoculated, and bacteria were allowed to grow for 3–5 hours, until OD_{600} reached 0.4–0.6. Expression of GST-CBP fusion protein was induced with overnight at room temperature using 0.5 mM IPTG. Bacteria were harvested by centrifugation at 1,500 *g* for 15 minutes. The pellet was resuspended in 10–15 ml ice-cold PBS and an equal volume of BC100 buffer. Following sonication, Triton X-100 was added until reaching a final concentration of 1%. Lysates were clarified at 13,300 *g* for 30 minutes. The supernatant was transferred to a new tube. 100 μl glutathione agarose beads (Pierce, catalog no. 16110) was added to the supernatant and incubated at 4℃ overnight. The beads were washed 3 times with 20 ml BC500 (500 mM NaCl, 20% glycerol, 20 mM Tris-Cl pH 7.9, 0.1% NP-40) and 2 times with 20 ml BC100. GST-tagged CBP protein was eluted for 2 hours at 4℃ with 20 mM reduced glutathione (Thermo Scientific, catalog no. 78259).

In vitro acetylation and deacetylation assays

Acetylation reactions of 10 μl volume contained 50 mM HEPES (pH 8.0), 10% glycerol, 1 mM DTT, 1 mM PMSF, 10 mM sodium butyrate, 100 μM acetyl-CoA, 2 μg LRP130 purified protein, and 100 ng CBP-HAT domain protein (1,319–1,710 aa). The reaction mixture was incubated at 30℃ for 1.5 hours. Subsequently, an equal volume of 2× LDS loading buffer was added, and the reactions were analyzed by immunoblotting overnight at 4℃ with anti–acetylated lysine antibody (Cell Signaling, catalog no. 9441). For in vitro deacetylation assay, acetylated LRP130 protein was recovered by binding to

Ni-NTA beads (Qiagen, catalog no. 30410) and washed 3–4 times with 1 ml wash buffer (50 mM NaH_2PO_4, 300 mM NaCl, 20 mM imidazole, pH 8.0), 1 minute per wash, at room temperature. Acetylated LRP130 protein was eluted with 50 μl of 250 mM imidazole at 4°C for 2 hours. The elution buffer was changed to BC100 using a NucAway spin column (Invitrogen). Deacetylation was performed in a 20-μl reaction containing approximately 1 μg acetylated LRP130 protein, 2 μl purified SIRT3 (Cyclex kit, catalog no. CY-1153), and 500 μM NAD^+. The reactions were incubated at 30°C for 1.5 hours in a buffer containing 50 mM Tris-HCl (pH 9.0), 50 mM NaCl, 4 mM $MgCl_2$, 0.5 mM DTT, 0.2 mM PMSF, 0.02% NP-40, and 5% glycerol. Subsequently, the reaction was stopped by adding 4× LDS loading buffer, and the reactions were analyzed by immunoblotting overnight at 4°C using anti–acetylated lysine antibody (Cell Signaling, catalog no. 9441).

Identification of peptides using tandem mass spectrometry

Mass spectrometry studies were performed at the Proteomics and Mass Spectrometry Facility of University of Massachusetts Medical School, as previously reported (256). In brief, silver stained gel bands were rinsed in water and briefly incubated with ammonium bicarbonate (100 mM). Gel bands were next destained with a 1:1 ratio of potassium ferricyanide (30 mM) and sodium thiosulfate (100 mM), and transferred to new tubes containing 1 ml water for 1 hour. After removal of the water, gel slices were subjected to addition of 50 μl of 250 mM ammonium bicarbonate, reduced with 5 μl of 45 mM DTT for 30 minutes at 50°C, and then alkylated with 5 μl of 100 mM

iodoacetamide for 30 minutes at room temperature. The slices were then washed twice with 1 ml water, incubated in a 1:1 solution of 50 mM ammonium bicarbonate/acetonitrile at room temperature for 1 hour, soaked in 200 µl acetonitrile, removed, and dried in a SpeedVac. Samples were then digested with 50 µl of 2 ng/µl trypsin (Sigma-Aldrich) in 0.01% ProteaseMAX Surfactant (Promega) in 50 mM ammonium bicarbonate at 37°C for 21 hours. The supernatant of each sample was then removed and placed in a separate 0.5-ml tube, and each slice was further extracted with 100 µl acetonitrile/1% (v/v) formic acid (4:1), combined with respective supernatants of each sample, taken to dryness in a SpeedVac, and reconstituted in 20 µl of 0.1% TFA. LC-MS/MS analysis was done on a LTQ Orbitrap Velos mass spectrometer (Thermo Scientific) as previously reported (256), with the exception of using a 90-minute gradient for peptide elution. Raw data files were processed with either Mascot Distiller (Matrix Science) or Extract_MSN (Thermo Scientific), searched against the SwissProt database using the Mascot Search engine (Matrix Science). In brief, parent mass tolerances were set to 10 ppm, while fragment mass tolerances were set to 0.5 Da. Full tryptic specificity with 2 missed cleavages was used, and variable modifications of acetylation (protein N-term, lysine), pyro-glutamination (N-term glutamine), oxidation (methionine), and carbamidomethylation (cysteine) were considered. Further peptide annotation was achieved using Scaffold (Proteome Software), while relative quantification of acetylated peptides was performed using ProteoIQ (Nusep Inc.). Spectra of acetylated peptides were manually inspected to further validate assignments.

Metabolic labeling of mitochondrial proteins

Mouse primary hepatocytes were isolated as previously described (160). Cells were seeded in 6-well plates at 4.5×10^5 cells/well. After 16 hours, cells were treated with vehicle or 20 nM glucagon (Bachem) for 24 hours in starvation media (DMEM, 0.2% BSA, 2 mM sodium pyruvate). Cells were pretreated with 100 μg/ml cycloheximide (Sigma-Aldrich) and/or 100 μg/ml chloramphenicol (Sigma-Aldrich) as indicated for 10 minutes in methionine and cysteine-free starvation media containing vehicle or glucagon. Cells were then labeled with [^{35}S]-methionine and [^{35}S]-cysteine (50 μCi/ml, PerkinElmer) for 60 minutes and chased for 10 minutes in regular DMEM. Cells were washed with PBS twice and lysed in RIPA buffer supplemented with protease inhibitor cocktail (Sigma-Aldrich), followed by 3 freeze-thaw cycles. Lysates were cleared by centrifugation at 16,100 *g* for 10 minutes at 4℃. Protein concentration was determined by BCA assay (Thermo Scientific). 80 μg of protein (20 μg for total translation) were separated on a 15% polyacrylamide gel at 50 mA. The gel was fixed and stained using colloidal blue staining kit (Invitrogen) to confirm equal protein loading. The gel was then dried at 70℃ for 3 hours and exposed to a Biomax MR film (Carestream Health). Radioactivity in 5 μl of lysates was quantified using a liquid scintillation counter (Beckman Coulter) and normalized to protein concentration.

Palmitate oxidation assay

Palmitate oxidation was performed as previously described (126). Briefly, H2.35 mouse hepatoma cells were incubated in starvation medium (1% BSA, 25 mM HEPES, 1

mM sodium pyruvate in DMEM) in the presence of 0.5 mM NAD^+ for 16 hours. Cells were then incubated for 2 hours in preincubation medium (1% BSA, 25 mM HEPES, 0.25 mM sodium palmitate, 0.5 mM carnitine in DMEM), and subsequently, 0.5 μCi/well of 14C-palmitate was added for 90 minutes. The plate was frozen in liquid nitrogen, and 250 μl perchloric acid was added to each well. Filter paper moistened with 3N NaOH was immediately placed over each well and released CO_2.

Comparison of acetylated LRP130 sites across studies

To estimate the probability that, by chance, 2 studies (Study A and Study B) would identify a given number of acetylated residues in common, we used the hypergeometric distribution. If, of a total *N* acetylated LRP130 peptides, Study A identified *a* peptides and Study B identified *b* peptides, the probability that the sets of peptides identified by the 2 studies would have exactly *c* peptides in common, $0 \leq c \leq \min(230)$, is as follows.

$$p(c;N,a,b) = \frac{\binom{a}{c}\binom{N-a}{b-c}}{\binom{N}{b}}$$

(Equation 1)

Derivation. Conditioning on the peptides identified in Study A induces a separation of the peptides in Study B into 2 groups: the *a* peptides identified in Study A and the $N - a$ peptides not identified in Study A. If the 2 studies identify exactly *c* peptides in common,

Study B must identify c peptides among the a peptides and its remaining $b - c$ peptides among the $N - a$ peptides. The number of ways in which this can occur is the product of the binomial coefficients in the numerator. The total number of ways in which Study B can identify b peptides among the N is equal to the binomial coefficient in the denominator. This conditional probability applies to each of the possible sets of a peptides that Study A could identify. Because those sets are equally likely, the conditional probability is also the unconditional probability.

Assumptions. The application of the probabilities assumes there are 102 potentially acetylatable lysine residues in LRP130 and that, if acetylated, each residue would have equal probability of detection by mass spectrometry. It also assumes that mass spectrometry of LRP130 protein approaches 100% for each study. Because these conditions may not hold for every study, the probabilities are approximations.

Domain mapping and in vitro binding assay

Truncated mouse POLRMT clones expressing aas 1–340, 1–500, 1–650, and 1–710 were each generated by PCR. The products of these reactions were digested with BamHI and XbaI, then ligated in frame into pcDNA3.1 myc His B plasmid. Clones containing full-length and truncated POLRMT were subjected to in vitro transcription/translation using a TnT kit (Promega, catalog no. L4610). Full-length mouse LRP130 fused with an S-tag was immobilized on S-protein agarose (Novagen, catalog no. 69704), then washed with 25 mM HEPES and 0.125% Tween20 containing protease inhibitors. The translated products were subsequently treated with DNaseI and RNase for

10 minutes at room temperature and centrifuged for 10 minutes at 15,700 *g* at 4°C. The supernatants were incubated with immobilized S-tag LRP130 agarose. After incubation for 2 hours at 4°C, complexes were extensively washed with 25 mM HEPES, 0.125% Tween-20, and 0.125 M KCl, and c-myc was detected by immunoblotting.

Cellular respiration, complex activity, and isolation of mitochondria

Cellular respiration (123, 126), isolation of mitochondria (123, 126, 160), complex activity (126), and fractionation of mitochondria by alkaline treatment (257) were performed as previously described.

Statistics

2-tailed Student's *t* tests were used to analyze complex activity, mitochondrial content (using measures of mtDNA or fluorescence), protein quantification, and cellular respiration data. *P* values less than 0.05 were considered significant. 2-way ANOVA was used to assess differences in gene expression. Because mitochondrially encoded genes are transcribed as long polycistronic transcripts and thus tightly coordinated as a "gene set," we evaluated the entire set using a 2-way ANOVA, reporting a *P* value comparing differences among various groups (or treatments). *P* values less than 0.05 were considered significant. In contrast, nuclear-encoded genes were subjected to post-hoc analyses (as indicated in the figure legends), since they are not polycistronic genes that do not necessarily fit into a specific gene set. For these studies, Bonferroni-corrected

post-tests were implemented using a multiple comparison–adjusted α. All analyses were conducted using GraphPad Prism version 6.00.

Results

In liver, fasting coordinately induces mitochondrially encoded transcripts and OXPHOS capacity

Fasted liver is notable for ATP-consuming processes, and is thus dependent on OXPHOS. Given that induction of mitochondrially encoded transcripts stimulates OXPHOS, we wondered whether mitochondrially encoded transcripts and OXPHOS are coordinately induced in fasted liver of C57BL/6 mice. After fasting for 24 hours, mouse liver showed modestly increased mitochondrially encoded transcripts and OXPHOS capacity (Figure A.1A and C). Indicative of a normal fasted response, mRNA of *Pepck* and *G6p*, enzymes involved in gluconeogenesis, was induced, whereas that of *Scd1* and *Fasn*, enzymes involved in lipogenesis, was attenuated (Figure A.1B). Interestingly, the increase in complex IV activity that we observed (Figure A.1C) paralleled that reported by another group; however, alterations in mitochondrial content were not explored in the previous report (258).

Conceivably, changes in mitochondrially encoded transcripts and OXPHOS might be explained by increased mitochondrial content. We therefore quantified mitochondrial biogenesis using complementary genetic, biochemical, and protein assessments. While mRNA for *Pgc1a*, a potent regulator of mitochondrial biogenesis, was induced, there was no induction of *Tfam*, *Polrmt*, and *Tfb2m*, which comprise the basal transcription machinery of mitochondria, or of *Lrp130*, which stimulates the core machinery (Figure A.1B). Because genes comprising the basal transcription machinery are induced during

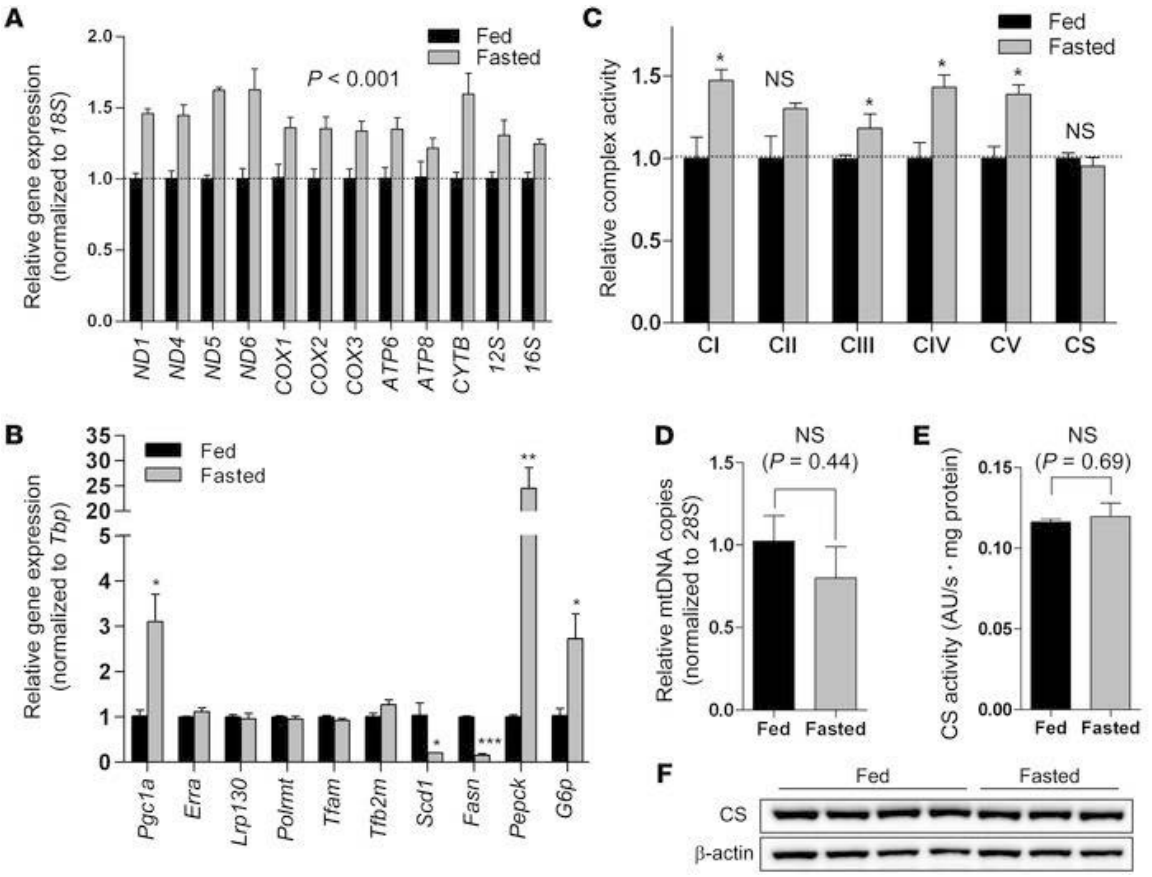

Figure A.1. Fasting coordinately induces mitochondrially encoded transcripts and OXPHOS in liver. (A) Hepatic gene expression of mitochondrially encoded transcripts in 24-hour fasted or fed C57BL/6 mice (n=3). (B) Expression of genes that regulate mitochondrial biogenesis, mitochondrial transcription, lipogenesis, and gluconeogenesis (n=3). (C) Complex activity of mitochondria isolated from liver of 24-hour fasted or fed C57BL/6 mice (n=3). CI–CV, complexes I–V; CS, citrate synthase. (D) Biochemical assessment of mitochondrial content using citrate synthase activity in whole liver homogenate (n=3). (E) Genetic assessment of mitochondrial content using mtDNA content (n=3). (F) Assessment of mitochondrial content by immunoblotting citrate synthase protein in whole liver homogenate (n=3–4). Data are mean ± SEM. *P < 0.05, **P < 0.01, ***P < 0.001, 2-way ANOVA, with (B and C) or without (A) Bonferroni post-test, or 2-tailed unpaired Student's t test (D and E).

mitochondrial biogenesis, their lack of induction was indicative of stable mitochondrial content. mtDNA content was unchanged (Figure A.1D), in support of unaltered mitochondrial mass. Because the activity of citrate synthase proved indistinguishable in isolated mitochondria (Figure A.1E), its activity in whole-liver homogenate permitted biochemical assessment of mitochondrial content. In agreement with genetic data, the activity and protein level for citrate synthase were unchanged (Figure A.1E and F), indicative of stable mitochondrial content regardless of feeding status. Hence, induction of *Pgc1a* was not associated with altered mitochondrial content in fasted liver. As previously reported in other systems (259, 260), these data imply that a certain threshold effect of PGC-1α coactivator activity is necessary to induce mitochondrial biogenesis.

Next, we sought to understand which nutrient signaling pathway influences mitochondrially encoded gene expression. Broadly, the fasting response is notable for a decline in insulin and an increase in glucagon, the latter of which activates intracellular cAMP signaling. Using cultured primary hepatocytes, we evaluated these possibilities. Withdrawal of insulin had no effect on the fasting-responsive genes *Pepck* and *G6p* or on mitochondrially encoded genes (Figure A.2A and C). As reported by others, glucagon induced both *Pepck* and *G6p* (Figure A.2C). Interestingly, mitochondrially encoded genes were also induced, while many nuclear encoded ETC genes were unaffected (Figure A.2A and B). Forskolin, which increases intracellular cAMP levels, induced mitochondrially encoded genes as well (Figure A.S1A and B), which indicates that the cAMP pathway governed by glucagon is likely responsible. Even in *Pgc1a* null primary hepatocytes, glucagon was still sufficient to induce mitochondrially

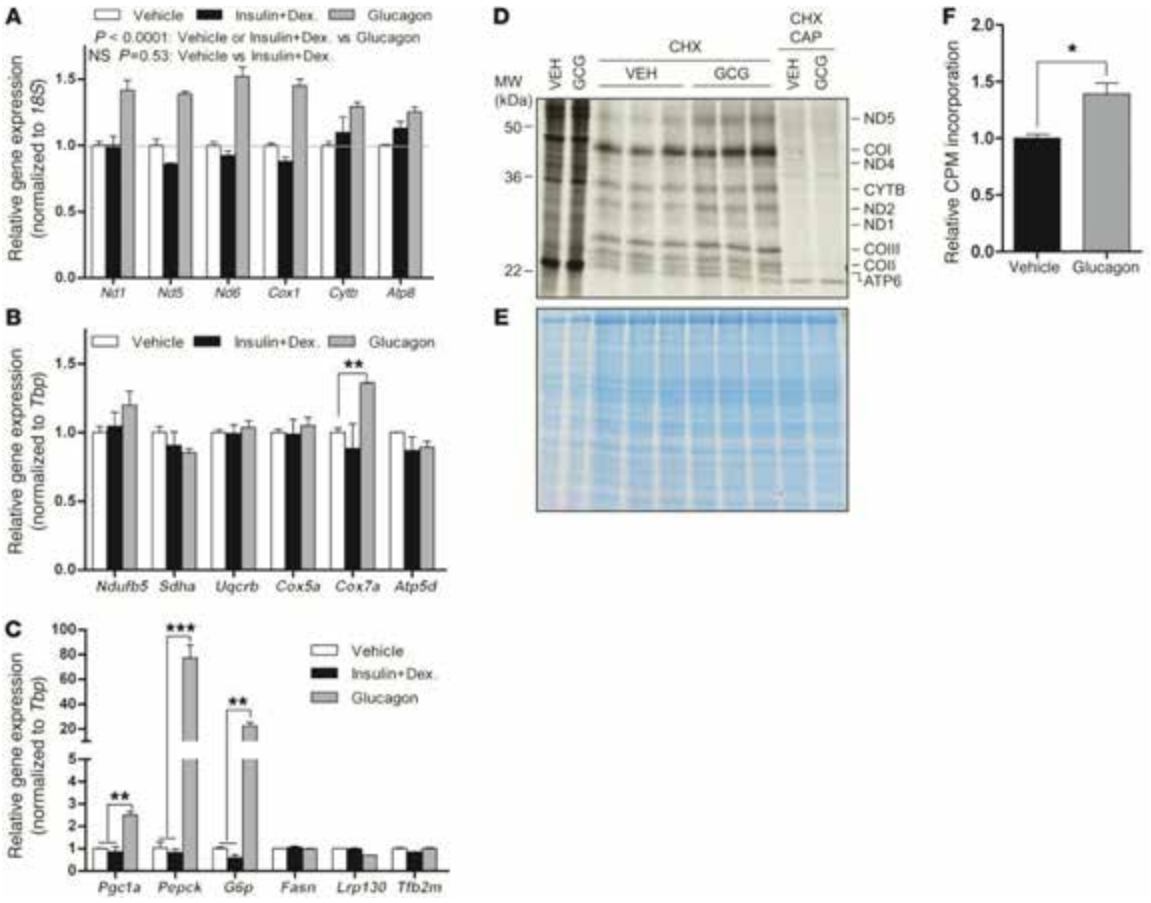

Figure A.2. Glucagon induces mitochondrially encoded genes and proteins. (A) Neither insulin/dexamethasone (Insulin+Dex) nor their withdrawal (Vehicle) had an effect on mitochondrially encoded gene expression; however, glucagon induced mitochondrially encoded gene expression. (B) Effect of glucagon on several nuclear encoded ETC subunits. (C) Effect of glucagon on fasting-responsive genes and regulators of mitochondrial content and function. (D) [^{35}S]-methionine labeling of cytoplasmic proteins (left 2 lanes) and mitochondrially encoded translation products, which were evident after inhibition of cytoplasmic translation with cycloheximide (CHX) (middle 6 lanes). Consistent with mitochondrial translation products, chloramphenicol (CAP) blocked their translation (right 2 lanes). GCG, glucagon. (E) Coomassie brilliant blue staining of the [^{35}S]-labeled gel, showing equal protein loading. (F) Quantification of mitochondrially encoded [^{35}S]-labeled proteins by scintillation courting (n = 3). Data are mean ± SEM. **P < 0.01, ***P < 0.001, 2-way ANOVA, with (B and C) or without (A) Bonferroni post-test, or 2-tailed unpaired Student's t test (F).

encoded genes, although the response was modestly blunted (Figure A.S1C and D). These data further support the observation that de novo biogenesis is not required. Induction of mitochondrially encoded genes was accompanied by an increase in mitochondrially encoded proteins (Figure A.2D–F). Even so, in both primary mouse hepatocytes and mouse liver, gene expression was largely unchanged for several nuclear encoded ETC subunits (Figure A.2B and Figure A.3A). Several nuclear encoded ETC proteins, however, were increased in fasting liver mitochondria (Figure A.3B and C), which indicates that they were modestly stabilized (or more efficiently translated) in the fasted state. Overall, these data are suggestive of a coordinated response that facilitates enhanced OXPHOS. Importantly, mitochondrially encoded proteins, which are central to the process, are regulated at the level of gene expression.

Finally, we used a different mouse strain to test the generality of the response. Similar to C57BL/6 mice, mitochondrially encoded genes were increased in 129S mice (Figure A.S2), although the induction of *Pepck*, *G6p* and other genes was less robust. Similar to C57BL/6 mice, induction of mitochondrially encoded genes in 129S mice was not attributable to alterations in mitochondrial content (Figure A.S2). These observations indicated that the fasting response is accompanied by increases in mitochondrially encoded transcripts and OXPHOS, independent of de novo mitochondrial biogenesis. Given that increased mitochondrially encoded gene expression enhances OXPHOS (126), these data might imply that induction of mitochondrially encoded genes in cooperation with nuclear encoded subunits increases the capacity for OXPHOS in fasted liver.

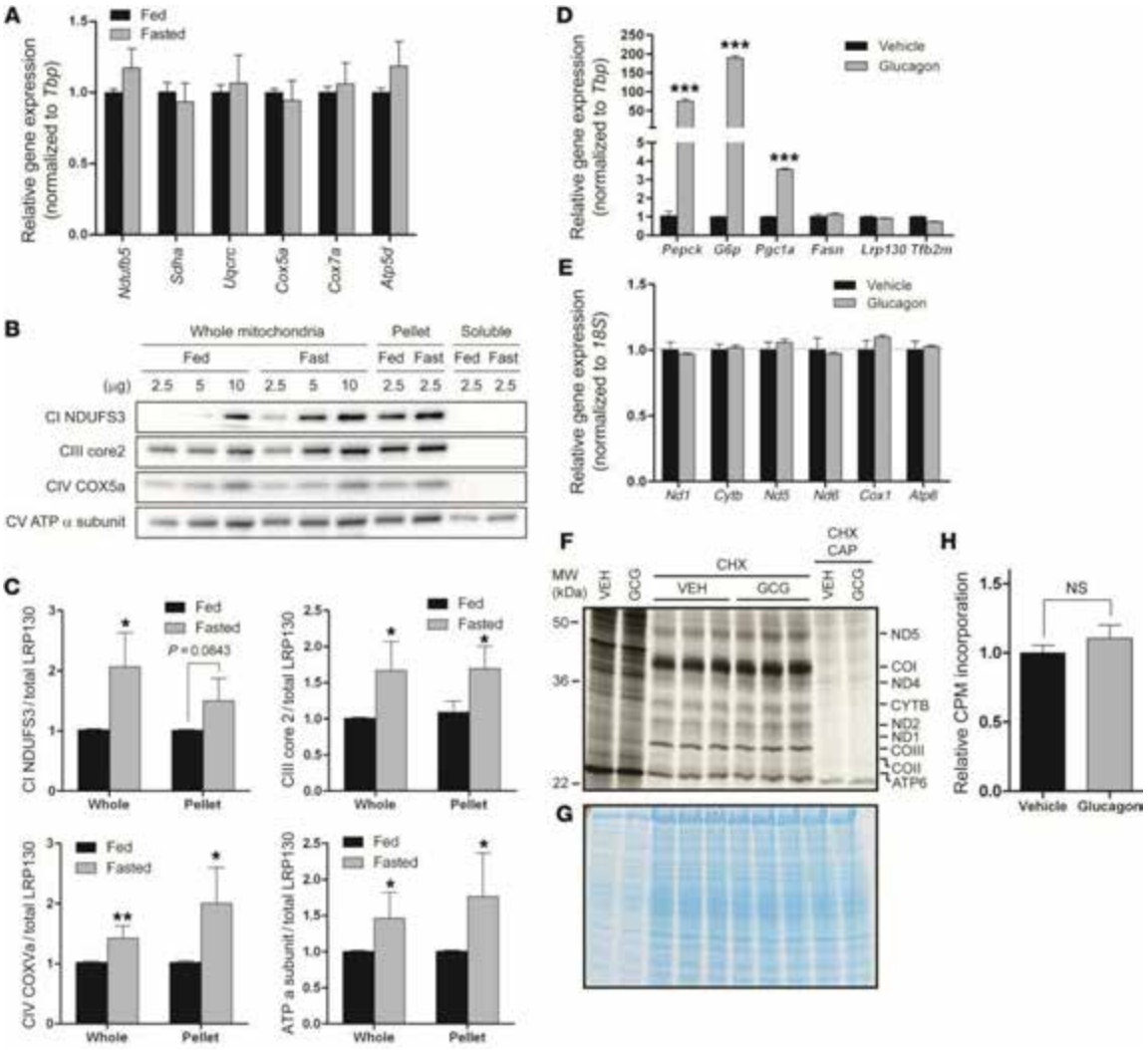

Figure A.3. Glucagon-mediated induction of mitochondrially encoded genes requires SIRT3. (A) Fasted mouse liver showed no change in gene expression for several nuclear encoded ETC genes (n=3–4). (B) Representative immunoblot of several nuclear encoded ETC subunits. Freshly isolated mitochondria were alkaline extracted with carbonate buffer, permitting assessment of the membrane fraction (Pellet) or soluble fraction. (C) Quantification of the several nuclear encoded ETC subunits (n=3–4). (D–H) In Sirt3 knockout primary hepatocytes, glucagon-mediated induction of fasting-responsive genes was unaltered (D); however, induction of mitochondrially encoded gene expression was completely abrogated (E; n=3) and no longer accompanied by increased mitochondrially encoded translation products (F and H). (G) Coomassie brilliant blue staining of [^{35}S]-labeled gel, showing equal protein loading. Similar results were obtained

using nicotinamide (Figure A.S1E and F). Data are mean ± SEM, except in C (mean ± SD). *P < 0.05, **P < 0.01, ***P < 0.001, 2-way ANOVA with Bonferroni post-test (A, D, and E) or 2-tailed unpaired Student's t test (C and H).

SIRT3 is necessary and sufficient for fasting-mediated induction of mitochondrially encoded transcripts and OXPHOS

By sensing the level of cellular NAD^+, sirtuins are important sensors of nutrient deprivation. To globally assess this, we treated primary hepatocytes with nicotinamide, which inhibits NAD^+-dependent sirtuin activity, and evaluated the response to glucagon. Nicotinamide had no effect on the fasting-responsive genes *Pepck* and *G6p* (Figure A.S1E). In contrast, nicotinamide abrogated induction of mitochondrially encoded genes (Figure A.S1F), which suggests that a NAD^+-dependent pathway is necessary for their induction. These data indicate that a NAD^+-dependent pathway, possibly via a sirtuin, mediates induction of mitochondrially encoded genes in the fasted response. SIRT3 protein is a sensor of nutrient deprivation that is induced in fasted liver mitochondria (234, 261). Moreover, prior studies in cell lines indicate that it influences cellular respiration (236-238); thus, SIRT3 might coordinate changes in energy metabolism with the fasted response. For these reasons, SIRT3 protein was an attractive candidate in the control of mitochondrially encoded gene expression and concomitant OXPHOS in fasted liver. We therefore challenged *Sirt3* KO primary hepatocytes with glucagon. Similar to nicotinamide-treated primary hepatocytes, glucagon stimulated several fasting-responsive genes in the *Sirt3* KO primary hepatocytes, but failed to induce mitochondrially encoded gene expression or mitochondrially encoded translation products (Figure A.3D–H).

Given that SIRT3 is implicated in energy metabolism in cell lines and is induced in fasted liver, we evaluated the fasting response in *Sirt3* KO mouse liver. Neither mitochondrially encoded transcripts nor OXPHOS were induced in fasted *Sirt3* KO liver,

despite a slight increase in mitochondrial content (Figure A.4A–F). Again, there was no change in nuclear encoded ETC subunits (Figure A.S3). Additionally, we depleted SIRT3 in C57BL/6 mouse liver using shRNA targeting *Sirt3* (Figure A.S4A). Again, both mitochondrially encoded gene expression and induction of OXPHOS were impaired, independent of mitochondrial content (Figure A.S4). Moreover, SIRT3 knockdown did not influence the general fasting response, as these mice proved indistinguishable from wild-type C57BL/6 mice (compare Figure A.1B and Figure A.S4D). These findings in 2 mouse models of SIRT3 deficiency argue that SIRT3 is required for induction of mitochondrially encoded transcripts and OXPHOS in fasted liver.

Next, we evaluated whether SIRT3 is sufficient to induce mitochondrially encoded gene expression. SIRT3 was ectopically expressed in mouse liver using adenovirus encoding *Sirt3* (Figure A.S5A–E). To minimize hormonal influences and genetic variations due to feeding status, food was briefly removed for 3 hours to clear the gastrointestinal tract of residual food. Brief food deprivation did not alter mitochondrially encoded transcripts or SIRT3 protein (data not shown), the latter of which is induced only after a longer fast (234). Even in the absence of potent fasting cues, ectopic expression of SIRT3 modestly induced mitochondrially encoded gene expression.

Induction of mitochondrially encoded genes was not associated with alterations in mitochondrial content (Figure A.S5D and E). This action proved cell autonomous, as mitochondrially encoded gene expression was also induced in H2.35 murine hepatoma cells stably expressing SIRT3 as well as in primary hepatocytes transduced for 36 hours with *Sirt3* adenovirus (Figure A.4G–L, and Figure A.S5F and G). Unlike primary

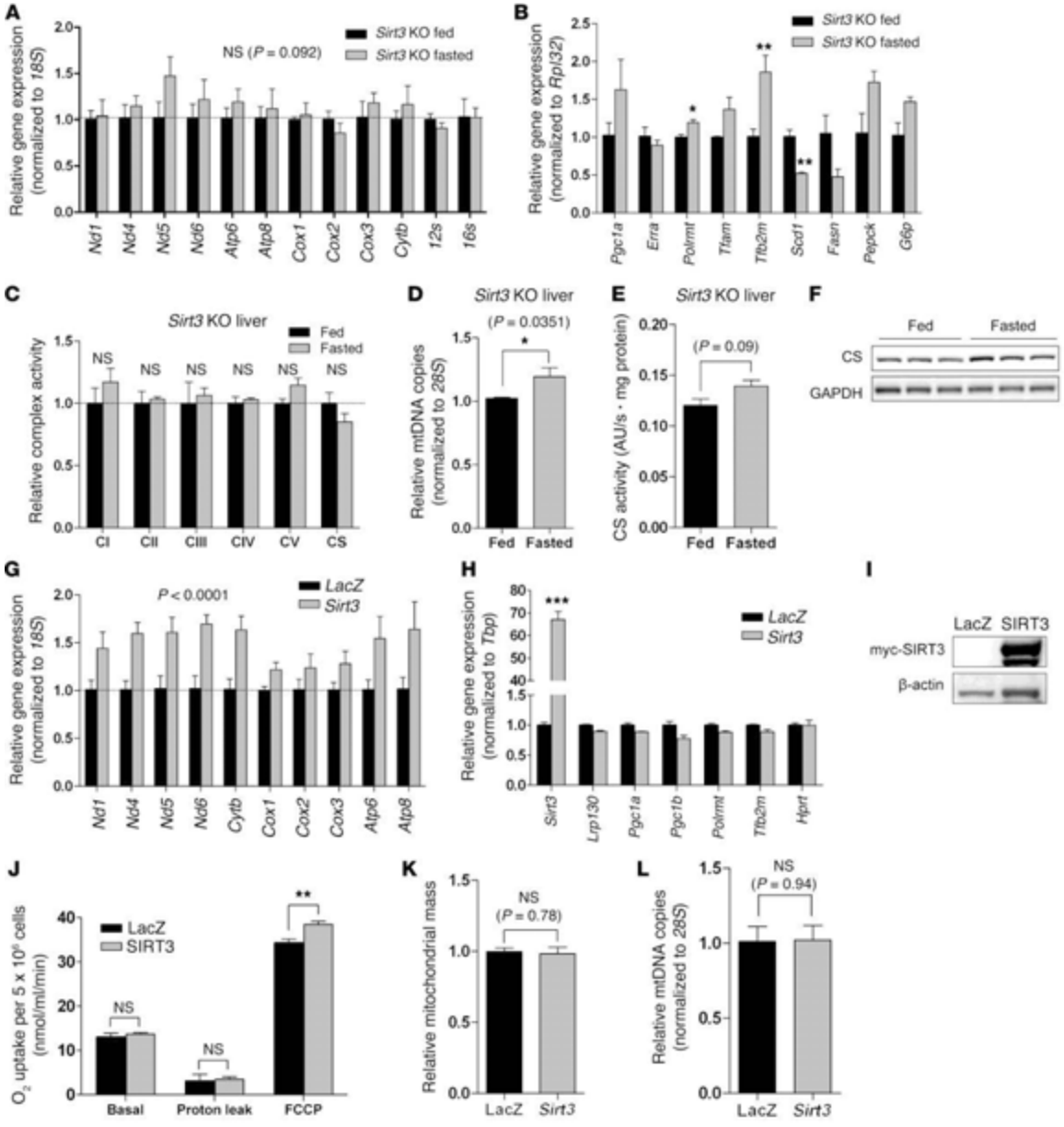

Figure A.4. In liver, SIRT3 is necessary and sufficient for fasting-mediated induction of mitochondrial encoded transcripts and OXPHOS. (A) Hepatic gene expression of mitochondrially encoded transcripts in 24-hour fasted Sirt3 KO mice (129S background) (n=3). (B) Expression of genes that regulate mitochondrial biogenesis, mitochondrial transcription, lipogenesis, and gluconeogenesis in Sirt3 KO liver (n=3). (C) Complex activity from liver of 24-hour fasted or fed Sirt3 KO mice (n=3). (D) Genetic assessment of mitochondrial content using mtDNA content (n=3). (E)

Biochemical assessment of mitochondrial content using citrate synthase activity in whole liver homogenate (n = 3). (F) Assessment of mitochondrial content by immunoblotting citrate synthase protein in whole liver homogenate (n=3). (G and H) Expression of (G) mitochondrially encoded transcripts and (H) genes that regulate mitochondrial biogenesis and mitochondrial transcription in H2.35 hepatoma cells stably expressing LacZ or SIRT3 (n=3). (I) Immunoblot showing expression of ectopically expressed myc-tagged SIRT3 protein. (J) Using a Clark-type oxygen electrode, cellular respiration — basal, proton leak, and maximal respiration (FCCP) — was assessed in H2.35 hepatoma cells stably expressing LacZ or SIRT3. (n=4). See Figure A.S6 for representative oxygen consumption curves. (K) Fluorescent assessment of mitochondrial content using MitoTracker Green FM (n=3). (L) Genetic assessment of mitochondrial content using mtDNA content (n=3). Data are mean ± SEM. *P < 0.05, **P < 0.01, ***P < 0.001, 2-way ANOVA, with (A and G) or without (B and H) Bonferroni post-test, or 2-tailed unpaired Student's t test (C–E and J–L).

hepatocytes, H2.35 hepatoma cells stably transduced with SIRT3 required supplementation with 500 μM NAD^+, a cofactor for SIRT3. Even though mechanisms involving NAD^+ uptake by mitochondria remain controversial, extracellular NAD^+ does increase the concentration of NAD^+ within mitochondria (262, 263). To make fair comparisons, LacZ H2.35 control cells were treated likewise.

Next, we evaluated OXPHOS in H2.35 cells stably expressing SIRT3. In cells replete with SIRT3, maximal cellular respiration was modestly induced about 12%, while basal respiration and proton leak were unchanged (Figure A.4J). Increased respiratory capacity was independent of de novo mitochondrial biogenesis (Figure A.4K and L). Using galactose, a fuel in which very little ATP is derived from glycolysis, maximal cellular respiration was increased about 37% (Figure A.S6). These data imply that, after a bout of fasting, induction of SIRT3 is both necessary and sufficient for the induction of mitochondrially encoded transcripts and OXPHOS.

SIRT3 activates mitochondrial transcription and promotes OXPHOS via LRP130

Induction of mitochondrially encoded transcripts stimulates OXPHOS (12). Mitochondrially encoded gene expression is the summation of transcription and degradation. Presumably, SIRT3 influenced one or both of these pathways. Transcription and RNA degradation can be assessed by metabolic labeling, using pulse and pulse-chase experiments, respectively (Figure A.5A). To assess mitochondrial transcription, we pulse-labeled cells with 4-thiouridine (4sU), a naturally occurring analog of UTP. After isolating RNA, 4sU-labeled transcripts were biotinylated, recovered on streptavidin

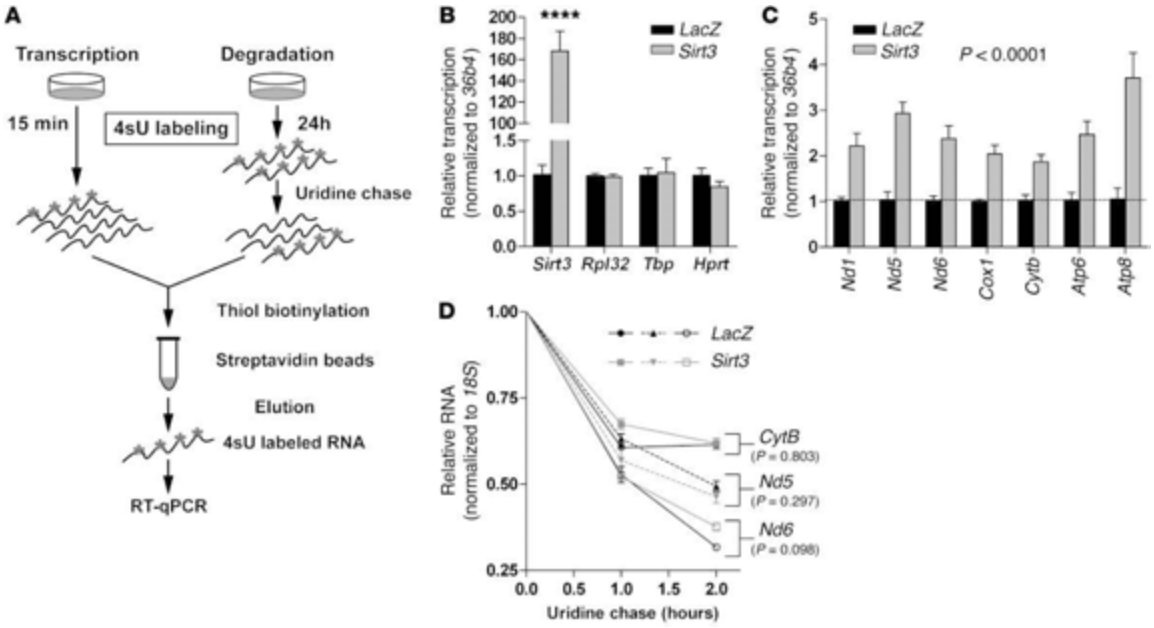

Figure A.5. SIRT3 induces mitochondrially encoded genes by stimulating mitochondrial transcription. (A) Metabolic labeling with 4sU. This method quantifies de novo transcripts, permitting assessment of mitochondrial transcription in whole cells. It can also be used to monitor transcript degradation. (B) Transcription of Sirt3, driven by the viral CMV promoter, was induced in cells replete with SIRT3, whereas transcription of several housekeeping genes was unchanged (n=3). (C) Cells stably expressing SIRT3 exhibited increased mitochondrial transcription (n=3). (D) Uridine was used to chase the 4sU label and assess transcript half-life. Half-lives of mitochondrial transcripts in H2.35 hepatoma cells stably expressing SIRT3 were unchanged. Data are mean ± SEM. ****P < 0.0001, 2-way ANOVA, with (B) or without (C) Bonferroni post-test.

beads, and quantified by quantitative PCR (qPCR). Because labeling is brief and much shorter than the half-life of most mitochondrially encoded transcripts, this method allows for quantitative assessment of transcription (253, 264, 265). Driven by a powerful CMV promoter, *Sirt3* mRNA served as a positive control for transcription (Figure A.5B). Several housekeeping genes were unchanged (Figure A.5B), indicative of specific transcription. Ectopic expression of SIRT3 induced mitochondrial transcription, but failed to influence transcript degradation (Figure A.5C and D). Akin to transcription in the nucleus, these data support the general observation that changes in gene expression are largely driven by transcription (264). Overall, these data indicate that SIRT3 induces mitochondrially encoded gene expression by stimulating mitochondrial transcription. Given that mitochondrial mass and mtDNA content were stable (Figure A.4 and Figure A.S5), induction by SIRT3 signified increased transcription per mitochondrial genome.

Next, we explored the mechanism by which SIRT3 influences mitochondrial transcription and OXPHOS. Independent of de novo mitochondrial biogenesis, it was previously reported that LRP130 interacts with POLRMT, culminating in enhanced mitochondrial transcription and attendant OXPHOS (126). We therefore wondered whether SIRT3 activates mitochondrial transcription and OXPHOS via LRP130. To test this, we ectopically expressed SIRT3 in cells deficient for LRP130. Using a previously validated RNAi (123, 126, 160), LRP130 knockdown in H2.35 cells was greater than 85% at the mRNA and protein levels (Figure A.6A and B). As previously reported (123, 126, 160), mitochondrially encoded transcripts were globally attenuated in LRP130-deficient cells, whereas genes involved in mitochondrial biogenesis and mitochondrial

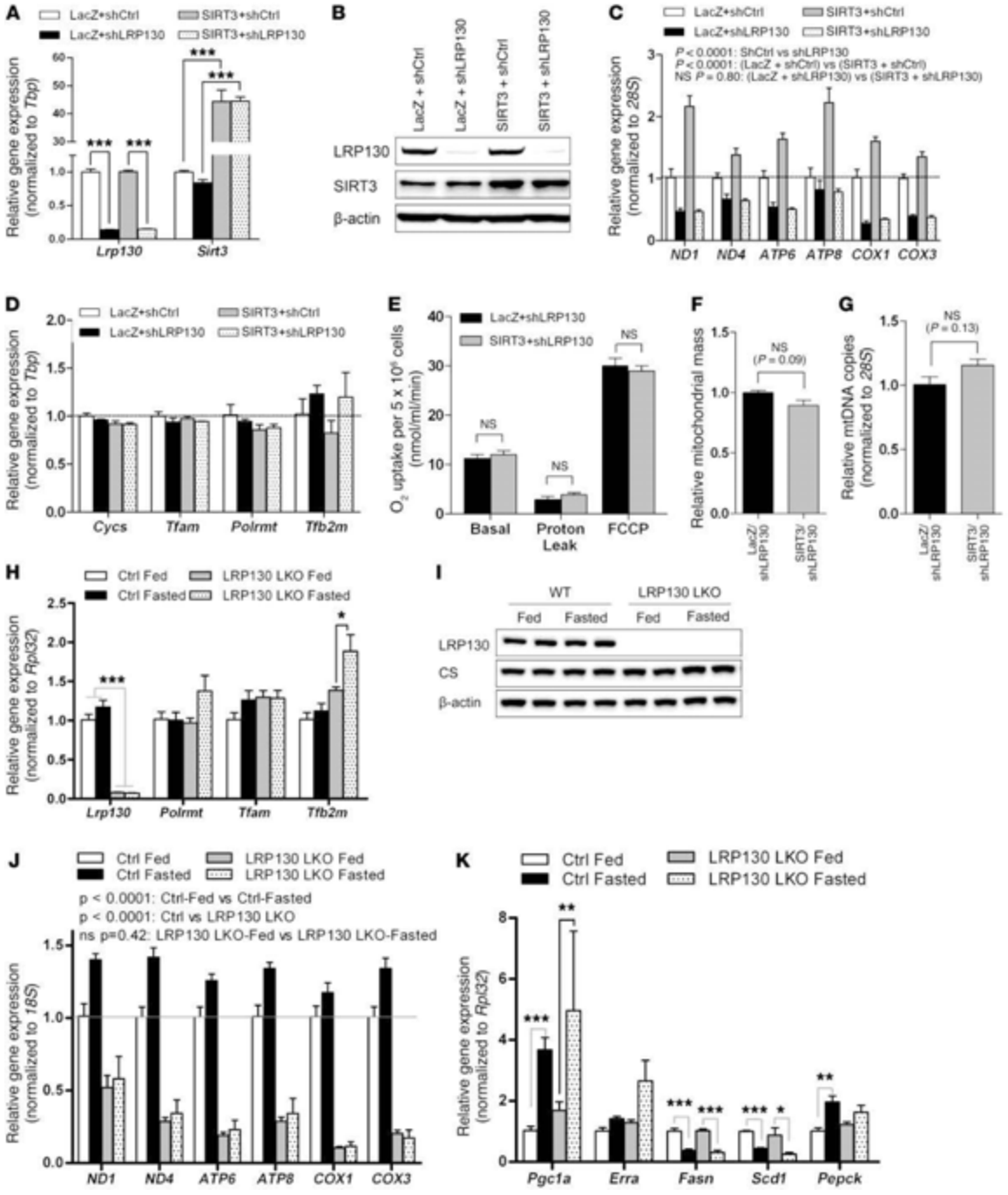

Figure A.6. SIRT3-mediated induction of mitochondrial transcription requires LRP130. (A–D) Gene expression of Lrp130 and Sirt3 (A), representative immunoblot of LRP130 and SIRT3 (B), gene expression of mitochondrially encoded transcripts (C), and expression of genes that regulate mitochondrial biogenesis and mitochondrial

transcription (D) in H2.35 hepatoma cells replete with LacZ or SIRT3, superimposed with control (shCtrl) or Lrp130 knockdown (shLRP130) (n=3). (E–G) H2.35 hepatoma cells replete with SIRT3 or LacZ, but deficient for LRP130, were used. (E) SIRT3 was no longer sufficient to influence maximal respiration, using a Clark-type oxygen electrode (n = 6). However, control shRNA SIRT3 cells retained increased respiratory capacity (see Figure A.S6). Assessment of mitochondrial content was unchanged, as assessed by (F) MitoTracker Green FM or (G) mtDNA content (n=3). (H–K) LRP130 liver-specific knockout (LRP130 LKO) mice were used. Hepatic gene (H) and protein (I) expression (n=4). (J) Effect of fasting on mitochondrially encoded genes in liver. (K) Effect of fasting on fasting-responsive genes in liver. Data are mean ± SEM. *P < 0.05, **P < 0.01, ***P < 0.001, 2-way ANOVA, with (A, D, H, and K) or without (C and J) Bonferroni post-test, or 2-tailed unpaired Student's t test (E–G).

transcription were unchanged (Figure A.6C and D). In cells deficient for LRP130, ectopically expressed SIRT3 failed to induce either mitochondrially encoded transcripts or OXPHOS (Figure A.6C and E). In contrast, OXPHOS was increased in control shRNA LacZ cells replete with SIRT3 protein (Figure A.S6), an induction similar to that shown in Figure A.4J. Effects on mitochondrial transcription and energy metabolism were not caused by altered mitochondrial content, as genetic and fluorescent markers of mitochondrial content were unperturbed (Figure A.6F and G). Finally, effects on mitochondrial transcription and energy metabolism were not caused by perturbation of TFB2M or POLRMT, which collectively comprise the basal transcription machinery. Specifically, cells deficient or replete with LRP130 protein did not alter POLRMT or TFB2M protein levels (Figure A.S7A and B).

Next, we fasted mice in which *Lrp130* was ablated in liver. To achieve liver-specific deletion of *Lrp130* in adult mice, animals harboring floxed *Lrp130* alleles were injected via tail vein with adeno-associated virus containing a vector coding for liver-specific cre recombinase (AAV-Cre), yielding liver-specific LRP130 KO mice (referred to herein as LRP130 LKO mice; Figure A.6H and I). After a 24-hour fast, mitochondrially encoded genes were induced in wild-type mice, but not LRP130 LKO mice (Figure A.6J), which indicates that LRP130 is required for induction of mitochondrially encoded genes in fasted liver. As previously reported, mitochondrially encoded gene expression was globally decreased in LRP130 LKO liver (Figure A.6J). Details of the $Lrp130^{flox/flox}$ allele are shown in Figure A.S7C. We additionally ectopically expressed SIRT3 in *Lrp130* KO primary hepatocytes. The ability of SIRT3 to induce

mitochondrially encoded genes was abrogated in *Lrp130* KO hepatocytes (Figure A.S8). Finally, we evaluated fatty acid in H2.35 cells stably expressing SIRT3 but deficient for LRP130, since fatty acid oxidation depends on OXPHOS. Antimycin A (which inhibits electron transfer and, hence, OXPHOS) served as a positive control. In the absence of LRP130, fatty acid oxidation was significantly impaired (Figure A.S8), which suggests that LRP130 is required for fatty acid oxidation. In summary, SIRT3 activated mitochondrial transcription and increased OXPHOS. This action was dependent on LRP130, a regulator of mitochondrial transcription and OXPHOS.

SIRT3 deacetylates LRP130 in fasted liver and increases its transcriptional activity

Given that nutrient deprivation induces mitochondrial SIRT3, we evaluated whether SIRT3 influences acetylation of LRP130 protein in fasted liver mitochondria. Compared with fed liver, LRP130 was deacetylated in fasted liver mitochondria, a state in which SIRT3 activity (and protein) was increased (Figure A.7A). Supporting regulation by SIRT3, LRP130 was hyperacetylated in SIRT3-deficient mouse liver (Figure A.7B). In accordance with cell-autonomous control, NAD^+ promoted deacetylation of LRP130 in H2.35 cells replete with SIRT3 (Figure A.7C). Buttressing these data, LRP130 coimmunoprecipitated with SIRT3 (Figure A.7D), but failed to immunoprecipitate with SIRT5 (data not shown), another — albeit less potent — deacetylase localized to mitochondria. To assess a functional interaction, we evaluated whether SIRT3 deacetylates purified LRP130 protein. Since mitochondrial acetylases have not been characterized, we used CREB-binding protein (CBP) to acetylate purified

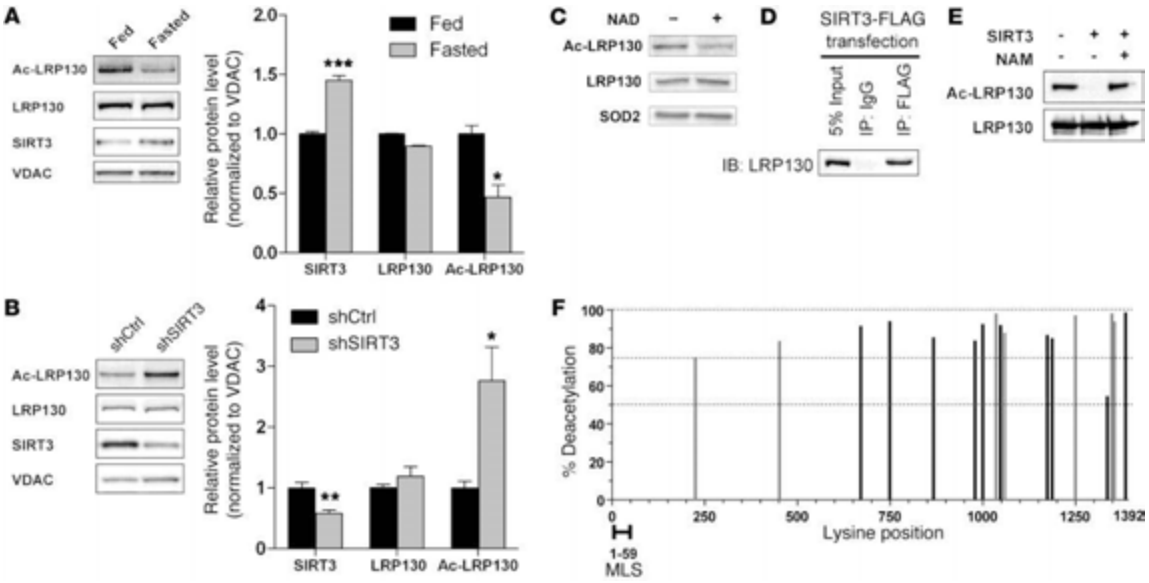

Figure A.7. During the fasted response, SIRT3 deacetylates LRP130 in liver mitochondria. (A) Representative immunoblot and protein quantification showing reduced acetylation of LRP130 (Ac-LRP130) in mitochondria isolated from fasted mouse liver (n=3 experiments). (B) Immunoblot and protein quantification showing hyperacetylation of LRP130 in mitochondria isolated from liver deficient for SIRT3 (n = 4). (C) Immunoblot showing deacetylation of LRP130 in H2.35 cells stably expressing SIRT3 upon treatment with 500 μM NAD^+. (D) SIRT3 and LRP130 coimmunoprecipitated, using ectopically expressed SIRT3-FLAG protein and endogenous LRP130. (E) Using purified proteins, SIRT3 robustly deacetylated the C terminus of LRP130. Deacetylation of LRP130 was inhibited by 12.5 mM nicotinamide (NAM). Shown is 1 representative of 4 independent experiments. Similar, but less robust, deacetylation was obtained for the N terminus of LRP130 (not shown). (F) Acetylated LRP130 fragments were incubated with control buffer or purified SIRT3 protein, then subjected to mass spectrometry. Lysines showing greater than 50% deacetylation by SIRT3 are graphed (gray and black bars). Percent deacetylation was calculated as 1 – (SIRT3 signal/control signal). 7 lysines were mutated to arginines (gray bars), generating LRP130-7KR, which mimics deacetylated protein. Data are mean ± SEM. *P < 0.05, **P < 0.01, ***P < 0.001, 2-tailed unpaired Student's t test (A and B).

LRP130 protein, an approach that is standard in the field (266, 267). In the presence of purified SIRT3 protein, acetylated LRP130 C-terminal protein was robustly deacetylated by SIRT3 (Figure A.7E). Similar, but less robust, results were obtained using N-terminal fragments of LRP130 (data not shown). Collectively, these data argue that SIRT3 deacetylates LRP130 in fasted liver. Finally, the conclusion that LRP130 is a bona fide target of SIRT3 was buttressed by a review of proteomic analyses (268-270), in which SIRT3 was found to be deficient in either cells or mouse liver (Figure A.S9).

Next, we used mass spectrometry to map 17 lysine residues of LRP130 sensitive to deacetylation by SIRT3 (Figure A.7F and Table A.S1). Sites with greater than 2-fold change were deemed positive. The mass spectrometry signal from the control reaction containing acetylated LRP130 protein was divided into the signal from the SIRT3 reaction. This ratio was subtracted from 1, yielding the arbitrary metric of percent deacetylation.

To evaluate the genetic and functional implications of LRP130 protein acetylation, we mutated 7 of 17 acetylated lysines to arginine (referred to herein as LRP130-7KR; Figure A.7F and Table A.S1). By mutating a lysine to an arginine, a mutated site retains its positive charge and functionally mimics deacetylated protein. Similarly, we generated a 7KQ mutant of LRP130 (LRP130-7KQ). Mutating a lysine to glutamine retains a neutral charge at the site and often mimics acetylated protein. 2 groups previously reported that LRP130 stimulates mitochondrial transcription (126, 271). In cell lysates, LRP130 interacted with both TFB2M and POLRMT (126), both of which comprise the basal transcription machinery of mitochondria (243). We therefore

reasoned that the acetylation status of LRP130 might influence its interaction with TFB2M and/or POLRMT. Because POLRMT and LRP130 migrate at similar molecular weights, we refined the level of interaction to aas 340–710 of POLRMT (Figure A.S10). This enabled us to use a 1–710 aa fragment of POLRMT, which is easily distinguished from LRP130. We evaluated whether LRP130-7KR (which mimics deacetylated protein) differentially interacts with either TFB2M or the 1–710 aa fragment of POLRMT. Compared with murine LRP130-WT, LRP130-7KR preferentially interacted with POLRMT, whereas differential binding of TFB2M was less apparent (Figure A.8A and B).

Next, we evaluated whether LRP130-7KR and LRP130-7KQ exhibited differential activity. We transiently expressed LRP130-WT or the murine LRP130 mutants in 293T cells deficient for endogenous human LRP130. We used this strategy to mitigate competition with endogenous LRP130 and to evaluate activity using physiologically relevant levels of LRP130 protein. Although human and mouse LRP130 share more than 75% homology at the protein level, the shRNA targeting human *LRP130* mRNA does not target mouse *Lrp130* mRNA. Knockdown of human LRP130 in 293T cells and reconstitution with murine LRP130 is shown in Figures A.S11 and A.S12. Endogenous SIRT3 activity was inhibited using 10 mM nicotinamide, a dose previously shown to impair NAD^+-dependent sirtuin activity in 293T cells. Compared with LRP130-WT, LRP130-7KR exhibited greater activity, as assessed by mitochondrial gene expression, mitochondrial transcription, and oxygen consumption (Figure A.8C, D, and F). The level of ectopically expressed LRP130 protein was comparable (Figure A.8E).

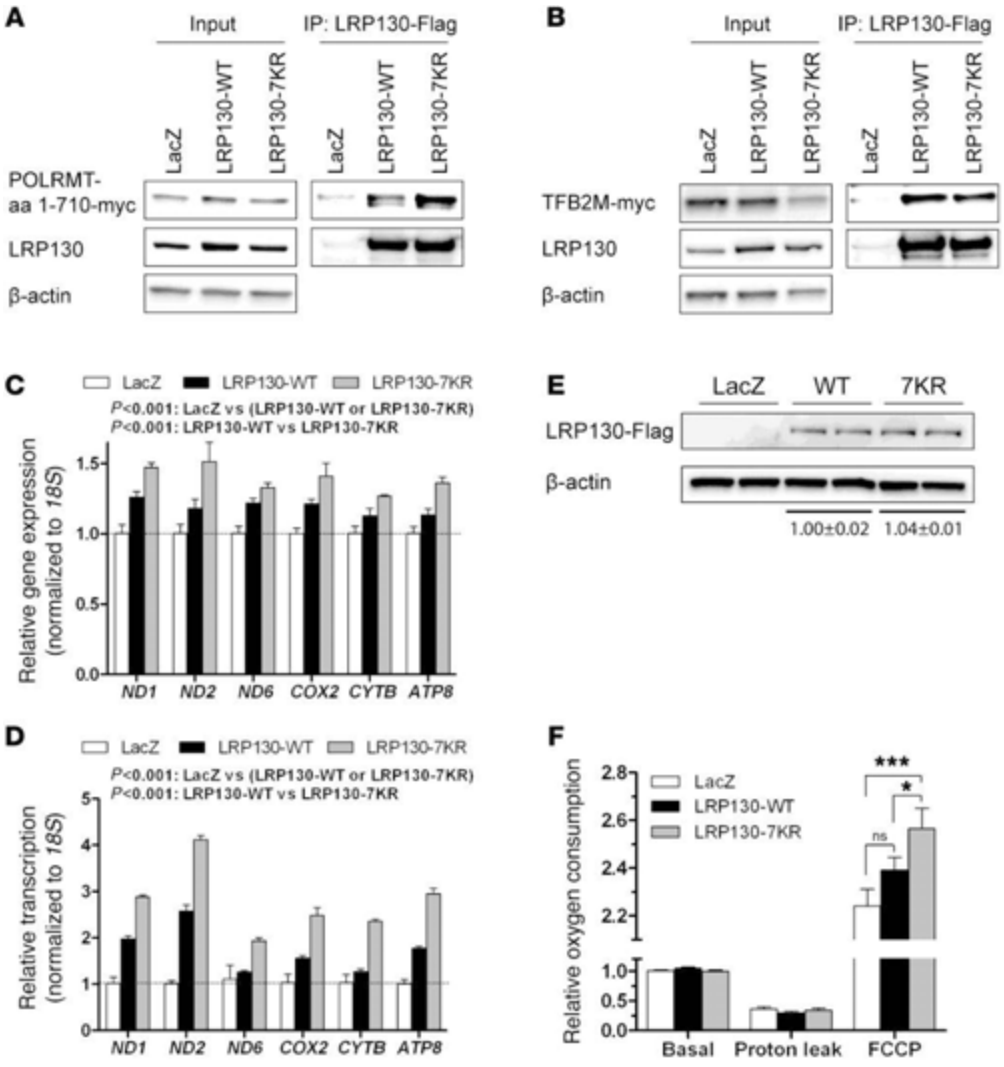

Figure A.8. LRP130-7KR stimulates mitochondrial transcription and promotes OXPHOS. (A) LRP130-7KR, which mimics deacetylated protein, showed increased affinity for aas 1–710 of POLRMT, a fragment that contains the catalytic domain. See Figure A.S10 for more detailed mapping. (B) In contrast, compared with LRP130-WT, LRP130-7KR showed no differential affinity for TFB2M. (C, D, and F) Using 293T cells, endogenous human LRP130 was knocked down >95%, then reconstituted with murine LRP130-WT or LRP130-7KR (see Figure A.S11). The shRNA targeting human LRP130 does not target mouse Lrp130 (not shown). Endogenous NAD^+-dependent sirtuin activity was inhibited with 10 mM nicotinamide for 16 hours. LRP130-7KR had greater (C) mitochondrially encoded gene expression (n=3), (D) mitochondrial transcription (n=3), and (F) maximal respiration (n=5) versus LRP130-WT. (E)

Immunoblot showing similar levels of ectopically expressed LRP130-WT and LRP130-7KR. See Figure A.S11 for total LRP130 protein. Data are mean ± SEM. *P < 0.05, ***P < 0.001, 2-way ANOVA (C and D) or 2-tailed unpaired Student's t test (F).

Interestingly, the effect on transcription was much greater than that on respiration, indicative of either a saturation effect or limitations of our experimental system. In contrast, LRP130-7KQ did not increase mitochondrially encoded gene expression (Figure A.S12), which suggests that deacetylation of LRP130 (as reflected by LRP130-7KR) increases its activity. Since SIRT3-dependent pathways were inhibited by nicotinamide, in terms of mitochondrial transcription and OXPHOS, these data indicate that LRP130 is a crucial mediator of SIRT3 action. Taken together, our results imply that deacetylation of LRP130 by SIRT3 enhances the activity of LRP130, which in turn stimulates mitochondrial transcription and OXPHOS.

In summary, we have identified a mechanism whereby nutrient sensing by SIRT3 induces mitochondrial transcription and enhances OXPHOS via LRP130 (Figure A.9). Moreover, our present findings indicate that SIRT3 coordinates activation of enzyme systems involved in fatty acid oxidation as well as OXPHOS. In fasted liver, our data support a model whereby activation of mitochondrial transcription increases OXPHOS capacity, and this enhanced bioenergetic efficiency would be predicted to support increased substrate oxidation.

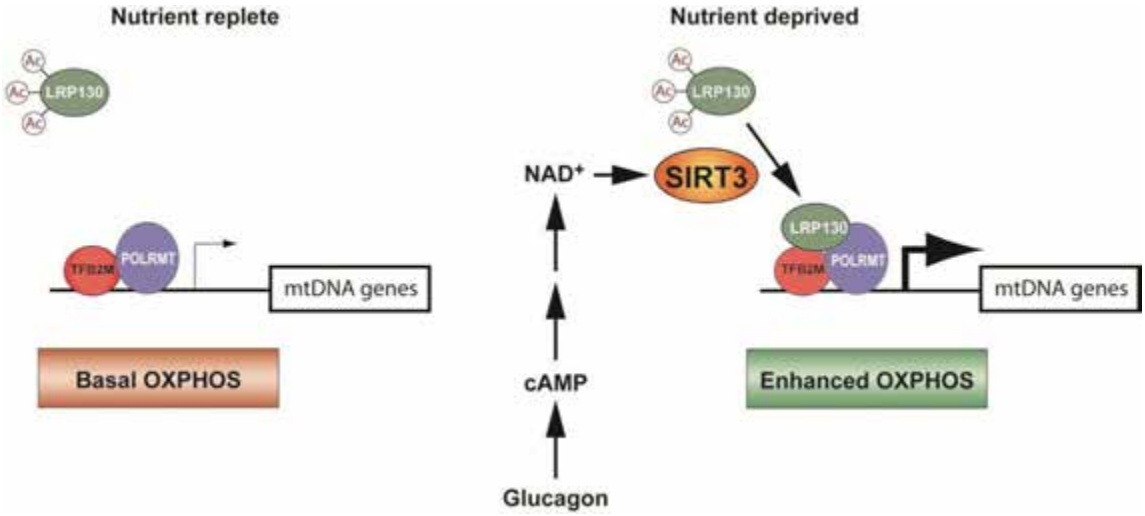

Figure A.9. In fasted liver, the transcription machinery of mitochondria sense nutrient deprivation via SIRT3, culminating in enhanced energy metabolism. In liver, SIRT3 is induced by nutrient deprivation. Specifically, glucagon, which activates cAMP signaling, increases SIRT3 activity, perhaps by indirectly increasing mitochondrial NAD^+ levels. LRP130 is then deacetylated and activated by SIRT3, which strengthens the LRP130-POLRMT interaction. This culminates in increased mitochondrial transcription and attendant OXPHOS. Presumably, processes dependent on OXPHOS — fatty acid oxidation, gluconeogenesis, ketogenesis, and ureagenesis — are augmented by increased respiratory capacity. To simplify the model, deacetylation of enzymes involved in fatty acid oxidation and ketogenesis, as well as SIRT3 action on individual OXPHOS subunits, are not illustrated.

Discussion

Here, we identified an unanticipated link between nutrient sensing and mitochondrial transcription that was critical for fasting-mediated induction of OXPHOS. In fasted liver, ATP synthesis is accompanied by a 20% increase in oxygen consumption (272, 273), enabling ATP-dependent processes such as gluconeogenesis and ureagenesis. While increases in nutrient flux and oxidation are essential, OXPHOS capacity is critical factor as well. We showed here that SIRT3 deacetylated LRP130 during the fasted response. Once deacetylated, LRP130 stimulated mitochondrial transcription to increase mitochondrially encoded gene expression and OPXHOS, independent of de novo mitochondrial biogenesis. In fasted liver, SIRT3 protein has previously been shown to plateau at 18–24 hours and activate enzyme systems involved in fatty acid oxidation, culminating in greater β-oxidation of fatty acids (234). At 24 hours, we observed SIRT3-mediated deacetylation of LRP130. We therefore propose that SIRT3 couples enhanced β-oxidation of fatty acids to increase OXPHOS capacity via LRP130. Presumably, this strategy permits metabolic matching between 2 enzyme systems that are linked by coenzyme cycling: shuttling of NAD^+ and NADH between fatty oxidative pathways and OXPHOS.

Governed by SIRT3 and LRP130, nutrient control of OXPHOS via mitochondrial transcription is a simple, yet elegant, model. Regarding control of OXPHOS, prior studies on SIRT3 implicated modifications of various subunits of the electron transport chain or alterations in mitochondrial content. In SIRT3-deficient cell lines, respiration is impaired and there is hyperacetylation of several respiratory complexes, including complex I (236,

239), succinate dehydrogenase (238), and complexes III and V (239). The stabilization of several nuclear encoded subunits may be related to their acetylation status, which might explain the differential regulation of complex activity previously reported by others (236). One limitation to interpreting these studies is that mutant subunits that mimic acetylated or deacetylated protein were not evaluated. It is therefore difficult to discern the functional relevance of these modifications.

In liver, the salutary actions of SIRT3 on OXPHOS do not require an increase in mitochondrial content. This is in contrast to immortalized, brown fat–like HIB1B cells, in which ectopic expression of SIRT3 was associated with increased *Pgc1a*, mitochondrial biogenesis, and concomitant OXPHOS (186). Using mouse models and cell culture, we did not observe changes in mitochondrial mass due to SIRT3, which suggests that the effect of SIRT3 on mitochondrial mass is restricted to certain cellular contexts. Notably, our results indicate a prominent role for SIRT3 in mitochondrial transcription, which promotes OXPHOS. Ectopic expression of SIRT3 in cells deficient for LRP130 protein failed to induce OXPHOS or mitochondrially encoded genes. Similarly, in liver deficient for LRP130, fasting failed to induce mitochondrially encoded gene expression. These data suggest that mechanisms independent of LRP130 are either trivial or operate downstream of mitochondrial transcription. For instance, in LRP130-deficient cells, reduction of mitochondrially encoded genes is associated with reduced OXPHOS subunits (123, 126, 133, 160), attenuation that might offset deacetylation of individual OXPHOS subunits. If normal mitochondrially encoded gene expression is a prerequisite for SIRT3-mediated activation of individual OXPHOS subunits, then ablation of LRP130

would abrogate any downstream effect. Additionally, LRP130 might influence factors involved in mitochondrial transcription. In our studies, neither POLRMT nor TFB2M, which comprise the initiation complex, were unchanged. Even so, we cannot exclude the possibility that other factors involved in transcription are not secondarily perturbed. Nevertheless, LRP130-deficient cells still retained some OXPHOS complexes, albeit less than those of wild-type cells. If activation of individual OXPHOS subunits were a predominant action of SIRT3, one would anticipate some enhancement of OXPHOS even in the absence of LRP130, a finding we failed to observe. Additionally, SIRT3 regulates several hundred mitochondrial proteins. Indeed, in other cellular systems, variegated actions of SIRT3 are not readily intuitive (274); hence, without further investigation, our findings predominantly relate to the fasted response. Nonetheless, even when NAD^+-dependent sirtuins were pharmacologically inhibited, LRP130-7KR had greater activity in terms of transcription and OXPHOS capacity. This indicates that isolated deacetylation of LRP130 is sufficient to stimulate mitochondrial transcription and OXPHOS. Although we cannot exclude direct effects of acetylation on OXPHOS complexes per se, our data highlight a significant pathway involving mitochondrial transcription and attendant OXPHOS mediated by SIRT3 and LRP130.

Our results indicate that SIRT3 influences mitochondrial transcription via LRP130. In concert with prior reports by us and others (126, 271), these data further support a role for LRP130 in the control of mitochondrial transcription. Some studies have reported that LRP130 stabilizes mitochondrial transcripts; however, such a role for LRP130 in SIRT3-mediated control of mitochondrial gene expression was not supported

here. As stated earlier, the LRP130-7KR mutant increased mitochondrially encoded transcripts, even when endogenous SIRT3 was inhibited. This suggests that deacetylation of basal mitochondrial transcription is not strictly required. Thus far, no differential acetylation has been reported for POLRMT or TFB2M, which collectively constitute the initiation complex. While our results suggest that deacetylation of LRP130 is sufficient to stimulate mitochondrial transcription and attendant OXPHOS, we cannot definitely exclude parallel deacetylation and activation of the basal transcription machinery. TFAM, a regulator of both mitochondrial transcription and replication, is acetylated in cells and mouse liver (269, 275), which is dependent on SIRT3 (269). After caloric restriction, there is a slight decrease in acetylation of TFAM; however, the functional and biological significance of this slight change is unknown, as an acetylation mutant was not evaluated (269). Although interesting and important, evaluating the basal transcription machinery in the context of biology will prove challenging, since ablation of its components completely interdicts OXPHOS, while in our study, ectopic expression of either TFB2M or POLRMT paradoxically attenuated mitochondrially encoded gene expression. This implies a finely tuned balance, limiting the tools and approaches available to decipher mechanisms. In terms of mitochondrially encoded gene expression, ablation of LRP130 still permitted some basal transcription, while its ectopic expression induced transcription. We therefore believe LRP130 is uniquely poised to specifically evaluate mitochondrial transcription and OXPHOS.

What are the broader questions pertinent to integrative physiology and disease? An increasing number of reports suggest that a mismatch between nutrient flux and

oxidative capacity promotes and/or exacerbates insulin resistance (230-232). In human and mouse studies, increased fatty acid flux in the setting of impaired tricarboxylic acid and/or OXPHOS activity is associated with insulin resistance (230, 232, 276, 277). SIRT3 activity is impaired in mice fed a high-fat diet for 16–24 weeks that develop insulin resistance (278). Additionally, ablation of SIRT3 leads to metabolic syndrome (239, 240), suggestive of a causal role. Although the notion is speculative, a decline in SIRT3 activity might lead to impaired OXPHOS in liver and exacerbate insulin resistance. One additional question to consider is whether pathways involved in OXPHOS and fatty acid oxidation exhibit differential sensitivity to SIRT3 activity, which might produce a mismatch between fatty acid oxidation and OXPHOS.

In conclusion, induction of SIRT3 by fasting induced OXPHOS by increasing mitochondrial gene expression. Upon deacetylation by SIRT3, LRP130 induced mitochondrial transcription, culminating in greater OXPHOS capacity. We hypothesize that greater OXPHOS capacity improves mitochondrial bioenergetic efficiency, thereby supporting parallel and downstream biochemical pathways.

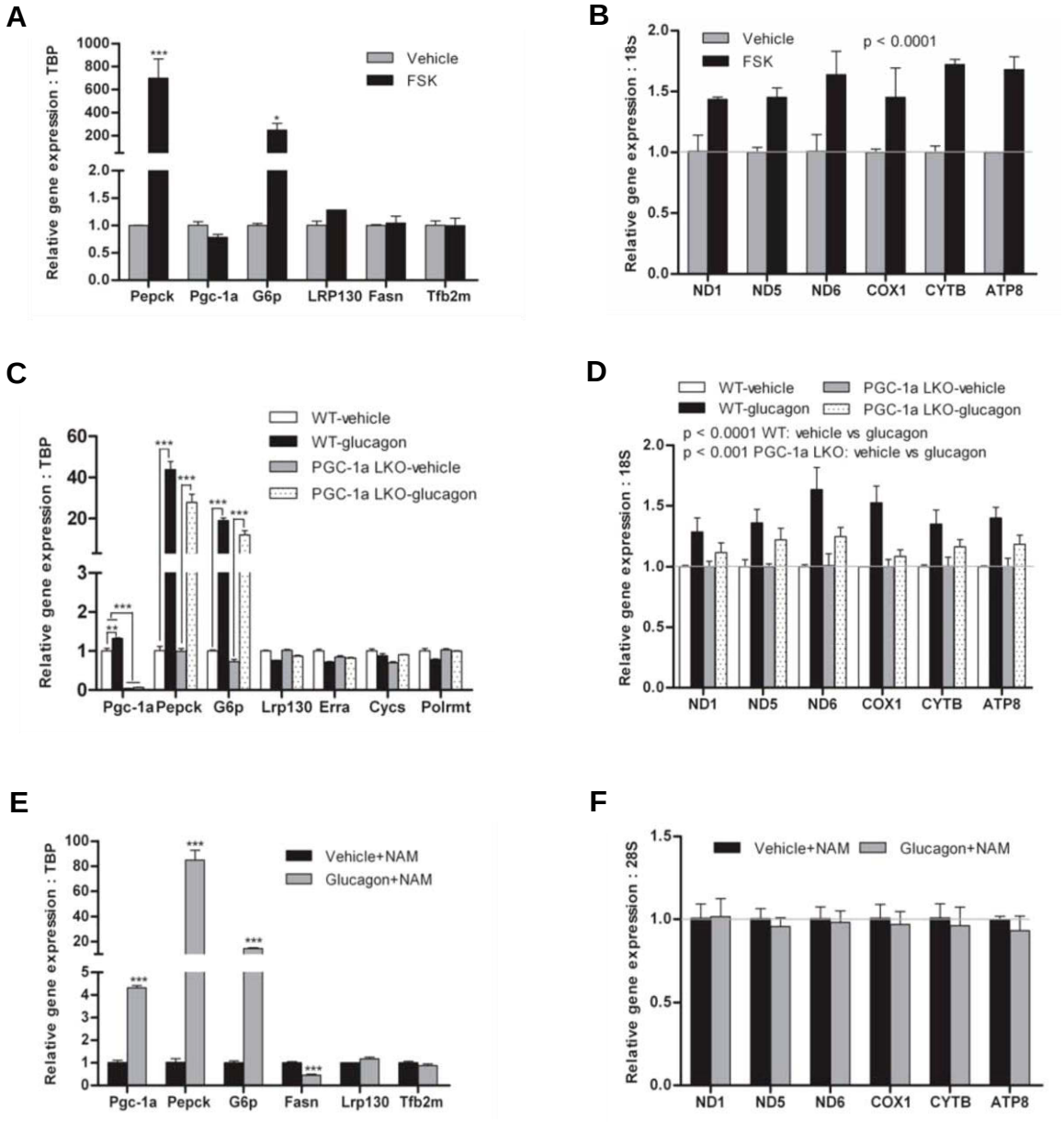

Figure A.S1. cAMP signaling mediates induction of mitochondrially encoded genes, Pgc-1α is not required for induction of mitochondrially encoded gene expression but NAD$^+$-dependent pathways are required. A) Following an 18 hour treatment with forskolin, which increases intra-cellular cAMP levels, Pepck and G6p, both of which are fasting responsive genes, were induced in primary hepatocytes. B) Treatment of primary hepatocytes with forskolin also induced mitochondrially encoded gene expression. C) In Pgc-1α null hepatocytes, glucagon induces fasting responsive genes similar to wild-type

cells. D) In Pgc-1α null hepatocytes, glucagon still induces mitochondrially encoded gene expression; but, the induction is modestly blunted. Note: induction of mitochondrially encoded gene expression by forskolin was normal in primary hepatocytes in which Pgc-1α was knocked down more than 75% (data not shown). E) Nicotinamide (NAM; an inhibitor of NAD^+)-dependent pathways did not alter glucagon mediated induction of fasting responsive genes; however, F) induction of mitochondrially encoded gene expression was completely abrogated (n=3). 2-way ANOVA for all studies. For nuclear encoded genes, a Bonferroni post test was also performed. *$p<0.05$, **$p<0.01$, ***$p<0.001$ (n=3).

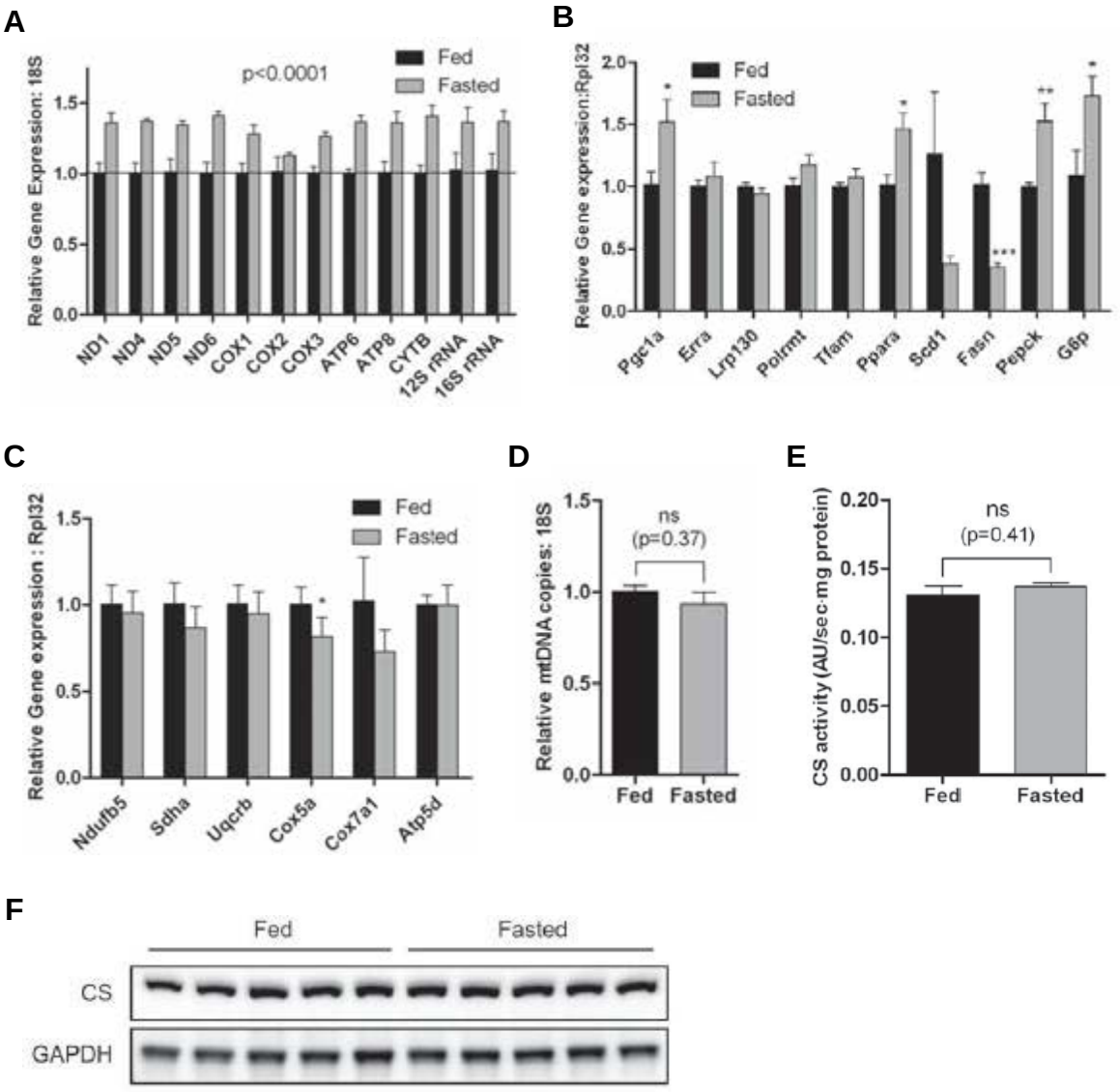

Figure A.S2. Fasting induces mitochondrially encoded genes in 129S mice. (A) Hepatic gene expression of mitochondrially encoded transcripts in 129S mice fasted for 24 hours (n=5). (B) Expression of genes that regulate mitochondrial biogenesis, mitochondrial transcription, lipogenesis and gluconeogenesis (n=5). (C) Expression of several nuclear encoded ETC genes. (D) Genetic assessment of mitochondrial content using mitochondrial DNA content (n=5). (E) Biochemical assessment of mitochondrial content using citrate synthase (CS) activity in whole liver homogenate (n=5). (F) Assessment of mitochondrial content using citrate synthase (CS) protein in whole liver homogenate (n=5). For gene expression, 2-way ANOVA with Bonferroni post test where indicated. (mean+s.e.m, *p<0.05, **p<0.01, ***p<0.001).

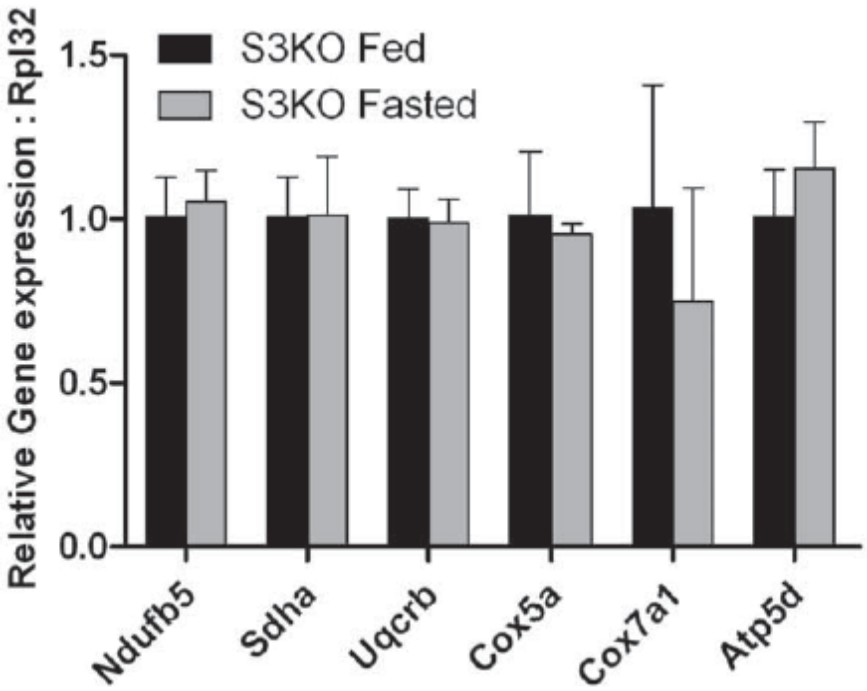

Figure A.S3. Effect of fasting in Sirtuin 3 knockout mouse liver (S3KO) on a 129S mice background. Gene expression of several nuclear encoded mitochondrially encoded genes in sirtuin 3 knockout mouse liver (S3KO) in the fed or fasted state (n=3). For gene expression, 2-way ANOVA with Bonferroni post test (p=ns for all comparisons). Error bars represent mean±s.e.m.

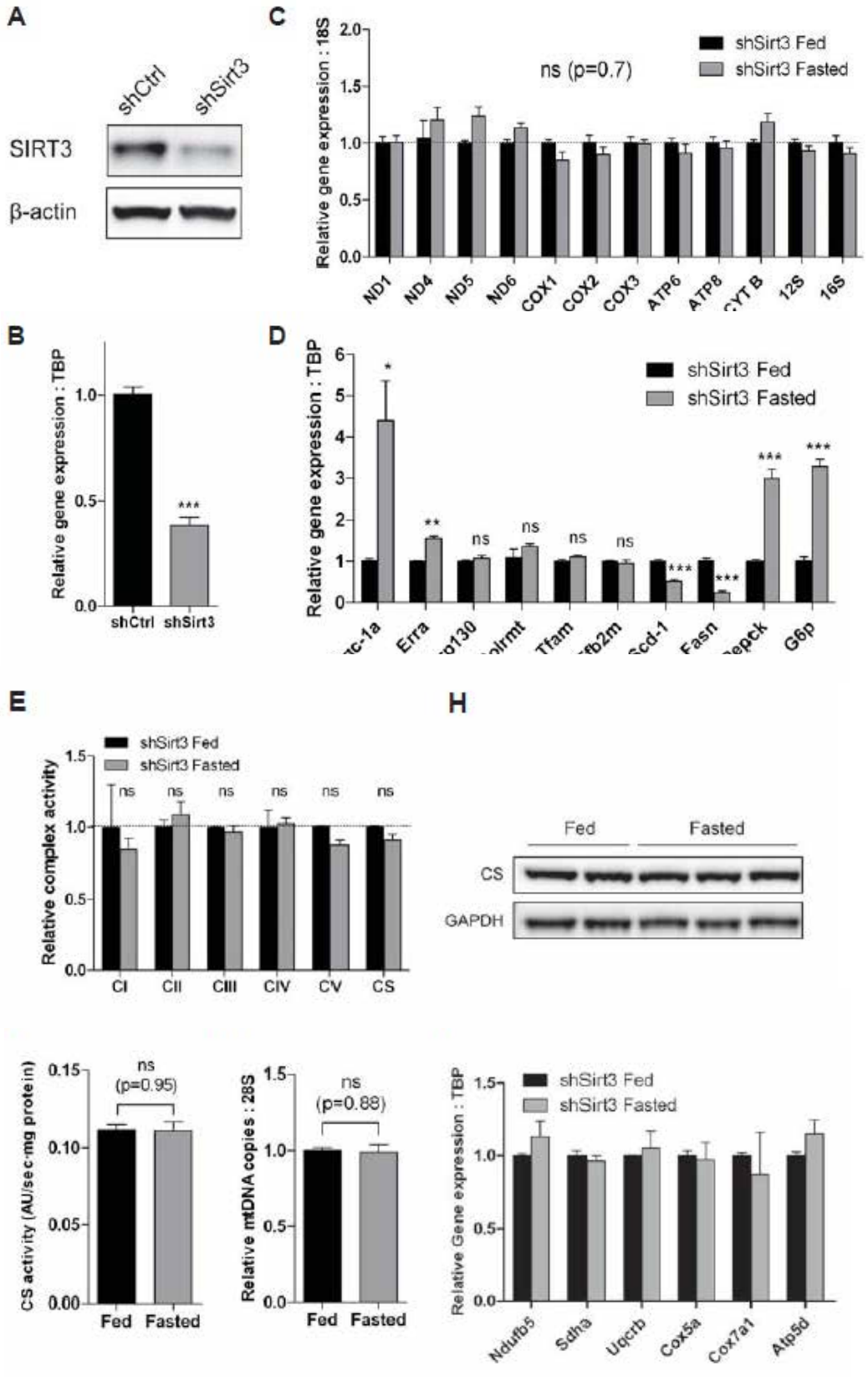
A
shCtrl
shSirt3
SIRT3
β-actin
B
Relative gene expression : TBP
shCtrl
shSirt3
C
Relative gene expression : 18S
ns (p=0.7)
shSirt3 Fed
shSirt3 Fasted
ND1
ND4
ND5
ND6
COX1
COX2
COX3
ATP6
ATP8
CYT B
12S
16S
D
Relative gene expression : TBP
shSirt3 Fed
shSirt3 Fasted
Erra
Tfam
Fasn
G6p
E
Relative complex activity
shSirt3 Fed
shSirt3 Fasted
CI
CII
CIII
CIV
CV
CS
H
Fed
Fasted
CS
GAPDH
CS activity (AU/sec·mg protein)
ns
(p=0.95)
Fed
Fasted
Relative mtDNA copies : 28S
ns
(p=0.88)
Fed
Fasted
Relative Gene expression : TBP
shSirt3 Fed
shSirt3 Fasted
Ndufb5
Sdha
Uqcrb
Cox5a
Cox7a1
Atp5d

Figure A.S4. In liver, knockdown of *Sirt3* in C57BL6 mouse liver impairs fasting-mediated induction of mitochondrially encoded genes and OXPHOS. (A) Protein expression in *Sirt3* deficient mouse liver. *Sirt3* knockdown was achieved by tail vein injecting adenovirus encoding shSirt3. Knockdown of SIRT3 protein in liver was confirmed by comparison with a control shRNA (shCtrl) (n=4). (B) Gene expression of *Sirt3* following its knockdown in mouse liver (n=3). (C) Hepatic gene expression of mitochondrially encoded transcripts in liver deficient for SIRT3. Mice were either in the fed state or fasted for 24 hours (n=3). (D) Expression of genes that regulate mitochondrial biogenesis, mitochondrial transcription, lipogenesis and gluconeogenesis in liver deficient for SIRT3 (n=3). (E) Complex activity of mitochondria isolated from shSirt3 mouse liver either in the fed state or after fasting for 24 hours (n=3). CI through CV denotes activities for complexes I through V. CS denotes citrate synthase . (F) Biochemical assessment of mitochondrial content using citrate synthase activity in whole liver homogenate (n=3). (G) Genetic assessment of mitochondrial content using mitochondrial DNA content (n=3). (H) Citrate synthase (CS) immunoblot. (I) Gene expression of several nuclear encoded electron transport chain subunits (n=3). For gene expression, 2-way ANOVA with Bonferroni post test where indicated. For complex activity and mitochondrial content, 2-tailed unpaired Student's t test. (mean+s.e.m, *$p<0.05$, **$p<0.01$, ***$p<0.001$)

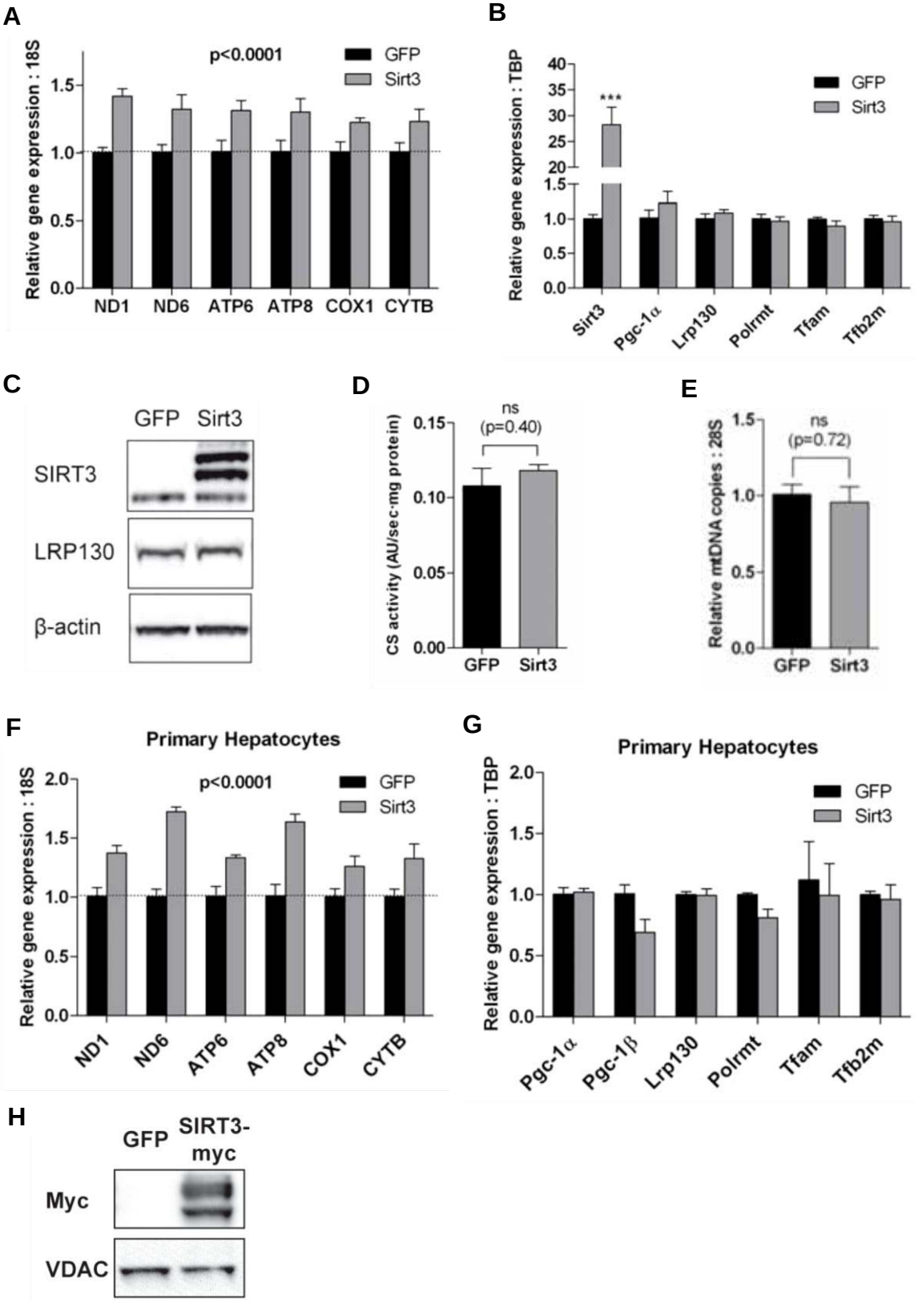
A
p<0.0001
GFP
Sirt3
Relative gene expression : 18S
ND1
ND6
ATP6
ATP8
COX1
CYTB
B
***
Relative gene expression : TBP
Sirt3
Pgc-1α
Lrp130
Polrmt
Tfam
Tfb2m
C
GFP
Sirt3
SIRT3
LRP130
β-actin
D
ns
(p=0.40)
CS activity (AU/sec·mg protein)
E
ns
(p=0.72)
Relative mtDNA copies : 28S
F
Primary Hepatocytes
G
Primary Hepatocytes
Pgc-1β
H
SIRT3-myc
Myc
VDAC

Figure A.S5. Ectopic expression of SIRT3 in mouse liver and primary hepatocytes induces mitochondrially encoded transcripts. (A) Hepatic gene expression of mitochondrially encoded transcripts in mouse liver transduced with adenovirus encoding either GFP or Sirt3 (n=4). (B) Expression of genes that influence mitochondrial biogenesis and mitochondrial transcription (n=4). (C) Immunoblot showing expression of ectopically expressed myc-tagged SIRT3 protein, following transduction of C57BL6 mouse liver with adenovirus. Note, ectopically expressed SIRT3 is myc-tagged, and thus, migrates at a slightly higher molecular weight. (D) Biochemical assessment of mitochondrial content using citrate synthase activity of whole liver homogenate (n=4). (E) Genetic assessment of mitochondrial content using mitochondrial DNA content (n=3). (F) Gene expression of mitochondrially encoded transcripts in primary hepatocytes transduced with adenovirus encoding either GFP or Sirt3 (n=3). (G) Expression of genes that influence mitochondrial biogenesis and mitochondrial transcription in primary hepatocytes (n=3). (H) Immunoblot showing expression of ectopically expressed myc-tagged SIRT3 protein in primary hepatocytes. For gene expression, 2-way ANOVA with Bonferroni post test where indicated. For mitochondrial content, 2-tailed unpaired Student's t test. (mean+s.e.m, ***$p<0.001$).

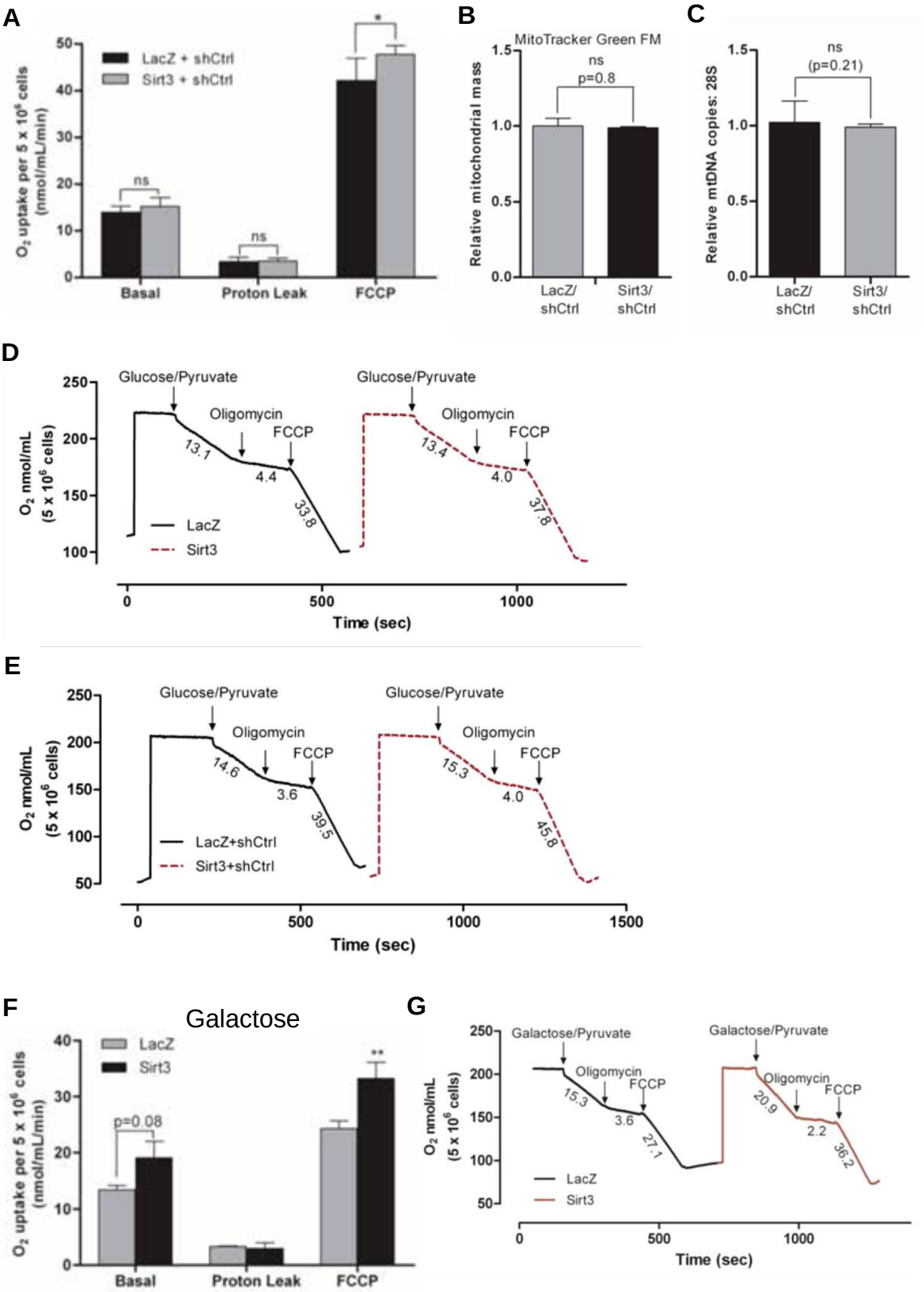
A
LacZ + shCtrl
Sirt3 + shCtrl
O2 uptake per 5 x 10^6 cells (nmol/mL/min)
ns
ns
*
Basal
Proton Leak
FCCP
B
MitoTracker Green FM
ns
p=0.8
Relative mitochondrial mass
LacZ/ shCtrl
Sirt3/ shCtrl
C
ns
(p=0.21)
Relative mtDNA copies; 28S
LacZ/ shCtrl
Sirt3/ shCtrl
D
Glucose/Pyruvate
Oligomycin
FCCP
13.1
4.4
33.8
13.4
4.0
37.8
LacZ
Sirt3
O2 nmol/mL (5 x 10^6 cells)
Time (sec)
E
Glucose/Pyruvate
Oligomycin
FCCP
14.6
3.6
39.5
15.3
4.0
45.8
LacZ+shCtrl
Sirt3+shCtrl
O2 nmol/mL (5 x 10^6 cells)
Time (sec)
F
Galactose
LacZ
Sirt3
p=0.08
**
O2 uptake per 5 x 10^6 cells (nmol/mL/min)
Basal
Proton Leak
FCCP
G
Galactose/Pyruvate
Oligomycin
FCCP
15.3
3.6
27.1
20.9
2.2
36.2
LacZ
Sirt3
O2 nmol/mL (5 x 10^6 cells)
Time (sec)

Figure A.S6. Respiration and mitochondrial content in H2.35 hepatoma cells with ectopic expression of *Sirt3*. (A) Cellular respiration in shControl H2.35 hepatoma cells replete with sirtuin 3 (Sirt3). 2-tailed unpaired Student's t test. (n=3-4, mean±std, *p < 0.05). (B) MitoTracker Green, a measure of mitochondrial biogenesis, was assessed in H2.35 hepatoma cells replete with sirtuin 3 (Sirt3) that co-express shControl RNA (shCtrl). (n=3, mean±s.e.m.). (C) Mitochondrial DNA content, a measure of mitochondrial content, was quantified in H2.35 hepatoma cells replete with sirtuin 3 (Sirt3) that co-express shControl RNA (shCtrl). 2-tailed unpaired Student's t test. (mean±s.e.m, *p<0.05). Representative oxygen consumption curves for (D) H2.35 heptoma cells expressing LacZ or Sirt3 as shown in Figure 3J and (E) those that co-express shControl RNA (shCtrl) as shown here in Fig. S6A. (F) Cellular respiration using galactose in H2.35 hepatoma cells that ectopically express LacZ or sirtuin 3 (Sirt3). 2-tailed unpaired Student's t test. (n=3-4, mean±std, *p < 0.05). Two hours prior to cell collection, medium was changed to galactose containing medium. Respiration was performed as described in materials and methods but galactose was used in *in lieu* of glucose. (G) Representative oxygen consumption curves for galactose respiration studies.

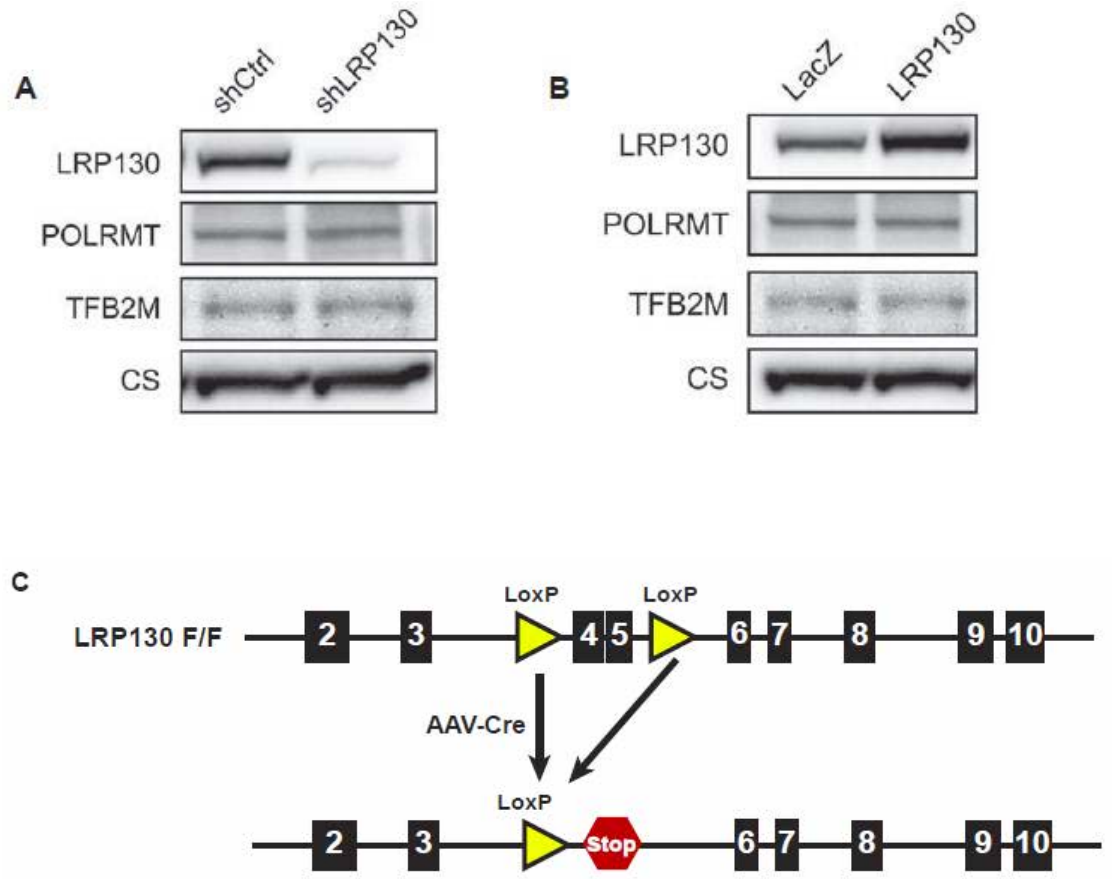

Figure A.S7. Effect of LRP130 protein level on the basal transcription machinery and a schematic of the LRP130 floxed allele. (A) Immunoblot of mitochondria isolated from H2.35 hepatoma cells, showing that deficiency of LRP130 does not alter the level of POLRMT or TFB2M protein. (B) Immunoblot of mitochondria isolated from H2.35 hepatoma cells, showing that ectopic expression of LRP130 does not alter the level of POLRMT or TFB2M protein. (C) Schematic of the floxed allele in LRP130 flox/flox (F/F) mice. To generate LRP130 liver-specific KO mice (LRP130 LKO), liver specific adeno-associated virus that expresses Cre recombinase (AAV-Cre) was tail vein injected into adult male LRP130 flox/flox mice of 8-12 weeks of age. Littermate control male wild-type mice were also injected with AAV-Cre.1 x 10(11) GC viral particles were tail vein injected per mouse. After 3 weeks, liver was harvested in either the fed or fasted state (Fig. 5H-K).

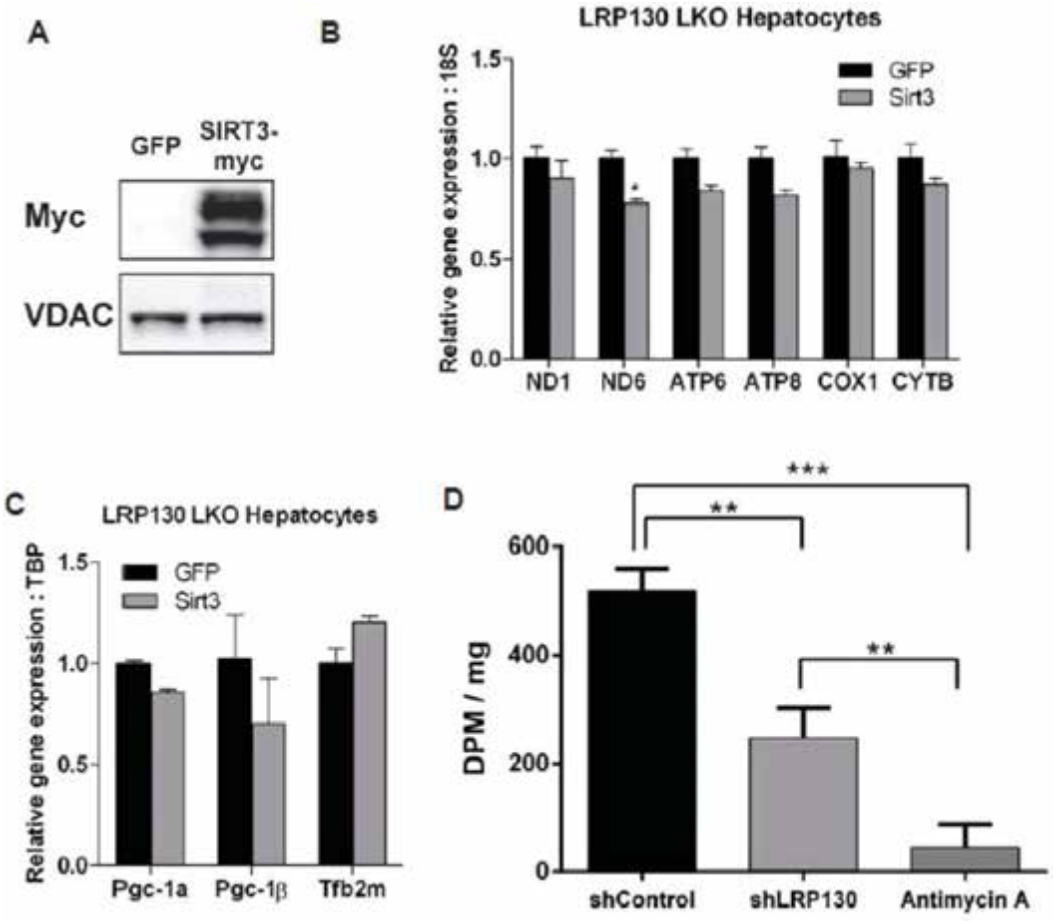

Figure A.S8: Effect of ectopic expression of SIRT3 in LRP130 deficient cells. (A) Immunoblot showing expression of ectopically expressed myc-tagged SIRT3 protein in LRP130 KO hepatocytes. (B) Gene expression of mitochondrially encoded transcripts in LRP130 KO hepatocytes transduced with adenovirus encoding either GFP or *Sirt3* (n=4). Note, in LRP130 KO hepatocytes, SIRT3 is no longer sufficient to induce mitochondrially encoded genes. (C) Expression of genes that influence mitochondrial biogenesis and mitochondrial transcription (n=4). D, Fatty acid oxidation of radiolabeled 14C-palmitate to CO2 in H2.35 cells stably expressing sirtuin 3 and treated with NAD^+ as describe in the methods section. Deficiency of LRP130 was associated with reduced fatty acid oxidation. Antimycin A, which inhibits the electron transport chain at complex III, serves as a positive control, showing nearly complete inhibition of fatty acid oxidation (n=3). In cells treated with nicotinamide there was no longer a difference between shControl (shCtrl) and shLRP130 cells (data not shown), suggesting strong interplay between sirtuin 3 and LRP130. 2-way ANOVA with Bonferroni post test where indicated. (mean±s.e.m, *$p<0.05$).

A

	Liu L	Rardin M	Hebert A	Sol E
Liu L	17*†			
Rardin M	2†	8		
Hebert A	3*	3	10	
Sol E	3*†	2	2	11

B

	Liu L	Rardin M	Hebert A	Sol E
Liu L	17			
Rardin M	225, 749	8		
Hebert A	867, 1036, 1048	186, 291, 462	10	
Sol E	749, 867	291, 749	291, 867	11

C

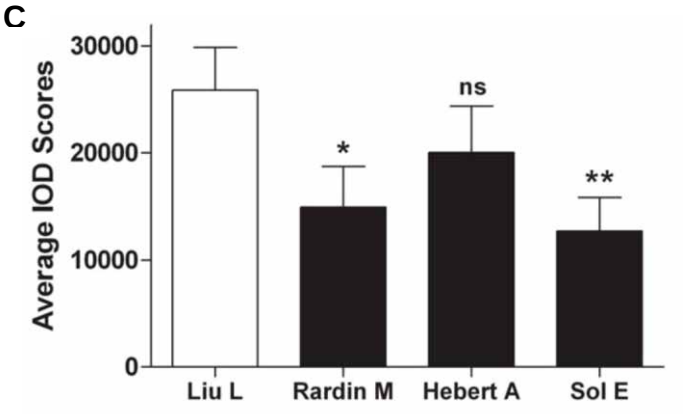

Figure A.S9. Comparison of acetylated lysines in LRP130 (LRPPRC) across various studies. (A) Pair wise overlap of acetylated lysine sites in this study (Liu L) compared with other studies that ablated sirtuin 3 in cells or mouse liver. Gray indicates the number of unique acetylated lysine peptides of LRP130 (LRPPRC) identified in a particular study. Blue represents the number of peptides common between two studies. *Indicates a unique site identified across three separate studies. †indicates another unique site shared across three separate studies. Using a hypergeometric distribution, the probability that shared acetylated sites between two or more studies arose from a non-random (biological) process was greater than 80% across all studies (see materials and methods for mathematical formula and derivation used). (B) Acetylated lysine residues shared across studies shown in panel A. For simplicity, mouse residues are reported for all studies, irrespective of whether or not the study was performed using mouse or human samples. (C) Average IOD (integrated optical density) binding scores established by Smith BC et al 2011 (ACS Chem. Biol.) was compared across studies. A high score indicates greater affinity for SIRT3.

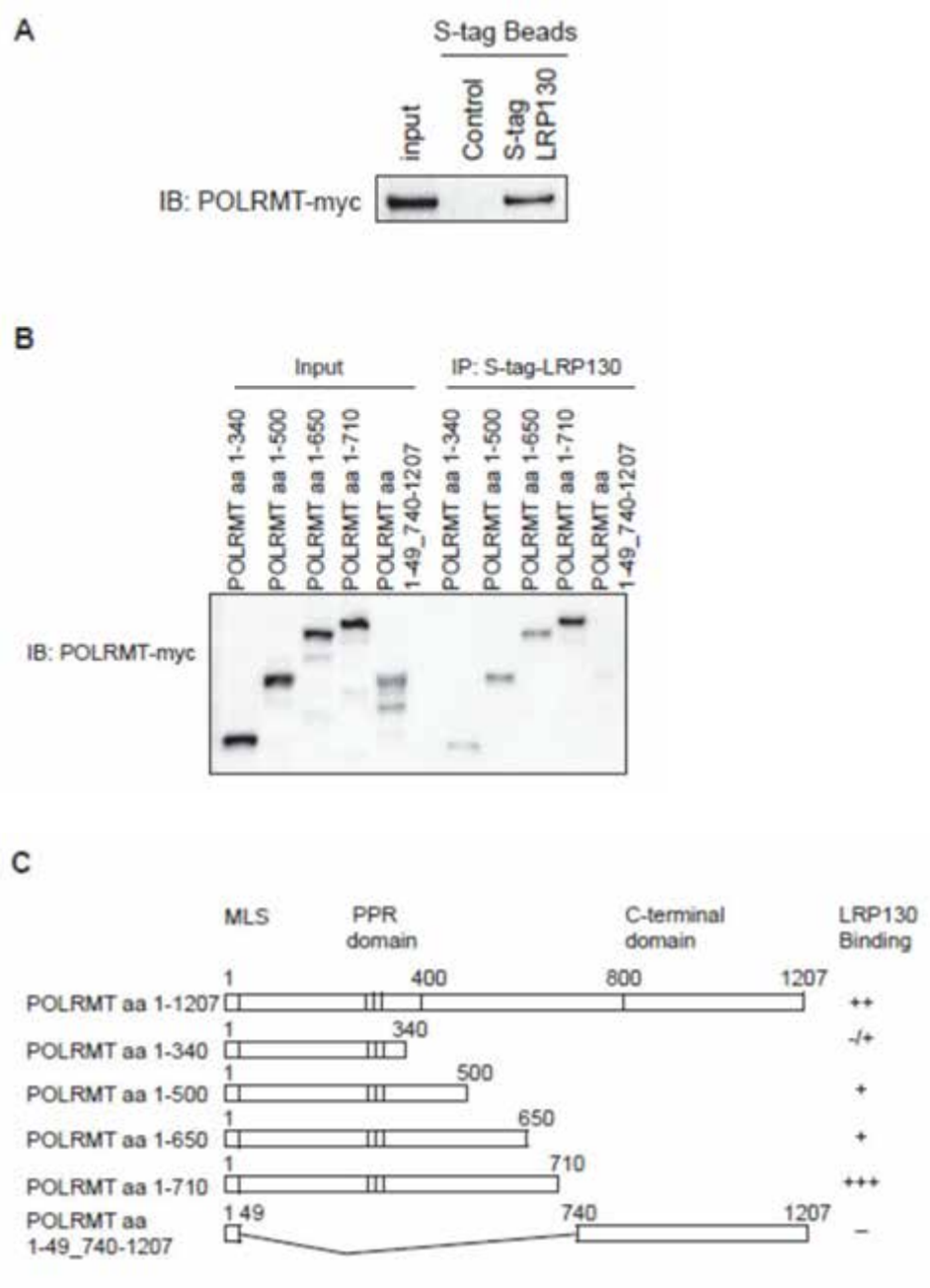

Figure A.S10. Mapping of the interaction between POLRMT and LRP130. (A) Immunoblot showing the interaction between *in vitro* translated POLRMT bearing a C-terminal myc tag and purified LRP130 protein containing an S-Tag. (B) Immunoblot of various fragments of POLRMT and their level of interaction with S-tagged full length purified LRP130 protein. (C) Schematic summarizing the interactions shown in (B).

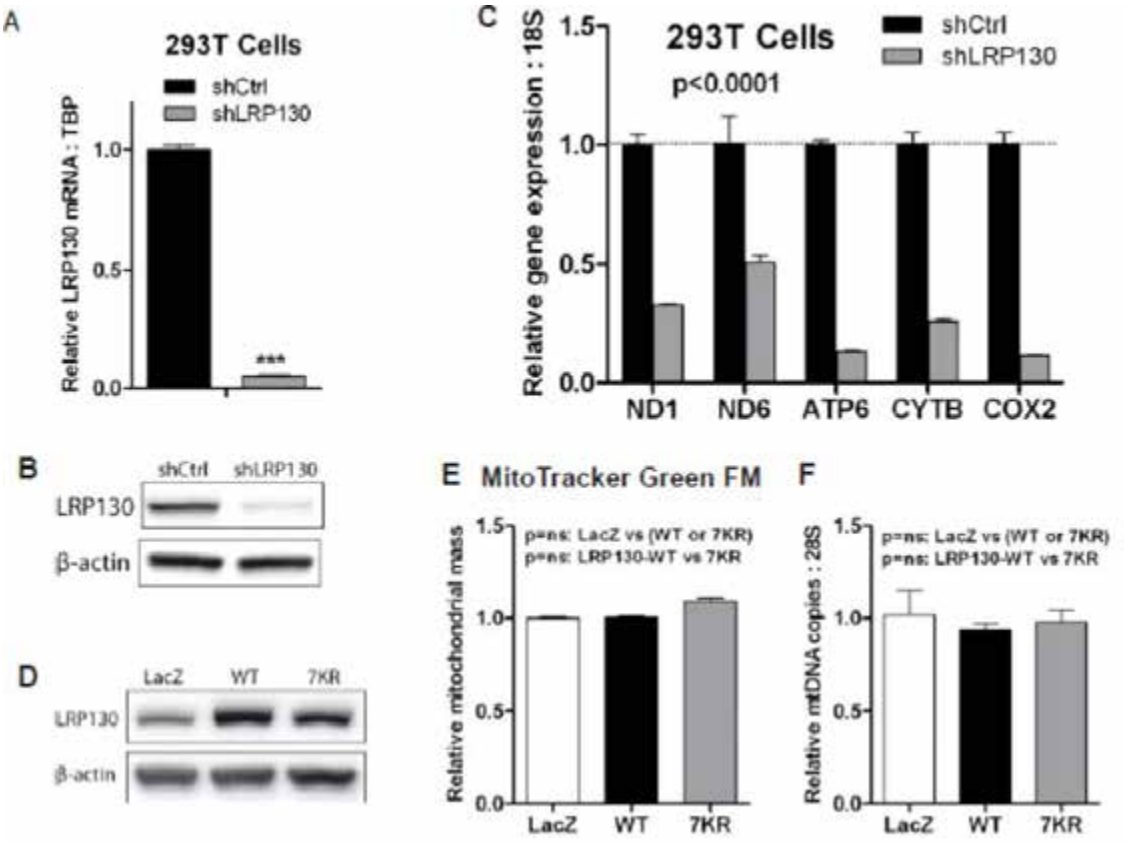

Figure A.S11. Knock-down of human LRP130 in 293T cells and reconstitution with mouse wild-type LRP130 or the LRP130 7KR mutant. (A) Using retrovirus, human LRP130 was stably knocked-down in 293T cells. The shRNA construct targeting human LRP130 does not affect murine LRP130 (data not shown). (B) Immunoblot confirming greater than 95% knock down of human *LRP130*. (C) As expected, 293T cells deficient for LRP130 have reduced expression of mitochondrially encoded genes. (D) Transient transfection of LacZ, murine wild-type LRP130 or the 7KR into 293T cells lacking human LRP130. A long exposure permitted comparison of the level of ectopically expressed murine LRP130 compared with the remaining endogenous human LRP130. Based on the knock-down of human LRP130, reconstitution with murine LRP130 is within a physiological range. (E) Fluorescent assessment of mitochondrial content using MitoTracker Green FM (n=3). (F) Genetic assessment of mitochondrial content using mitochondrial DNA content (n=3). For gene expression, Two-way ANOVA. For mitochondrial content, two-tailed unpaired Student's t test. (mean+s.e.m, ***p<0.001).

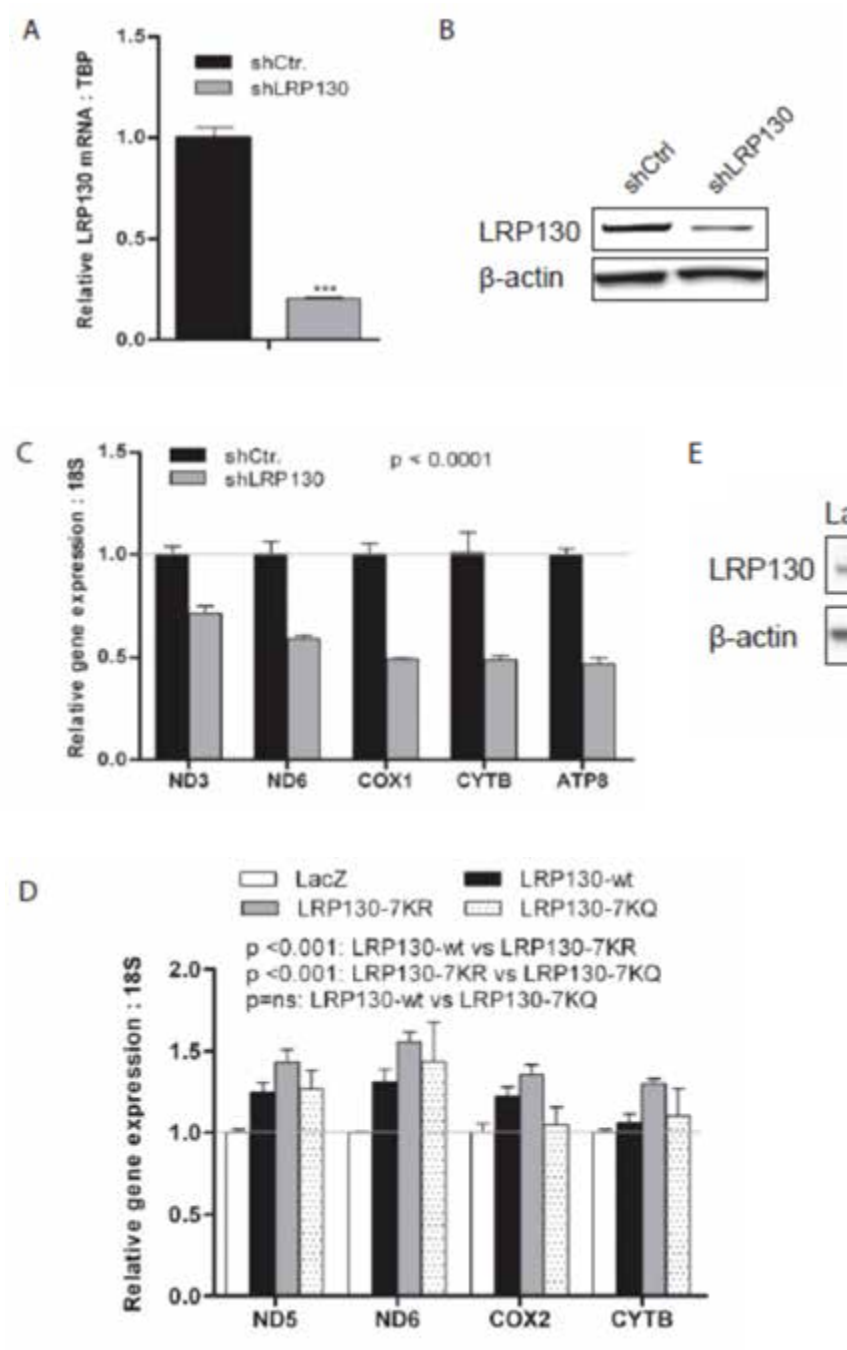

Figure A.S12. Knock-down of human LRP130 in 293T cells and reconstitution with mouse wild-type LRP130 or the LRP130 7KQ mutant. (A) Using transient transfection of a plasmid bearing a shRNA construct targeted to human *LRP130*, human *LRP130* was knocked down in 293T cells. The shRNA construct targeting human *LRP130* does not affect murine *Lrp130* (data not shown). (B) Immunoblot confirming

knock-down of human LRP130. (C) As expected, 293T cells deficient for LRP130 have reduced expression of mitochondrially encoded genes (n=3). (D) Gene expression following transient transfection of LacZ, murine wild-type LRP130, 7KR mutant and the 7KQ mutant into 293T cells deficient for human LRP130 (n=3). (E) A long exposure immunoblot permitted comparison of the level of ectopically expressed murine LRP130 compared with remaining endogenous human LRP130.

Table A.S1. Mass spectrometry intensities for lysines in murine LRP130 sensitive to deacetylation by SIRT3

Lysine	Ac-Ctrl	SIRT3	Rel Ac	Sequence	Species
225	148,400	37,700	0.25	G F M K T K D L P I T	Mouse
				G F M K T K D L P V T	Human
				G F M K T K D L P V T	Bovine
				G F M K T K D L P I T	Pig
				G F M K S K D L P I T	Chicken
452	58,790	9,759	0.17	G H Q K T K N V Q G I	Mouse
				G R R K E K N V Q G I	Human
				G H Q K E K N V Q G I	Bovine
				G Y Q K E K N V Q G I	Pig
				G F Q K E K N L K G V	Chicken
671	341,300	29,490	0.09	T L E K L K A E G Q P	Mouse
				T L E T L K A E N Q P	Human
				K L E K L K A E N Q P	Bovine
				K L E K L K S E N Q P	Pig
				K L E K R K A E N Q P	Chicken
749	131,800	8,111	0.06	I L D T A K Y V A L V	Mouse
				V L D T G K Y V G L V	Human
				V L D T G K Y V R L V	Bovine
				V L D T G K Y L G L V	Pig
				A L D S G K Y I A L V	Chicken
867	202,000	29,620	0.15	C K L V E K G E T D L	Mouse
				C K L V E K G E T D L	Human
				C K L I E K G E T E L	Bovine
				C R L I E K G K T E L	Pig
				C R L I E K G D T E L	Chicken
979	568,100	92,830	0.16	D A A W T K M Q E E N	Mouse
				D A V W N K I Q E E N	Human
				D A V W N K M Q E E N	Bovine
				D A V W N K M Q E E N	Pig
				E A V W T K I Q E E N	Chicken
1000	291,200	22,170	0.08	L A E I L K T S N Q E	Mouse
				L A E I L R E G N Q E	Human
				L A E I L R N N N Q D	Bovine
				L A E I L R N S N Q E	Pig
				L A D I F E K N G Q V	Chicken
1036	1,160,000	25,000	0.02	E D V T E K T L L S N	Mouse
				E P D F Q K D I L I A	Human
				E V N L Q K E L L N A	Bovine
				Q G N L Q K E L L K A	Pig
				E - - - E R K I R M L	Chicken
1048	2,007,000	165,000	0.08	K L K K S K D A Y N I	Mouse
				R L N Q K K G A Y D I	Human
				R T R R N K D A F N I	Bovine
				R K R K N R D A F N I	Pig
				K K N S A R E A Y N V	Chicken

Lysine	Ac-Ctrl	SIRT3	Rel Ac	Sequence	Species
1059	94,900	11,700	0.12	F L K A E K Q N V V F	Mouse
				F L N A K E Q N I V F	Human
				F L T A K K Q N I V F	Bovine
				F L K A K R Q N I V F	Pig
				F L K N Q G K - S D Y	Chicken
1174	4,216,000	567,300	0.13	- I G L S K M V F I N	Mouse
				S I G L S K M V F I N	Human
				S I G L S R M V F I N	Bovine
				S I G L S R M V F I N	Pig
				S I G L S P S L I S N	Chicken
1187	767,100	116,000	0.15	A L A Q M K N N K L D	Mouse
				A L A Q I K N N N I D	Human
				A L A Q I K N N N I D	Bovine
				A L A Q I K N N D I D	Pig
				A L A H T N N N D L D	Chicken
1250	373,700	11,900	0.03	Q F A L Y K P V T D L	Mouse
				Q F A I Y K P V T D F	Human
				Q F A V Y K P V T D L	Bovine
				Q F A V Y K P V T D L	Pig
				Q F G I Y R P V T D L	Chicken
1336	72,222,000	32,967,000	0.46	D V A S A K A L Y E Y	Mouse
				D V T S A K A L Y E H	Human
				D V A S A K A L Y E S	Bovine
				D V T S A K E L Y E N	Pig
				D V A S V K A V Y E K	Chicken
1348	1,950,000	39,600	0.02	T A K N L K L D D L F	Mouse
				T A K N T K L D D L F	Human
				T A K N V K L N D L F	Bovine
				T A K D T K L N D L F	Pig
				K E K N I Q L P E L S	Chicken
1355	1,334,000	84,900	0.06	D D L F L K R Y A A L	Mouse
				D D L F L K R Y A S L	Human
				N D L F L K R Y A V L	Bovine
				N D L F L K R Y A V L	Pig
				P E L S L K S L A A F	Chicken
1385	1,788,000	28,000	0.02	Y I K Q L K E A R E S	Mouse
				Y A Q Q L R K L R E N	Human
				Y A K Q L K E S K E T	Bovine
				Y A K Q L K E S K E N	Pig
				Y V E E W R K R R L E	Chicken

Shown in columns 2 and 3 are mass spectrometry intensities for lysines in murine LRP130 sensitive to deacetylation by SIRT3, that is, those sites showing less than 50%

acetylation when treated with SIRT3 and NAD^+. ‘Rel Ac’ denotes relative acetylation, derived by dividing the intensity of the SIRT3 sample by the acetylated control sample (Ac-Ctrl). Bolded lysine positions in column 1 were mutated in this study, generating a 7KR LRP130 mutant. Highlighted in light gray are lysine residues in mouse and various other species. In some species, lysine residues were replaced with arginine residues, which mimic deacetylation and are highlighted in dark gray.

Table A.S2. Mouse primers used for RT-qPCR.

Primer	Forward (5' -> 3')	Reverse (5' -> 3')
12S (Rnr1)	CCCCGCTCTACCTCACCAT	AATACCTTTTTAGGGTTTGCTGAAGA
16S (Rnr2)	GCCTGCCCAGTGACTAAAGTTT	AACAAGTGATTATGCTACCTTTGCA
18S (Rn18s)	AGTCCCTGCCCTTTGTACACA	CGATCCGAGGGCCTCACTA
28S (Rn28s1)	GAATCCGCTAAGGAGTGTGTAACA	CTCCAGCGCCATCCATTT
36B4 (Rplp0)	TGCAGATCGGGTACCCAACT	ACGCGCTTGTACCCATTGA
ATP6	AATTACAGGCTTCCGACACAAAC	TGGAATTAGTGAAATTGGAGTTCCT
ATP8	GCCACAACTAGATACATCAACATGATT	GGTTGTTAGTGATTTTGGTGAAGGT
COX1	TTTTCAGGCTTCACCCTAGATGA	CCTACGAATATGATGGCGAAGTG
COX2	TGAAGACGTCCTCCACTCATGA	GCCTGGGATGGCATCAGTT
COX3	GCAGGATTCTTCTGAGCGTTCT	GTCAGCAGCCTCCTAGATCATGT
CYTB	AGACAACTACATACCAGCTAATCCACTAA	GAATGGCGTATGCAAATAGGAAA
Erra (Esrra)	GCAGGGCAGTGGGAAGCTA	CCTCTTGAAGAAGGCTTTGCA
Fasn	CGGGTTCGTGAAACTGATAAA	CATGGTTGACAGCAAAATGG
G6p (G6pc)	ATGACTTTGGGATCCAGTCG	TGGAACCAGATGGGAAAGAG
Hprt	TGGCCATCTGCCTAGTAAAGC	GGCTCATAGTGCAAATCAAAAGTC
Lrp130 (Lrpprc)	TTCAGTGCTCTCGTCACAGG	GTCGCGGTCCATGAAGTAAT
ND1	CCCCTTCGACCTGACAGAAG	GGGCCGGCTGCGTATT
ND4	ATCACTCCTATTCTGCCTAGCAAAC	GAAGTCCTCGGGCCATAATTATAGT
ND5	CGGACGAACAGACGCAAATA	CAAACTATAGCTAAAATGAATCCGATGT
ND6	ACAAAGATCACCCAGCTACTACCAT	TTGATGATGTTGGAGTTATGTTGGA
Pepck (Pck1)	CATATGCTGATCCTGGGCATAAC	CAAACTTCATCCAGGCAATGTC
Pgc-1a (Ppargc1a)	GCCGTGTGATTTACGTTGGTAA	AAAACTTCAAAGCGGTCTCTCAA
Pgc-1b (Ppargc1b)	GCCTCTCCAGGCAGGTTCA	TAGAGAACTCAGTCCAGAAGGCTTT
Polrmt	TCTTCAAAAGTCTACAGGAGATGTTCAC	TGAGGTTGGCACTCTCAGTCA
Rpl32	CGCAAGTTCCTGGTCCACAATGTC	GCTCTTTCTACGATGGCTTTTCGG
Sirt3	TACAGGCCCAATGTCACTCA	ACAGACCGTGCATGTAGCTG
Tbp	ACCCTTCACCAATGACTCCTATG	TGACTGCAGCAAATCGCTTGG
Tfam	CCGAAGTGTTTTTCCAGCAT	GGCTGCAATTTTCCTAACCA
Tfb2m	AGAGCCGTTGCCTGATTCTG	CCGATCGATTCCTGGATGTC

Where indicated official gene symbols are shown in brackets.

Table A.S3. Human primers used for RT-qPCR

Primer	Forward (5' -> 3')	Reverse (5' -> 3')
ND1	CCCTAAAACCCGCCACATCT	GAGCGATGGTGAGAGCTAAGGT
ND2	GACATCCGGCCTGCTTCTT	TACGTTTAGTGAGGGAGAGATTTGG
ND6	CCCCGAGCAATCTCAATTACA	TGATTATGGGCGTTGATTAGTAGTAGTT
COX2	CCGACTACGGCGGACTAATC	CGCCTGGTTCTAGGAATAATGG
ATP8	CCCTCACCAAAGCCCATAAA	GAATGAAGCGAACAGATTTTCGT
CYTB	AACCGCCTTTTCATCAATCG	AGCGGATGATTCAGCCATAATT
TBP	GCACAGGAGCCAAGAGTGAA	TCACAGCTCCCCACCATGTT
18S (RNA18S5)	CGCAGCTAGGAATAATGGAATAGG	CATGGCCTCAGTTCCGAAA
28S (RNA28S5)	CCCAGTGCTCTGAATGTCAA	ATGACGAGGCATTTGGCTAC
36B4 (RPLP0)	GCGACCTGGAAGTCCAACTA	TGTCTGCTCCCACAATGAAA
LRP130 (LRPPRC)	CGAGGACCGACGGAAGCT	AATGCTCCTCCTTGGCCTGTA

Where indicated official gene symbols are shown in brackets.

Bibliography

1. Gessner K. Historiae Animalium: I De Quadrupedibus viviparis. 1551.

2. Sheldon EF. The so-called hibernating gland in mammals: a form of adipose tissue. *The Anatomical Record.* 1924;28(5):331-47.

3. Smith RE. Thermogenic activity of the hibernating gland in the cold-acclimated rat. *Physiologist.* 1961;4(Aug.):113.

4. Young P, Arch JR, and Ashwell M. Brown adipose tissue in the parametrial fat pad of the mouse. *FEBS Lett.* 1984;167(1):10-4.

5. Loncar D, Bedrica L, Mayer J, Cannon B, Nedergaard J, Afzelius BA, and Svajger A. The effect of intermittent cold treatment on the adipose tissue of the cat. Apparent transformation from white to brown adipose tissue. *J Ultrastruct Mol Struct Res.* 1986;97(1-3):119-29.

6. Cousin B, Cinti S, Morroni M, Raimbault S, Ricquier D, Penicaud L, and Casteilla L. Occurrence of brown adipocytes in rat white adipose tissue: molecular and morphological characterization. *J Cell Sci.* 1992;103 (Pt 4)(931-42.

7. Shabalina IG, Petrovic N, de Jong JM, Kalinovich AV, Cannon B, and Nedergaard J. UCP1 in brite/beige adipose tissue mitochondria is functionally thermogenic. *Cell Rep.* 2013;5(5):1196-203.

8. Wu J, Cohen P, and Spiegelman BM. Adaptive thermogenesis in adipocytes: is beige the new brown? *Genes Dev.* 2013;27(3):234-50.

9. Kajimura S, and Saito M. A new era in brown adipose tissue biology: molecular control of brown fat development and energy homeostasis. *Annu Rev Physiol.* 2014;76(225-49.

10. Wu J, Bostrom P, Sparks LM, Ye L, Choi JH, Giang AH, Khandekar M, Virtanen KA, Nuutila P, Schaart G, et al. Beige adipocytes are a distinct type of thermogenic fat cell in mouse and human. *Cell.* 2012;150(2):366-76.

11. Harms M, and Seale P. Brown and beige fat: development, function and therapeutic potential. *Nat Med.* 2013;19(10):1252-63.

12. Rosenwald M, Perdikari A, Rulicke T, and Wolfrum C. Bi-directional interconversion of brite and white adipocytes. *Nat Cell Biol.* 2013;15(6):659-67.

13. Cousin B, Casteilla L, Dani C, Muzzin P, Revelli JP, and Penicaud L. Adipose tissues from various anatomical sites are characterized by different patterns of gene expression and regulation. *Biochem J.* 1993;292 (Pt 3)(873-6.

14. Seale P, Bjork B, Yang W, Kajimura S, Chin S, Kuang S, Scime A, Devarakonda S, Conroe HM, Erdjument-Bromage H, et al. PRDM16 controls a brown fat/skeletal muscle switch. *Nature.* 2008;454(7207):961-7.

15. Wirsén C. Distribution of adrenergic nerve fibers in brown and white adipose tissue. *Compr Physiol 2011.*Supplement 15: Handbook of Physiology, Adipose Tissue: 197-9. First published in print 1965.

16. Himms-Hagen J. Neural control of brown adipose tissue thermogenesis, hypertrophy, and atrophy. *Front Neuroendocrinol.* 1991;12(38-93.

17. Hausberger FX, and Widelitz MM. Distribution of labeled erythrocytes in adipose tissue and muscle in the rat. *Am J Physiol.* 1963;204(649-52.

18. Foster DO, and Frydman ML. Tissue distribution of cold-induced thermogenesis in conscious warm- or cold-acclimated rats reevaluated from changes in tissue blood flow: the dominant role of brown adipose tissue in the replacement of shivering by nonshivering thermogenesis. *Can J Physiol Pharmacol.* 1979;57(3):257-70.

19. Heldmaier G, and Buchberger A. Sources of heat during nonshivering thermogenesis in Djungarian hamsters: a dominant role of brown adipose tissue during cold adaptation. *J Comp Physiol B.* 1985;156(2):237-45.

20. Power GG. Biology of temperature: the mammalian fetus. *J Dev Physiol.* 1989;12(6):295-304.

21. Rabi T, Cassuto Y, and Gutman A. Lipolysis in brown adipose tissue of cold- and heat-acclimated hamsters. *J Appl Physiol Respir Environ Exerc Physiol.* 1977;43(6):1007-11.

22. Bartelt A, Bruns OT, Reimer R, Hohenberg H, Ittrich H, Peldschus K, Kaul MG, Tromsdorf UI, Weller H, Waurisch C, et al. Brown adipose tissue activity controls triglyceride clearance. *Nat Med.* 2011;17(2):200-5.

23. Nedergaard J, Bengtsson T, and Cannon B. New powers of brown fat: fighting the metabolic syndrome. *Cell Metab.* 2011;13(3):238-40.

24. Gunawardana SC, and Piston DW. Reversal of type 1 diabetes in mice by brown adipose tissue transplant. *Diabetes.* 2012;61(3):674-82.

25. Stanford KI, Middelbeek RJ, Townsend KL, An D, Nygaard EB, Hitchcox KM, Markan KR, Nakano K, Hirshman MF, Tseng YH, et al. Brown adipose tissue regulates glucose homeostasis and insulin sensitivity. *J Clin Invest.* 2013;123(1):215-23.

26. Liu X, Zheng Z, Zhu X, Meng M, Li L, Shen Y, Chi Q, Wang D, Zhang Z, Li C, et al. Brown adipose tissue transplantation improves whole-body energy metabolism. *Cell Res.* 2013;23(6):851-4.

27. Lin FT, and Lane MD. CCAAT/enhancer binding protein alpha is sufficient to initiate the 3T3-L1 adipocyte differentiation program. *Proc Natl Acad Sci U S A.* 1994;91(19):8757-61.

28. Tontonoz P, Hu E, and Spiegelman BM. Stimulation of adipogenesis in fibroblasts by PPAR gamma 2, a lipid-activated transcription factor. *Cell.* 1994;79(7):1147-56.

29. Yeh WC, Cao Z, Classon M, and McKnight SL. Cascade regulation of terminal adipocyte differentiation by three members of the C/EBP family of leucine zipper proteins. *Genes Dev.* 1995;9(2):168-81.

30. Tanaka T, Yoshida N, Kishimoto T, and Akira S. Defective adipocyte differentiation in mice lacking the C/EBPbeta and/or C/EBPdelta gene. *EMBO J.* 1997;16(24):7432-43.

31. Rosen ED, Hsu CH, Wang X, Sakai S, Freeman MW, Gonzalez FJ, and Spiegelman BM. C/EBPalpha induces adipogenesis through PPARgamma: a unified pathway. *Genes Dev.* 2002;16(1):22-6.

32. Lefterova MI, Zhang Y, Steger DJ, Schupp M, Schug J, Cristancho A, Feng D, Zhuo D, Stoeckert CJ, Jr., Liu XS, et al. PPARgamma and C/EBP factors orchestrate adipocyte biology via adjacent binding on a genome-wide scale. *Genes Dev.* 2008;22(21):2941-52.

33. Puigserver P, Wu Z, Park CW, Graves R, Wright M, and Spiegelman BM. A cold-inducible coactivator of nuclear receptors linked to adaptive thermogenesis. *Cell.* 1998;92(6):829-39.

34. Wu Z, Puigserver P, Andersson U, Zhang C, Adelmant G, Mootha V, Troy A, Cinti S, Lowell B, Scarpulla RC, et al. Mechanisms controlling mitochondrial biogenesis and respiration through the thermogenic coactivator PGC-1. *Cell.* 1999;98(1):115-24.

35. Kressler D, Schreiber SN, Knutti D, and Kralli A. The PGC-1-related protein PERC is a selective coactivator of estrogen receptor alpha. *J Biol Chem.* 2002;277(16):13918-25.

36. Uldry M, Yang W, St-Pierre J, Lin J, Seale P, and Spiegelman BM. Complementary action of the PGC-1 coactivators in mitochondrial biogenesis and brown fat differentiation. *Cell Metab.* 2006;3(5):333-41.

37. Fog CK, Galli GG, and Lund AH. PRDM proteins: important players in differentiation and disease. *Bioessays.* 2012;34(1):50-60.

38. Kajimura S, Seale P, Kubota K, Lunsford E, Frangioni JV, Gygi SP, and Spiegelman BM. Initiation of myoblast to brown fat switch by a PRDM16-C/EBP-beta transcriptional complex. *Nature.* 2009;460(7259):1154-8.

39. Kajimura S, Seale P, Tomaru T, Erdjument-Bromage H, Cooper MP, Ruas JL, Chin S, Tempst P, Lazar MA, and Spiegelman BM. Regulation of the brown and white fat gene programs through a PRDM16/CtBP transcriptional complex. *Genes Dev.* 2008;22(10):1397-409.

40. Rajakumari S, Wu J, Ishibashi J, Lim HW, Giang AH, Won KJ, Reed RR, and Seale P. EBF2 determines and maintains brown adipocyte identity. *Cell Metab.* 2013;17(4):562-74.

41. Wang W, Kissig M, Rajakumari S, Huang L, Lim HW, Won KJ, and Seale P. Ebf2 is a selective marker of brown and beige adipogenic precursor cells. *Proc Natl Acad Sci U S A.* 2014;111(40):14466-71.

42. de Jesus LA, Carvalho SD, Ribeiro MO, Schneider M, Kim SW, Harney JW, Larsen PR, and Bianco AC. The type 2 iodothyronine deiodinase is essential for adaptive thermogenesis in brown adipose tissue. *J Clin Invest.* 2001;108(9):1379-85.

43. Zhou Z, Yon Toh S, Chen Z, Guo K, Ng CP, Ponniah S, Lin SC, Hong W, and Li P. Cidea-deficient mice have lean phenotype and are resistant to obesity. *Nat Genet.* 2003;35(1):49-56.

44. Ricquier D. Uncoupling protein 1 of brown adipocytes, the only uncoupler: a historical perspective. *Front Endocrinol (Lausanne).* 2011;2(85.

45. Forner F, Kumar C, Luber CA, Fromme T, Klingenspor M, and Mann M. Proteome differences between brown and white fat mitochondria reveal specialized metabolic functions. *Cell Metab.* 2009;10(4):324-35.

46. Shinoda K, Luijten IH, Hasegawa Y, Hong H, Sonne SB, Kim M, Xue R, Chondronikola M, Cypess AM, Tseng YH, et al. Genetic and functional characterization of clonally derived adult human brown adipocytes. *Nat Med.* 2015;21(4):389-94.

47. Lidell ME, Betz MJ, Dahlqvist Leinhard O, Heglind M, Elander L, Slawik M, Mussack T, Nilsson D, Romu T, Nuutila P, et al. Evidence for two types of brown adipose tissue in humans. *Nat Med.* 2013;19(5):631-4.

48. Heaton JM. The distribution of brown adipose tissue in the human. *J Anat.* 1972;112(Pt 1):35-9.

49. Huttunen P, Hirvonen J, and Kinnula V. The occurrence of brown adipose tissue in outdoor workers. *Eur J Appl Physiol Occup Physiol.* 1981;46(4):339-45.

50. English JT, Patel SK, and Flanagan MJ. Association of pheochromocytomas with brown fat tumors. *Radiology.* 1973;107(2):279-81.

51. Ricquier D, Nechad M, and Mory G. Ultrastructural and biochemical characterization of human brown adipose tissue in pheochromocytoma. *J Clin Endocrinol Metab.* 1982;54(4):803-7.

52. Lean ME, James WP, Jennings G, and Trayhurn P. Brown adipose tissue in patients with phaeochromocytoma. *Int J Obes.* 1986;10(3):219-27.

53. Cypess AM, Lehman S, Williams G, Tal I, Rodman D, Goldfine AB, Kuo FC, Palmer EL, Tseng YH, Doria A, et al. Identification and importance of brown adipose tissue in adult humans. *N Engl J Med.* 2009;360(15):1509-17.

54. van Marken Lichtenbelt WD, Vanhommerig JW, Smulders NM, Drossaerts JM, Kemerink GJ, Bouvy ND, Schrauwen P, and Teule GJ. Cold-activated brown adipose tissue in healthy men. *N Engl J Med.* 2009;360(15):1500-8.

55. Virtanen KA, Lidell ME, Orava J, Heglind M, Westergren R, Niemi T, Taittonen M, Laine J, Savisto NJ, Enerback S, et al. Functional brown adipose tissue in healthy adults. *N Engl J Med.* 2009;360(15):1518-25.

56. Saito M, Okamatsu-Ogura Y, Matsushita M, Watanabe K, Yoneshiro T, Nio-Kobayashi J, Iwanaga T, Miyagawa M, Kameya T, Nakada K, et al. High incidence of metabolically active brown adipose tissue in healthy adult humans: effects of cold exposure and adiposity. *Diabetes.* 2009;58(7):1526-31.

57. Sharp LZ, Shinoda K, Ohno H, Scheel DW, Tomoda E, Ruiz L, Hu H, Wang L, Pavlova Z, Gilsanz V, et al. Human BAT possesses molecular signatures that resemble beige/brite cells. *PLoS One.* 2012;7(11):e49452.

58. Cypess AM, White AP, Vernochet C, Schulz TJ, Xue R, Sass CA, Huang TL, Roberts-Toler C, Weiner LS, Sze C, et al. Anatomical localization, gene expression profiling and functional characterization of adult human neck brown fat. *Nat Med.* 2013;19(5):635-9.

59. Jespersen NZ, Larsen TJ, Peijs L, Daugaard S, Homoe P, Loft A, de Jong J, Mathur N, Cannon B, Nedergaard J, et al. A classical brown adipose tissue mRNA

signature partly overlaps with brite in the supraclavicular region of adult humans. *Cell Metab.* 2013;17(5):798-805.

60. Wikstrom JD, Mahdaviani K, Liesa M, Sereda SB, Si Y, Las G, Twig G, Petrovic N, Zingaretti C, Graham A, et al. Hormone-induced mitochondrial fission is utilized by brown adipocytes as an amplification pathway for energy expenditure. *EMBO J.* 2014;33(5):418-36.

61. Justo R, Oliver J, and Gianotti M. Brown adipose tissue mitochondrial subpopulations show different morphological and thermogenic characteristics. *Mitochondrion.* 2005;5(1):45-53.

62. Rodriguez-Cuenca S, Pujol E, Justo R, Frontera M, Oliver J, Gianotti M, and Roca P. Sex-dependent thermogenesis, differences in mitochondrial morphology and function, and adrenergic response in brown adipose tissue. *J Biol Chem.* 2002;277(45):42958-63.

63. Loncar D. Convertible adipose tissue in mice. *Cell Tissue Res.* 1991;266(1):149-61.

64. Schreiber SN, Knutti D, Brogli K, Uhlmann T, and Kralli A. The transcriptional coactivator PGC-1 regulates the expression and activity of the orphan nuclear receptor estrogen-related receptor alpha (ERRalpha). *J Biol Chem.* 2003;278(11):9013-8.

65. Nicholls DG. The bioenergetics of brown adipose tissue mitochondria. *FEBS Lett.* 1976;61(2):103-10.

66. Nicholls DG, Bernson VS, and Heaton GM. The identification of the component in the inner membrane of brown adipose tissue mitochondria responsible for regulating energy dissipation. *Experientia Suppl.* 1978;32(89-93.

67. Cannon B, Romert L, Sundin U, and Barnard T. Morphology and biochemical properties of perirenal adipose tissue from lamb (Ovis aries). A comparison with brown adipose tissue. *Comp Biochem Physiol B.* 1977;56(1):87-99.

68. Cannon B, Sundin U, and Romert L. Palmitoyl coenzyme A: a possible physiological regulator of nucleotide binding to brown adipose tissue mitochondria. *FEBS Lett.* 1977;74(1):43-6.

69. Strieleman PJ, and Shrago E. Specific interaction of fatty acyl-CoA esters with brown adipose tissue mitochondria. *Am J Physiol.* 1985;248(6 Pt 1):E699-705.

70. Fedorenko A, Lishko PV, and Kirichok Y. Mechanism of fatty-acid-dependent UCP1 uncoupling in brown fat mitochondria. *Cell.* 2012;151(2):400-13.

71. Williamson JR. Control of energy metabolism in hamster brown adipose tissue. *J Biol Chem.* 1970;245(8):2043-50.

72. Cooney GJ, and Newsholme EA. The maximum capacity of glycolysis in brown adipose tissue and its relationship to control of the blood glucose concentration. *FEBS Lett.* 1982;148(2):198-200.

73. Lambeth DO, Tews KN, Adkins S, Frohlich D, and Milavetz BI. Expression of two succinyl-CoA synthetases with different nucleotide specificities in mammalian tissues. *J Biol Chem.* 2004;279(35):36621-4.

74. Christoffolete MA, Linardi CC, de Jesus L, Ebina KN, Carvalho SD, Ribeiro MO, Rabelo R, Curcio C, Martins L, Kimura ET, et al. Mice with targeted disruption of the Dio2 gene have cold-induced overexpression of the uncoupling protein 1 gene but fail to increase brown adipose tissue lipogenesis and adaptive thermogenesis. *Diabetes.* 2004;53(3):577-84.

75. Yu XX, Lewin DA, Forrest W, and Adams SH. Cold elicits the simultaneous induction of fatty acid synthesis and beta-oxidation in murine brown adipose tissue: prediction from differential gene expression and confirmation in vivo. *FASEB J.* 2002;16(2):155-68.

76. Cadoudal T, Distel E, Durant S, Fouque F, Blouin JM, Collinet M, Bortoli S, Forest C, and Benelli C. Pyruvate dehydrogenase kinase 4: regulation by thiazolidinediones and implication in glyceroneogenesis in adipose tissue. *Diabetes.* 2008;57(9):2272-9.

77. Yan J, Lawson JE, and Reed LJ. Role of the regulatory subunit of bovine pyruvate dehydrogenase phosphatase. *Proc Natl Acad Sci U S A.* 1996;93(10):4953-6.

78. Huang B, Gudi R, Wu P, Harris RA, Hamilton J, and Popov KM. Isoenzymes of pyruvate dehydrogenase phosphatase. DNA-derived amino acid sequences, expression, and regulation. *J Biol Chem.* 1998;273(28):17680-8.

79. Cannon B, and Nedergaard J. Brown adipose tissue: function and physiological significance. *Physiol Rev.* 2004;84(1):277-359.

80. Sakakibara I, Fujino T, Ishii M, Tanaka T, Shimosawa T, Miura S, Zhang W, Tokutake Y, Yamamoto J, Awano M, et al. Fasting-induced hypothermia and reduced energy production in mice lacking acetyl-CoA synthetase 2. *Cell Metab.* 2009;9(2):191-202.

81. Fujino T, Kondo J, Ishikawa M, Morikawa K, and Yamamoto TT. Acetyl-CoA synthetase 2, a mitochondrial matrix enzyme involved in the oxidation of acetate. *J Biol Chem.* 2001;276(14):11420-6.

82. Agius L, and Williamson DH. The utilization of ketone bodies by the interscapular brown adipose tissue of the rat. *Biochim Biophys Acta.* 1981;666(1):127-32.

83. Muller S, Balaz M, Stefanicka P, Varga L, Amri EZ, Ukropec J, Wollscheid B, and Wolfrum C. Proteomic Analysis of Human Brown Adipose Tissue Reveals Utilization of Coupled and Uncoupled Energy Expenditure Pathways. *Sci Rep.* 2016;6(30030.

84. Guzun R, Gonzalez-Granillo M, Karu-Varikmaa M, Grichine A, Usson Y, Kaambre T, Guerrero-Roesch K, Kuznetsov A, Schlattner U, and Saks V. Regulation of respiration in muscle cells in vivo by VDAC through interaction with the cytoskeleton and MtCK within Mitochondrial Interactosome. *Biochim Biophys Acta.* 2012;1818(6):1545-54.

85. Kazak L, Chouchani ET, Jedrychowski MP, Erickson BK, Shinoda K, Cohen P, Vetrivelan R, Lu GZ, Laznik-Bogoslavski D, Hasenfuss SC, et al. A creatine-driven substrate cycle enhances energy expenditure and thermogenesis in beige fat. *Cell.* 2015;163(3):643-55.

86. Anderson S, Bankier AT, Barrell BG, de Bruijn MH, Coulson AR, Drouin J, Eperon IC, Nierlich DP, Roe BA, Sanger F, et al. Sequence and organization of the human mitochondrial genome. *Nature.* 1981;290(5806):457-65.

87. Smeitink JA, Loeffen JL, Triepels RH, Smeets RJ, Trijbels JM, and van den Heuvel LP. Nuclear genes of human complex I of the mitochondrial electron transport chain: state of the art. *Hum Mol Genet.* 1998;7(10):1573-9.

88. Ahn CS, and Metallo CM. Mitochondria as biosynthetic factories for cancer proliferation. *Cancer Metab.* 2015;3(1):1.

89. Chalah A, and Khosravi-Far R. The mitochondrial death pathway. *Adv Exp Med Biol.* 2008;615(25-45.

90. Yun J, and Finkel T. Mitohormesis. *Cell Metab.* 2014;19(5):757-66.

91. Butow RA, and Avadhani NG. Mitochondrial signaling: the retrograde response. *Mol Cell.* 2004;14(1):1-15.

92. Epstein CB, Waddle JA, Hale Wt, Dave V, Thornton J, Macatee TL, Garner HR, and Butow RA. Genome-wide responses to mitochondrial dysfunction. *Mol Biol Cell.* 2001;12(2):297-308.

93. Liu Z, and Butow RA. A transcriptional switch in the expression of yeast tricarboxylic acid cycle genes in response to a reduction or loss of respiratory function. *Mol Cell Biol.* 1999;19(10):6720-8.

94. Traven A, Wong JM, Xu D, Sopta M, and Ingles CJ. Interorganellar communication. Altered nuclear gene expression profiles in a yeast mitochondrial dna mutant. *J Biol Chem.* 2001;276(6):4020-7.

95. Rohas LM, St-Pierre J, Uldry M, Jager S, Handschin C, and Spiegelman BM. A fundamental system of cellular energy homeostasis regulated by PGC-1alpha. *Proc Natl Acad Sci U S A.* 2007;104(19):7933-8.

96. Zhao Q, Wang J, Levichkin IV, Stasinopoulos S, Ryan MT, and Hoogenraad NJ. A mitochondrial specific stress response in mammalian cells. *EMBO J.* 2002;21(17):4411-9.

97. Yoneda T, Benedetti C, Urano F, Clark SG, Harding HP, and Ron D. Compartment-specific perturbation of protein handling activates genes encoding mitochondrial chaperones. *J Cell Sci.* 2004;117(Pt 18):4055-66.

98. Haynes CM, Yang Y, Blais SP, Neubert TA, and Ron D. The matrix peptide exporter HAF-1 signals a mitochondrial UPR by activating the transcription factor ZC376.7 in C. elegans. *Mol Cell.* 2010;37(4):529-40.

99. Nargund AM, Pellegrino MW, Fiorese CJ, Baker BM, and Haynes CM. Mitochondrial import efficiency of ATFS-1 regulates mitochondrial UPR activation. *Science.* 2012;337(6094):587-90.

100. Houtkooper RH, Mouchiroud L, Ryu D, Moullan N, Katsyuba E, Knott G, Williams RW, and Auwerx J. Mitonuclear protein imbalance as a conserved longevity mechanism. *Nature.* 2013;497(7450):451-7.

101. Mouchiroud L, Houtkooper RH, Moullan N, Katsyuba E, Ryu D, Canto C, Mottis A, Jo YS, Viswanathan M, Schoonjans K, et al. The NAD(+)/Sirtuin Pathway Modulates Longevity through Activation of Mitochondrial UPR and FOXO Signaling. *Cell.* 2013;154(2):430-41.

102. Lee YK, Jee BA, Kwon SM, Yoon YS, Xu WG, Wang HJ, Wang XW, Thorgeirsson SS, Lee JS, Woo HG, et al. Identification of a mitochondrial defect gene signature reveals NUPR1 as a key regulator of liver cancer progression. *Hepatology.* 2015;62(4):1174-89.

103. Ballinger SW. Beyond retrograde and anterograde signalling: mitochondrial-nuclear interactions as a means for evolutionary adaptation and contemporary disease susceptibility. *Biochem Soc Trans.* 2013;41(1):111-7.

104. Jones AW, Yao Z, Vicencio JM, Karkucinska-Wieckowska A, and Szabadkai G. PGC-1 family coactivators and cell fate: roles in cancer, neurodegeneration,

cardiovascular disease and retrograde mitochondria-nucleus signalling. *Mitochondrion.* 2012;12(1):86-99.

105. Lin J, Wu PH, Tarr PT, Lindenberg KS, St-Pierre J, Zhang CY, Mootha VK, Jager S, Vianna CR, Reznick RM, et al. Defects in adaptive energy metabolism with CNS-linked hyperactivity in PGC-1alpha null mice. *Cell.* 2004;119(1):121-35.

106. Leone TC, Lehman JJ, Finck BN, Schaeffer PJ, Wende AR, Boudina S, Courtois M, Wozniak DF, Sambandam N, Bernal-Mizrachi C, et al. PGC-1alpha deficiency causes multi-system energy metabolic derangements: muscle dysfunction, abnormal weight control and hepatic steatosis. *PLoS Biol.* 2005;3(4):e101.

107. Kleiner S, Mepani RJ, Laznik D, Ye L, Jurczak MJ, Jornayvaz FR, Estall JL, Chatterjee Bhowmick D, Shulman GI, and Spiegelman BM. Development of insulin resistance in mice lacking PGC-1alpha in adipose tissues. *Proc Natl Acad Sci U S A.* 2012;109(24):9635-40.

108. Lelliott CJ, Medina-Gomez G, Petrovic N, Kis A, Feldmann HM, Bjursell M, Parker N, Curtis K, Campbell M, Hu P, et al. Ablation of PGC-1beta results in defective mitochondrial activity, thermogenesis, hepatic function, and cardiac performance. *PLoS Biol.* 2006;4(11):e369.

109. Enguix N, Pardo R, Gonzalez A, Lopez VM, Simo R, Kralli A, and Villena JA. Mice lacking PGC-1beta in adipose tissues reveal a dissociation between mitochondrial dysfunction and insulin resistance. *Mol Metab.* 2013;2(3):215-26.

110. Villena JA, Hock MB, Chang WY, Barcas JE, Giguere V, and Kralli A. Orphan nuclear receptor estrogen-related receptor alpha is essential for adaptive thermogenesis. *Proc Natl Acad Sci U S A.* 2007;104(4):1418-23.

111. Luo J, Sladek R, Carrier J, Bader JA, Richard D, and Giguere V. Reduced fat mass in mice lacking orphan nuclear receptor estrogen-related receptor alpha. *Mol Cell Biol.* 2003;23(22):7947-56.

112. Ikeda K, Shiba S, Horie-Inoue K, Shimokata K, and Inoue S. A stabilizing factor for mitochondrial respiratory supercomplex assembly regulates energy metabolism in muscle. *Nat Commun.* 2013;4(2147.

113. Vartak R, Porras CA, and Bai Y. Respiratory supercomplexes: structure, function and assembly. *Protein Cell.* 2013;4(8):582-90.

114. Scarpulla RC. Transcriptional paradigms in mammalian mitochondrial biogenesis and function. *Physiol Rev.* 2008;88(2):611-38.

115. Vernochet C, Mourier A, Bezy O, Macotela Y, Boucher J, Rardin MJ, An D, Lee KY, Ilkayeva OR, Zingaretti CM, et al. Adipose-specific deletion of TFAM increases mitochondrial oxidation and protects mice against obesity and insulin resistance. *Cell Metab.* 2012;16(6):765-76.

116. Vernochet C, Damilano F, Mourier A, Bezy O, Mori MA, Smyth G, Rosenzweig A, Larsson NG, and Kahn CR. Adipose tissue mitochondrial dysfunction triggers a lipodystrophic syndrome with insulin resistance, hepatosteatosis, and cardiovascular complications. *FASEB J.* 2014;28(10):4408-19.

117. Kim SJ, Kwon MC, Ryu MJ, Chung HK, Tadi S, Kim YK, Kim JM, Lee SH, Park JH, Kweon GR, et al. CRIF1 is essential for the synthesis and insertion of oxidative phosphorylation polypeptides in the mammalian mitochondrial membrane. *Cell Metab.* 2012;16(2):274-83.

118. Shin J, Lee SH, Kwon MC, Yang DK, Seo HR, Kim J, Kim YY, Im SK, Abel ED, Kim KT, et al. Cardiomyocyte specific deletion of Crif1 causes mitochondrial cardiomyopathy in mice. *PLoS One.* 2013;8(1):e53577.

119. Ryu MJ, Kim SJ, Kim YK, Choi MJ, Tadi S, Lee MH, Lee SE, Chung HK, Jung SB, Kim HJ, et al. Crif1 deficiency reduces adipose OXPHOS capacity and triggers inflammation and insulin resistance in mice. *PLoS Genet.* 2013;9(3):e1003356.

120. Shi Y, Lan F, Matson C, Mulligan P, Whetstine JR, Cole PA, Casero RA, and Shi Y. Histone demethylation mediated by the nuclear amine oxidase homolog LSD1. *Cell.* 2004;119(7):941-53.

121. Pedersen MT, and Helin K. Histone demethylases in development and disease. *Trends Cell Biol.* 2010;20(11):662-71.

122. Duteil D, Metzger E, Willmann D, Karagianni P, Friedrichs N, Greschik H, Gunther T, Buettner R, Talianidis I, Metzger D, et al. LSD1 promotes oxidative metabolism of white adipose tissue. *Nat Commun.* 2014;5(4093.

123. Cooper MP, Uldry M, Kajimura S, Arany Z, and Spiegelman BM. Modulation of PGC-1 coactivator pathways in brown fat differentiation through LRP130. *J Biol Chem.* 2008;283(46):31960-7.

124. Mootha VK, Lepage P, Miller K, Bunkenborg J, Reich M, Hjerrild M, Delmonte T, Villeneuve A, Sladek R, Xu F, et al. Identification of a gene causing human cytochrome c oxidase deficiency by integrative genomics. *Proc Natl Acad Sci U S A.* 2003;100(2):605-10.

125. Merante F, Petrova-Benedict R, MacKay N, Mitchell G, Lambert M, Morin C, De Braekeleer M, Laframboise R, Gagne R, and Robinson BH. A biochemically

distinct form of cytochrome oxidase (COX) deficiency in the Saguenay-Lac-Saint-Jean region of Quebec. *Am J Hum Genet.* 1993;53(2):481-7.

126. Liu L, Sanosaka M, Lei S, Bestwick ML, Frey JH, Jr., Surovtseva YV, Shadel GS, and Cooper MP. LRP130 protein remodels mitochondria and stimulates fatty acid oxidation. *J Biol Chem.* 2011;286(48):41253-64.

127. Ruzzenente B, Metodiev MD, Wredenberg A, Bratic A, Park CB, Camara Y, Milenkovic D, Zickermann V, Wibom R, Hultenby K, et al. LRPPRC is necessary for polyadenylation and coordination of translation of mitochondrial mRNAs. *EMBO J.* 2012;31(2):443-56.

128. Mourier A, Ruzzenente B, Brandt T, Kuhlbrandt W, and Larsson NG. Loss of LRPPRC causes ATP synthase deficiency. *Hum Mol Genet.* 2014;23(10):2580-92.

129. Liu L, Nam M, Fan W, Akie TE, Hoaglin DC, Gao G, Keaney JF, Jr., and Cooper MP. Nutrient sensing by the mitochondrial transcription machinery dictates oxidative phosphorylation. *J Clin Invest.* 2014;124(2):768-84.

130. Bratic A, Wredenberg A, Gronke S, Stewart JB, Mourier A, Ruzzenente B, Kukat C, Wibom R, Habermann B, Partridge L, et al. The bicoid stability factor controls polyadenylation and expression of specific mitochondrial mRNAs in Drosophila melanogaster. *PLoS Genet.* 2011;7(10):e1002324.

131. Barkan A, Rojas M, Fujii S, Yap A, Chong YS, Bond CS, and Small I. A combinatorial amino acid code for RNA recognition by pentatricopeptide repeat proteins. *PLoS Genet.* 2012;8(8):e1002910.

132. Sterky FH, Ruzzenente B, Gustafsson CM, Samuelsson T, and Larsson NG. LRPPRC is a mitochondrial matrix protein that is conserved in metazoans. *Biochem Biophys Res Commun.* 2010;398(4):759-64.

133. Gohil VM, Nilsson R, Belcher-Timme CA, Luo B, Root DE, and Mootha VK. Mitochondrial and nuclear genomic responses to loss of LRPPRC expression. *J Biol Chem.* 2010;285(18):13742-7.

134. Feldmann HM, Golozoubova V, Cannon B, and Nedergaard J. UCP1 ablation induces obesity and abolishes diet-induced thermogenesis in mice exempt from thermal stress by living at thermoneutrality. *Cell Metab.* 2009;9(2):203-9.

135. Inokuma K, Okamatsu-Ogura Y, Omachi A, Matsushita Y, Kimura K, Yamashita H, and Saito M. Indispensable role of mitochondrial UCP1 for antiobesity effect of beta3-adrenergic stimulation. *Am J Physiol Endocrinol Metab.* 2006;290(5):E1014-21.

136. Matthias A, Ohlson KB, Fredriksson JM, Jacobsson A, Nedergaard J, and Cannon B. Thermogenic responses in brown fat cells are fully UCP1-dependent. UCP2 or UCP3 do not substitute for UCP1 in adrenergically or fatty scid-induced thermogenesis. *J Biol Chem.* 2000;275(33):25073-81.

137. Xu F, Morin C, Mitchell G, Ackerley C, and Robinson BH. The role of the LRPPRC (leucine-rich pentatricopeptide repeat cassette) gene in cytochrome oxidase assembly: mutation causes lowered levels of COX (cytochrome c oxidase) I and COX III mRNA. *Biochem J.* 2004;382(Pt 1):331-6.

138. Akie TE, Liu L, Nam M, Lei S, and Cooper MP. OXPHOS-Mediated Induction of NAD+ Promotes Complete Oxidation of Fatty Acids and Interdicts Non-Alcoholic Fatty Liver Disease. *PLoS One.* 2015;10(5):e0125617.

139. Spinazzi M, Casarin A, Pertegato V, Salviati L, and Angelini C. Assessment of mitochondrial respiratory chain enzymatic activities on tissues and cultured cells. *Nat Protoc.* 2012;7(6):1235-46.

140. del Mar Gonzalez-Barroso M, Pecqueur C, Gelly C, Sanchis D, Alves-Guerra MC, Bouillaud F, Ricquier D, and Cassard-Doulcier AM. Transcriptional activation of the human ucp1 gene in a rodent cell line. Synergism of retinoids, isoproterenol, and thiazolidinedione is mediated by a multipartite response element. *J Biol Chem.* 2000;275(41):31722-32.

141. Goto T, Lee JY, Teraminami A, Kim YI, Hirai S, Uemura T, Inoue H, Takahashi N, and Kawada T. Activation of peroxisome proliferator-activated receptor-alpha stimulates both differentiation and fatty acid oxidation in adipocytes. *J Lipid Res.* 2011;52(5):873-84.

142. Siersbaek MS, Loft A, Aagaard MM, Nielsen R, Schmidt SF, Petrovic N, Nedergaard J, and Mandrup S. Genome-wide profiling of peroxisome proliferator-activated receptor gamma in primary epididymal, inguinal, and brown adipocytes reveals depot-selective binding correlated with gene expression. *Mol Cell Biol.* 2012;32(17):3452-63.

143. Graves RA, Tontonoz P, and Spiegelman BM. Analysis of a tissue-specific enhancer: ARF6 regulates adipogenic gene expression. *Mol Cell Biol.* 1992;12(3):1202-8.

144. Schoonjans K, Peinado-Onsurbe J, Lefebvre AM, Heyman RA, Briggs M, Deeb S, Staels B, and Auwerx J. PPARalpha and PPARgamma activators direct a distinct tissue-specific transcriptional response via a PPRE in the lipoprotein lipase gene. *EMBO J.* 1996;15(19):5336-48.

145. Zhou J, Febbraio M, Wada T, Zhai Y, Kuruba R, He J, Lee JH, Khadem S, Ren S, Li S, et al. Hepatic fatty acid transporter Cd36 is a common target of LXR, PXR, and PPARgamma in promoting steatosis. *Gastroenterology.* 2008;134(2):556-67.

146. Arimura N, Horiba T, Imagawa M, Shimizu M, and Sato R. The peroxisome proliferator-activated receptor gamma regulates expression of the perilipin gene in adipocytes. *J Biol Chem.* 2004;279(11):10070-6.

147. Liemburg-Apers DC, Schirris TJ, Russel FG, Willems PH, and Koopman WJ. Mitoenergetic Dysfunction Triggers a Rapid Compensatory Increase in Steady-State Glucose Flux. *Biophys J.* 2015;109(7):1372-86.

148. Puigserver P, Herron D, Gianotti M, Palou A, Cannon B, and Nedergaard J. Induction and degradation of the uncoupling protein thermogenin in brown adipocytes in vitro and in vivo. *Biochem J.* 1992;284(393-8.

149. Bachman ES, Dhillon H, Zhang CY, Cinti S, Bianco AC, Kobilka BK, and Lowell BB. betaAR signaling required for diet-induced thermogenesis and obesity resistance. *Science.* 2002;297(5582):843-5.

150. Finck BN, and Kelly DP. PGC-1 coactivators: inducible regulators of energy metabolism in health and disease. *J Clin Invest.* 2006;116(3):615-22.

151. Imai T, Takakuwa R, Marchand S, Dentz E, Bornert JM, Messaddeq N, Wendling O, Mark M, Desvergne B, Wahli W, et al. Peroxisome proliferator-activated receptor gamma is required in mature white and brown adipocytes for their survival in the mouse. *Proc Natl Acad Sci U S A.* 2004;101(13):4543-7.

152. Wang F, Mullican SE, DiSpirito JR, Peed LC, and Lazar MA. Lipoatrophy and severe metabolic disturbance in mice with fat-specific deletion of PPARgamma. *Proc Natl Acad Sci U S A.* 2013;110(46):18656-61.

153. Choi JH, Banks AS, Estall JL, Kajimura S, Bostrom P, Laznik D, Ruas JL, Chalmers MJ, Kamenecka TM, Bluher M, et al. Anti-diabetic drugs inhibit obesity-linked phosphorylation of PPARgamma by Cdk5. *Nature.* 2010;466(7305):451-6.

154. Sears IB, MacGinnitie MA, Kovacs LG, and Graves RA. Differentiation-dependent expression of the brown adipocyte uncoupling protein gene: regulation by peroxisome proliferator-activated receptor gamma. *Mol Cell Biol.* 1996;16(7):3410-9.

155. Amuthan G, Biswas G, Ananadatheerthavarada HK, Vijayasarathy C, Shephard HM, and Avadhani NG. Mitochondrial stress-induced calcium signaling, phenotypic changes and invasive behavior in human lung carcinoma A549 cells. *Oncogene.* 2002;21(51):7839-49.

156. Biswas G, Adebanjo OA, Freedman BD, Anandatheerthavarada HK, Vijayasarathy C, Zaidi M, Kotlikoff M, and Avadhani NG. Retrograde Ca2+ signaling in C2C12 skeletal myocytes in response to mitochondrial genetic and metabolic stress: a novel mode of inter-organelle crosstalk. *EMBO J.* 1999;18(3):522-33.

157. Amuthan G, Biswas G, Zhang SY, Klein-Szanto A, Vijayasarathy C, and Avadhani NG. Mitochondria-to-nucleus stress signaling induces phenotypic changes, tumor progression and cell invasion. *EMBO J.* 2001;20(8):1910-20.

158. Lytton J, Westlin M, Burk SE, Shull GE, and MacLennan DH. Functional comparisons between isoforms of the sarcoplasmic or endoplasmic reticulum family of calcium pumps. *J Biol Chem.* 1992;267(20):14483-9.

159. Seale P, Conroe HM, Estall J, Kajimura S, Frontini A, Ishibashi J, Cohen P, Cinti S, and Spiegelman BM. Prdm16 determines the thermogenic program of subcutaneous white adipose tissue in mice. *J Clin Invest.* 2011;121(1):96-105.

160. Cooper MP, Qu L, Rohas LM, Lin J, Yang W, Erdjument-Bromage H, Tempst P, and Spiegelman BM. Defects in energy homeostasis in Leigh syndrome French Canadian variant through PGC-1alpha/LRP130 complex. *Genes Dev.* 2006;20(21):2996-3009.

161. Walli RA. Interrelation of aerobic glycolysis and lipogenesis in isolated perfused liver of well-fed rats. *Biochim Biophys Acta.* 1978;539(1):62-80.

162. Wang Z, Qi C, Krones A, Woodring P, Zhu X, Reddy JK, Evans RM, Rosenfeld MG, and Hunter T. Critical roles of the p160 transcriptional coactivators p/CIP and SRC-1 in energy balance. *Cell Metab.* 2006;3(2):111-22.

163. Puigserver P, Adelmant G, Wu Z, Fan M, Xu J, O'Malley B, and Spiegelman BM. Activation of PPARgamma coactivator-1 through transcription factor docking. *Science.* 1999;286(5443):1368-71.

164. Arnould T, Vankoningsloo S, Renard P, Houbion A, Ninane N, Demazy C, Remacle J, and Raes M. CREB activation induced by mitochondrial dysfunction is a new signaling pathway that impairs cell proliferation. *EMBO J.* 2002;21(1-2):53-63.

165. Hayato R, Higure Y, Kuba M, Nagai H, Yamashita H, and Kuba K. beta(3)-Adrenergic activation of sequential Ca(2+) release from mitochondria and the endoplasmic reticulum and the subsequent Ca(2+) entry in rodent brown adipocytes. *Cell Calcium.* 2011;49(6):400-14.

166. Sun W, Uchida K, Suzuki Y, Zhou Y, Kim M, Takayama Y, Takahashi N, Goto T, Wakabayashi S, Kawada T, et al. Lack of TRPV2 impairs thermogenesis in mouse brown adipose tissue. *EMBO Rep.* 2016;17(3):383-99.

167. Ma S, Yu H, Zhao Z, Luo Z, Chen J, Ni Y, Jin R, Ma L, Wang P, Zhu Z, et al. Activation of the cold-sensing TRPM8 channel triggers UCP1-dependent thermogenesis and prevents obesity. *J Mol Cell Biol.* 2012;4(2):88-96.

168. Brini M, Pinton P, King MP, Davidson M, Schon EA, and Rizzuto R. A calcium signaling defect in the pathogenesis of a mitochondrial DNA inherited oxidative phosphorylation deficiency. *Nat Med.* 1999;5(8):951-4.

169. Burelle Y, Bemeur C, Rivard ME, Thompson Legault J, Boucher G, Consortium L, Morin C, Coderre L, and Des Rosiers C. Mitochondrial vulnerability and increased susceptibility to nutrient-induced cytotoxicity in fibroblasts from leigh syndrome French canadian patients. *PLoS One.* 2015;10(3):e0120767.

170. Tian XY, Ganeshan K, Hong C, Nguyen KD, Qiu Y, Kim J, Tangirala RK, Tontonoz P, and Chawla A. Thermoneutral Housing Accelerates Metabolic Inflammation to Potentiate Atherosclerosis but Not Insulin Resistance. *Cell Metab.* 2016;23(1):165-78.

171. Chae S, Ahn BY, Byun K, Cho YM, Yu MH, Lee B, Hwang D, and Park KS. A systems approach for decoding mitochondrial retrograde signaling pathways. *Sci Signal.* 2013;6(264):rs4.

172. Rizzuto R, De Stefani D, Raffaello A, and Mammucari C. Mitochondria as sensors and regulators of calcium signalling. *Nat Rev Mol Cell Biol.* 2012;13(9):566-78.

173. Deluca HF, and Engstrom GW. Calcium uptake by rat kidney mitochondria. *Proc Natl Acad Sci U S A.* 1961;47(1744-50.

174. Vasington FD, and Murphy JV. Ca ion uptake by rat kidney mitochondria and its dependence on respiration and phosphorylation. *J Biol Chem.* 1962;237(2670-7.

175. Kirichok Y, Krapivinsky G, and Clapham DE. The mitochondrial calcium uniporter is a highly selective ion channel. *Nature.* 2004;427(6972):360-4.

176. De Stefani D, Raffaello A, Teardo E, Szabo I, and Rizzuto R. A forty-kilodalton protein of the inner membrane is the mitochondrial calcium uniporter. *Nature.* 2011;476(7360):336-40.

177. Baughman JM, Perocchi F, Girgis HS, Plovanich M, Belcher-Timme CA, Sancak Y, Bao XR, Strittmatter L, Goldberger O, Bogorad RL, et al. Integrative genomics

identifies MCU as an essential component of the mitochondrial calcium uniporter. *Nature.* 2011;476(7360):341-5.

178. Perocchi F, Gohil VM, Girgis HS, Bao XR, McCombs JE, Palmer AE, and Mootha VK. MICU1 encodes a mitochondrial EF hand protein required for Ca(2+) uptake. *Nature.* 2010;467(7313):291-6.

179. Patron M, Raffaello A, Granatiero V, Tosatto A, Merli G, De Stefani D, Wright L, Pallafacchina G, Terrin A, Mammucari C, et al. The mitochondrial calcium uniporter (MCU): molecular identity and physiological roles. *J Biol Chem.* 2013;288(15):10750-8.

180. Ksenzenko M, Konstantinov AA, Khomutov GB, Tikhonov AN, and Ruuge EK. Effect of electron transfer inhibitors on superoxide generation in the cytochrome bc1 site of the mitochondrial respiratory chain. *FEBS Lett.* 1983;155(1):19-24.

181. Raimundo N, Song L, Shutt TE, McKay SE, Cotney J, Guan MX, Gilliland TC, Hohuan D, Santos-Sacchi J, and Shadel GS. Mitochondrial stress engages E2F1 apoptotic signaling to cause deafness. *Cell.* 2012;148(4):716-26.

182. Chouchani ET, Kazak L, Jedrychowski MP, Lu GZ, Erickson BK, Szpyt J, Pierce KA, Laznik-Bogoslavski D, Vetrivelan R, Clish CB, et al. Mitochondrial ROS regulate thermogenic energy expenditure and sulfenylation of UCP1. *Nature.* 2016;532(7597):112-6.

183. Sims JL, Berger SJ, and Berger NA. Effects of nicotinamide on NAD and poly(ADP-ribose) metabolism in DNA-damaged human lymphocytes. *J Supramol Struct Cell Biochem.* 1981;16(3):281-8.

184. Bai P, Canto C, Oudart H, Brunyanszki A, Cen Y, Thomas C, Yamamoto H, Huber A, Kiss B, Houtkooper RH, et al. PARP-1 inhibition increases mitochondrial metabolism through SIRT1 activation. *Cell Metab.* 2011;13(4):461-8.

185. Qiang L, Wang L, Kon N, Zhao W, Lee S, Zhang Y, Rosenbaum M, Zhao Y, Gu W, Farmer SR, et al. Brown remodeling of white adipose tissue by SirT1-dependent deacetylation of Ppargamma. *Cell.* 2012;150(3):620-32.

186. Shi T, Wang F, Stieren E, and Tong Q. SIRT3, a mitochondrial sirtuin deacetylase, regulates mitochondrial function and thermogenesis in brown adipocytes. *J Biol Chem.* 2005;280(14):13560-7.

187. Finley LW, Carracedo A, Lee J, Souza A, Egia A, Zhang J, Teruya-Feldstein J, Moreira PI, Cardoso SM, Clish CB, et al. SIRT3 opposes reprogramming of cancer cell metabolism through HIF1alpha destabilization. *Cancer Cell.* 2011;19(3):416-28.

188. King MP, and Attardi G. Human cells lacking mtDNA: repopulation with exogenous mitochondria by complementation. *Science.* 1989;246(4929):500-3.

189. Khutornenko AA, Roudko VV, Chernyak BV, Vartapetian AB, Chumakov PM, and Evstafieva AG. Pyrimidine biosynthesis links mitochondrial respiration to the p53 pathway. *Proc Natl Acad Sci U S A.* 2010;107(29):12828-33.

190. Kozak LP, Kozak UC, and Clarke GT. Abnormal brown and white fat development in transgenic mice overexpressing glycerol 3-phosphate dehydrogenase. *Genes Dev.* 1991;5(12A):2256-64.

191. Prochazka M, Kozak UC, and Kozak LP. A glycerol-3-phosphate dehydrogenase null mutant in BALB/cHeA mice. *J Biol Chem.* 1989;264(8):4679-83.

192. Mili S, and Pinol-Roma S. LRP130, a pentatricopeptide motif protein with a noncanonical RNA-binding domain, is bound in vivo to mitochondrial and nuclear RNAs. *Mol Cell Biol.* 2003;23(14):4972-82.

193. Topisirovic I, Siddiqui N, Lapointe VL, Trost M, Thibault P, Bangeranye C, Pinol-Roma S, and Borden KL. Molecular dissection of the eukaryotic initiation factor 4E (eIF4E) export-competent RNP. *EMBO J.* 2009;28(8):1087-98.

194. Sobek S, Dalla Rosa I, Pommier Y, Bornholz B, Kalfalah F, Zhang H, Wiesner RJ, von Kleist-Retzow JC, Hillebrand F, Schaal H, et al. Negative regulation of mitochondrial transcription by mitochondrial topoisomerase I. *Nucleic Acids Res.* 2013;41(21):9848-57.

195. Seo BB, Matsuno-Yagi A, and Yagi T. Modulation of oxidative phosphorylation of human kidney 293 cells by transfection with the internal rotenone-insensitive NADH-quinone oxidoreductase (NDI1) gene of Saccharomyces cerevisiae. *Biochim Biophys Acta.* 1999;1412(1):56-65.

196. Kubota N, Terauchi Y, Miki H, Tamemoto H, Yamauchi T, Komeda K, Satoh S, Nakano R, Ishii C, Sugiyama T, et al. PPAR gamma mediates high-fat diet-induced adipocyte hypertrophy and insulin resistance. *Mol Cell.* 1999;4(4):597-609.

197. He W, Barak Y, Hevener A, Olson P, Liao D, Le J, Nelson M, Ong E, Olefsky JM, and Evans RM. Adipose-specific peroxisome proliferator-activated receptor gamma knockout causes insulin resistance in fat and liver but not in muscle. *Proc Natl Acad Sci U S A.* 2003;100(26):15712-7.

198. Lustig Y, Ruas JL, Estall JL, Lo JC, Devarakonda S, Laznik D, Choi JH, Ono H, Olsen JV, and Spiegelman BM. Separation of the gluconeogenic and mitochondrial functions of PGC-1{alpha} through S6 kinase. *Genes Dev.* 2011;25(12):1232-44.

199. Wright DC, Han DH, Garcia-Roves PM, Geiger PC, Jones TE, and Holloszy JO. Exercise-induced mitochondrial biogenesis begins before the increase in muscle PGC-1alpha expression. *J Biol Chem.* 2007;282(1):194-9.

200. Wright DC, Geiger PC, Han DH, Jones TE, and Holloszy JO. Calcium induces increases in peroxisome proliferator-activated receptor gamma coactivator-1alpha and mitochondrial biogenesis by a pathway leading to p38 mitogen-activated protein kinase activation. *J Biol Chem.* 2007;282(26):18793-9.

201. Cheng H, Lederer WJ, and Cannell MB. Calcium sparks: elementary events underlying excitation-contraction coupling in heart muscle. *Science.* 1993;262(5134):740-4.

202. Hogan PG, Chen L, Nardone J, and Rao A. Transcriptional regulation by calcium, calcineurin, and NFAT. *Genes Dev.* 2003;17(18):2205-32.

203. Vijgen GH, Bouvy ND, Teule GJ, Brans B, Schrauwen P, and van Marken Lichtenbelt WD. Brown adipose tissue in morbidly obese subjects. *PLoS One.* 2011;6(2):e17247.

204. Orava J, Nuutila P, Noponen T, Parkkola R, Viljanen T, Enerback S, Rissanen A, Pietilainen KH, and Virtanen KA. Blunted metabolic responses to cold and insulin stimulation in brown adipose tissue of obese humans. *Obesity (Silver Spring).* 2013;21(11):2279-87.

205. Vijgen GH, Bouvy ND, Teule GJ, Brans B, Hoeks J, Schrauwen P, and van Marken Lichtenbelt WD. Increase in brown adipose tissue activity after weight loss in morbidly obese subjects. *J Clin Endocrinol Metab.* 2012;97(7):E1229-33.

206. Min SY, Kady J, Nam M, Rojas-Rodriguez R, Berkenwald A, Kim JH, Noh HL, Kim JK, Cooper MP, Fitzgibbons T, et al. Human 'brite/beige' adipocytes develop from capillary networks, and their implantation improves metabolic homeostasis in mice. *Nat Med.* 2016;22(3):312-8.

207. Valerio A, Cardile A, Cozzi V, Bracale R, Tedesco L, Pisconti A, Palomba L, Cantoni O, Clementi E, Moncada S, et al. TNF-alpha downregulates eNOS expression and mitochondrial biogenesis in fat and muscle of obese rodents. *J Clin Invest.* 2006;116(10):2791-8.

208. Shimizu I, Aprahamian T, Kikuchi R, Shimizu A, Papanicolaou KN, MacLauchlan S, Maruyama S, and Walsh K. Vascular rarefaction mediates whitening of brown fat in obesity. *J Clin Invest.* 2014;124(5):2099-112.

209. Goodbody AE, and Trayhurn P. GDP binding to brown-adipose-tissue mitochondria of diabetic--obese (db/db) mice. Decreased binding in both the obese and pre-obese states. *Biochem J.* 1981;194(3):1019-22.

210. Masaki T, Yoshimatsu H, Chiba S, and Sakata T. Impaired response of UCP family to cold exposure in diabetic (db/db) mice. *Am J Physiol Regul Integr Comp Physiol.* 2000;279(4):R1305-9.

211. Atgie C, Marette A, Desautels M, Tulp O, and Bukowiecki LJ. Specific decrease of mitochondrial thermogenic capacity in brown adipose tissue of obese SHR/N-cp rats. *Am J Physiol.* 1993;265(6 Pt 1):C1674-80.

212. Lettieri Barbato D, Tatulli G, Vegliante R, Cannata SM, Bernardini S, Ciriolo MR, and Aquilano K. Dietary fat overload reprograms brown fat mitochondria. *Front Physiol.* 2015;6(272.

213. Rong JX, Qiu Y, Hansen MK, Zhu L, Zhang V, Xie M, Okamoto Y, Mattie MD, Higashiyama H, Asano S, et al. Adipose mitochondrial biogenesis is suppressed in db/db and high-fat diet-fed mice and improved by rosiglitazone. *Diabetes.* 2007;56(7):1751-60.

214. Takahashi Y, and Ide T. Dietary n-3 fatty acids affect mRNA level of brown adipose tissue uncoupling protein 1, and white adipose tissue leptin and glucose transporter 4 in the rat. *Br J Nutr.* 2000;84(2):175-84.

215. Kim M, Goto T, Yu R, Uchida K, Tominaga M, Kano Y, Takahashi N, and Kawada T. Fish oil intake induces UCP1 upregulation in brown and white adipose tissue via the sympathetic nervous system. *Sci Rep.* 2015;5(18013.

216. Bargut TC, Silva-e-Silva AC, Souza-Mello V, Mandarim-de-Lacerda CA, and Aguila MB. Mice fed fish oil diet and upregulation of brown adipose tissue thermogenic markers. *Eur J Nutr.* 2016;55(1):159-69.

217. Prpic V, Watson PM, Frampton IC, Sabol MA, Jezek GE, and Gettys TW. Adaptive changes in adipocyte gene expression differ in AKR/J and SWR/J mice during diet-induced obesity. *J Nutr.* 2002;132(11):3325-32.

218. Cypess AM, Chen YC, Sze C, Wang K, English J, Chan O, Holman AR, Tal I, Palmer MR, Kolodny GM, et al. Cold but not sympathomimetics activates human brown adipose tissue in vivo. *Proc Natl Acad Sci U S A.* 2012;109(25):10001-5.

219. van der Lans AA, Hoeks J, Brans B, Vijgen GH, Visser MG, Vosselman MJ, Hansen J, Jorgensen JA, Wu J, Mottaghy FM, et al. Cold acclimation recruits human brown fat and increases nonshivering thermogenesis. *J Clin Invest.* 2013;123(8):3395-403.

220. Carey AL, Formosa MF, Van Every B, Bertovic D, Eikelis N, Lambert GW, Kalff V, Duffy SJ, Cherk MH, and Kingwell BA. Ephedrine activates brown adipose tissue in lean but not obese humans. *Diabetologia.* 2013;56(1):147-55.

221. Ouellet V, Labbe SM, Blondin DP, Phoenix S, Guerin B, Haman F, Turcotte EE, Richard D, and Carpentier AC. Brown adipose tissue oxidative metabolism contributes to energy expenditure during acute cold exposure in humans. *J Clin Invest.* 2012;122(2):545-52.

222. Orava J, Nuutila P, Lidell ME, Oikonen V, Noponen T, Viljanen T, Scheinin M, Taittonen M, Niemi T, Enerback S, et al. Different metabolic responses of human brown adipose tissue to activation by cold and insulin. *Cell Metab.* 2011;14(2):272-9.

223. Mohell N, and Dicker A. The beta-adrenergic radioligand [3H]CGP-12177, generally classified as an antagonist, is a thermogenic agonist in brown adipose tissue. *Biochem J.* 1989;261(2):401-5.

224. Himms-Hagen J, Cui J, Danforth E, Jr., Taatjes DJ, Lang SS, Waters BL, and Claus TH. Effect of CL-316,243, a thermogenic beta 3-agonist, on energy balance and brown and white adipose tissues in rats. *Am J Physiol.* 1994;266(4 Pt 2):R1371-82.

225. Arch JR. Challenges in beta(3)-Adrenoceptor Agonist Drug Development. *Ther Adv Endocrinol Metab.* 2011;2(2):59-64.

226. Cypess AM, Weiner LS, Roberts-Toler C, Franquet Elia E, Kessler SH, Kahn PA, English J, Chatman K, Trauger SA, Doria A, et al. Activation of human brown adipose tissue by a beta3-adrenergic receptor agonist. *Cell Metab.* 2015;21(1):33-8.

227. Kawamoto S, Niwa H, Tashiro F, Sano S, Kondoh G, Takeda J, Tabayashi K, and Miyazaki J. A novel reporter mouse strain that expresses enhanced green fluorescent protein upon Cre-mediated recombination. *FEBS Lett.* 2000;470(3):263-8.

228. Shim M, Foley J, Anna C, Mishina Y, and Eling T. Embryonic expression of cyclooxygenase-2 causes malformations in axial skeleton. *J Biol Chem.* 2010;285(21):16206-17.

229. Odegaard JI, Lee MW, Sogawa Y, Bertholet AM, Locksley RM, Weinberg DE, Kirichok Y, Deo RC, and Chawla A. Perinatal Licensing of Thermogenesis by IL-33 and ST2. *Cell.* 2016;166(4):841-54.

230. Finck BN, Bernal-Mizrachi C, Han DH, Coleman T, Sambandam N, LaRiviere LL, Holloszy JO, Semenkovich CF, and Kelly DP. A potential link between muscle

peroxisome proliferator- activated receptor-alpha signaling and obesity-related diabetes. *Cell Metab.* 2005;1(2):133-44.

231. Koves TR, Ussher JR, Noland RC, Slentz D, Mosedale M, Ilkayeva O, Bain J, Stevens R, Dyck JR, Newgard CB, et al. Mitochondrial overload and incomplete fatty acid oxidation contribute to skeletal muscle insulin resistance. *Cell Metab.* 2008;7(1):45-56.

232. Satapati S, Sunny NE, Kucejova B, Fu X, He TT, Mendez-Lucas A, Shelton JM, Perales JC, Browning JD, and Burgess SC. Elevated TCA cycle function in the pathology of diet-induced hepatic insulin resistance and fatty liver. *J Lipid Res.* 2012;53(6):1080-92.

233. Houtkooper RH, Pirinen E, and Auwerx J. Sirtuins as regulators of metabolism and healthspan. *Nat Rev Mol Cell Biol.* 2012;13(4):225-38.

234. Hirschey MD, Shimazu T, Goetzman E, Jing E, Schwer B, Lombard DB, Grueter CA, Harris C, Biddinger S, Ilkayeva OR, et al. SIRT3 regulates mitochondrial fatty-acid oxidation by reversible enzyme deacetylation. *Nature.* 2010;464(7285):121-5.

235. Shimazu T, Hirschey MD, Hua L, Dittenhafer-Reed KE, Schwer B, Lombard DB, Li Y, Bunkenborg J, Alt FW, Denu JM, et al. SIRT3 deacetylates mitochondrial 3-hydroxy-3-methylglutaryl CoA synthase 2 and regulates ketone body production. *Cell Metab.* 2010;12(6):654-61.

236. Ahn BH, Kim HS, Song S, Lee IH, Liu J, Vassilopoulos A, Deng CX, and Finkel T. A role for the mitochondrial deacetylase Sirt3 in regulating energy homeostasis. *Proc Natl Acad Sci U S A.* 2008;105(38):14447-52.

237. Cimen H, Han MJ, Yang Y, Tong Q, Koc H, and Koc EC. Regulation of succinate dehydrogenase activity by SIRT3 in mammalian mitochondria. *Biochemistry.* 2010;49(2):304-11.

238. Finley LW, Haas W, Desquiret-Dumas V, Wallace DC, Procaccio V, Gygi SP, and Haigis MC. Succinate dehydrogenase is a direct target of sirtuin 3 deacetylase activity. *PLoS One.* 2011;6(8):e23295.

239. Jing E, Emanuelli B, Hirschey MD, Boucher J, Lee KY, Lombard D, Verdin EM, and Kahn CR. Sirtuin-3 (Sirt3) regulates skeletal muscle metabolism and insulin signaling via altered mitochondrial oxidation and reactive oxygen species production. *Proc Natl Acad Sci U S A.* 2011;108(35):14608-13.

240. Hirschey MD, Shimazu T, Jing E, Grueter CA, Collins AM, Aouizerat B, Stancakova A, Goetzman E, Lam MM, Schwer B, et al. SIRT3 deficiency and

mitochondrial protein hyperacetylation accelerate the development of the metabolic syndrome. *Mol Cell.* 2011;44(2):177-90.

241. Tiranti V, Savoia A, Forti F, D'Apolito MF, Centra M, Rocchi M, and Zeviani M. Identification of the gene encoding the human mitochondrial RNA polymerase (h-mtRPOL) by cyberscreening of the Expressed Sequence Tags database. *Hum Mol Genet.* 1997;6(4):615-25.

242. Masters BS, Stohl LL, and Clayton DA. Yeast mitochondrial RNA polymerase is homologous to those encoded by bacteriophages T3 and T7. *Cell.* 1987;51(1):89-99.

243. Shutt TE, Lodeiro MF, Cotney J, Cameron CE, and Shadel GS. Core human mitochondrial transcription apparatus is a regulated two-component system in vitro. *Proc Natl Acad Sci U S A.* 2010;107(27):12133-8.

244. Fisher RP, and Clayton DA. A transcription factor required for promoter recognition by human mitochondrial RNA polymerase. Accurate initiation at the heavy- and light-strand promoters dissected and reconstituted in vitro. *J Biol Chem.* 1985;260(20):11330-8.

245. Fisher RP, and Clayton DA. Purification and characterization of human mitochondrial transcription factor 1. *Mol Cell Biol.* 1988;8(8):3496-509.

246. Fisher RP, Lisowsky T, Parisi MA, and Clayton DA. DNA wrapping and bending by a mitochondrial high mobility group-like transcriptional activator protein. *J Biol Chem.* 1992;267(5):3358-67.

247. Ekstrand MI, Falkenberg M, Rantanen A, Park CB, Gaspari M, Hultenby K, Rustin P, Gustafsson CM, and Larsson NG. Mitochondrial transcription factor A regulates mtDNA copy number in mammals. *Hum Mol Genet.* 2004;13(9):935-44.

248. Kanki T, Ohgaki K, Gaspari M, Gustafsson CM, Fukuoh A, Sasaki N, Hamasaki N, and Kang D. Architectural role of mitochondrial transcription factor A in maintenance of human mitochondrial DNA. *Mol Cell Biol.* 2004;24(22):9823-34.

249. Kaufman BA, Durisic N, Mativetsky JM, Costantino S, Hancock MA, Grutter P, and Shoubridge EA. The mitochondrial transcription factor TFAM coordinates the assembly of multiple DNA molecules into nucleoid-like structures. *Mol Biol Cell.* 2007;18(9):3225-36.

250. Morin C, Mitchell G, Larochelle J, Lambert M, Ogier H, Robinson BH, and De Braekeleer M. Clinical, metabolic, and genetic aspects of cytochrome C oxidase deficiency in Saguenay-Lac-Saint-Jean. *Am J Hum Genet.* 1993;53(2):488-96.

251. Bibb MJ, Van Etten RA, Wright CT, Walberg MW, and Clayton DA. Sequence and gene organization of mouse mitochondrial DNA. *Cell.* 1981;26(2 Pt 2):167-80.

252. Gao GP, and Sena-Esteves M. In: Green MRS, J. ed. *Molecular Cloning, Vol 2: A Laboratory Manual*. New York: Cold Spring Harbor Laboratory Press; 2012:1209-313.

253. Dolken L, Ruzsics Z, Radle B, Friedel CC, Zimmer R, Mages J, Hoffmann R, Dickinson P, Forster T, Ghazal P, et al. High-resolution gene expression profiling for simultaneous kinetic parameter analysis of RNA synthesis and decay. *RNA.* 2008;14(9):1959-72.

254. Fan W, and Luo J. SIRT1 regulates UV-induced DNA repair through deacetylating XPA. *Mol Cell.* 2010;39(2):247-58.

255. Baur JA, Pearson KJ, Price NL, Jamieson HA, Lerin C, Kalra A, Prabhu VV, Allard JS, Lopez-Lluch G, Lewis K, et al. Resveratrol improves health and survival of mice on a high-calorie diet. *Nature.* 2006;444(7117):337-42.

256. Paquette N, Conlon J, Sweet C, Rus F, Wilson L, Pereira A, Rosadini CV, Goutagny N, Weber AN, Lane WS, et al. Serine/threonine acetylation of TGFbeta-activated kinase (TAK1) by Yersinia pestis YopJ inhibits innate immune signaling. *Proc Natl Acad Sci U S A.* 2012;109(31):12710-5.

257. Schwer B, North BJ, Frye RA, Ott M, and Verdin E. The human silent information regulator (Sir)2 homologue hSIRT3 is a mitochondrial nicotinamide adenine dinucleotide-dependent deacetylase. *J Cell Biol.* 2002;158(4):647-57.

258. Casas F, Pineau T, Rochard P, Rodier A, Daury L, Dauca M, Cabello G, and Wrutniak-Cabello C. New molecular aspects of regulation of mitochondrial activity by fenofibrate and fasting. *FEBS Lett.* 2000;482(1-2):71-4.

259. St-Pierre J, Drori S, Uldry M, Silvaggi JM, Rhee J, Jager S, Handschin C, Zheng K, Lin J, Yang W, et al. Suppression of reactive oxygen species and neurodegeneration by the PGC-1 transcriptional coactivators. *Cell.* 2006;127(2):397-408.

260. Rodgers JT, Lerin C, Haas W, Gygi SP, Spiegelman BM, and Puigserver P. Nutrient control of glucose homeostasis through a complex of PGC-1alpha and SIRT1. *Nature.* 2005;434(7029):113-8.

261. Caton PW, Holness MJ, Bishop-Bailey D, and Sugden MC. PPARalpha-LXR as a novel metabolostatic signalling axis in skeletal muscle that acts to optimize substrate selection in response to nutrient status. *Biochem J.* 2011;437(3):521-30.

262. Pittelli M, Felici R, Pitozzi V, Giovannelli L, Bigagli E, Cialdai F, Romano G, Moroni F, and Chiarugi A. Pharmacological effects of exogenous NAD on mitochondrial bioenergetics, DNA repair, and apoptosis. *Mol Pharmacol.* 2011;80(6):1136-46.

263. Nikiforov A, Dolle C, Niere M, and Ziegler M. Pathways and subcellular compartmentation of NAD biosynthesis in human cells: from entry of extracellular precursors to mitochondrial NAD generation. *J Biol Chem.* 2011;286(24):21767-78.

264. Rabani M, Levin JZ, Fan L, Adiconis X, Raychowdhury R, Garber M, Gnirke A, Nusbaum C, Hacohen N, Friedman N, et al. Metabolic labeling of RNA uncovers principles of RNA production and degradation dynamics in mammalian cells. *Nat Biotechnol.* 2011;29(5):436-42.

265. Schwanhausser B, Busse D, Li N, Dittmar G, Schuchhardt J, Wolf J, Chen W, and Selbach M. Global quantification of mammalian gene expression control. *Nature.* 2011;473(7347):337-42.

266. Schwer B, Bunkenborg J, Verdin RO, Andersen JS, and Verdin E. Reversible lysine acetylation controls the activity of the mitochondrial enzyme acetyl-CoA synthetase 2. *Proc Natl Acad Sci U S A.* 2006;103(27):10224-9.

267. Sundaresan NR, Samant SA, Pillai VB, Rajamohan SB, and Gupta MP. SIRT3 is a stress-responsive deacetylase in cardiomyocytes that protects cells from stress-mediated cell death by deacetylation of Ku70. *Mol Cell Biol.* 2008;28(20):6384-401.

268. Sol EM, Wagner SA, Weinert BT, Kumar A, Kim HS, Deng CX, and Choudhary C. Proteomic investigations of lysine acetylation identify diverse substrates of mitochondrial deacetylase sirt3. *PLoS One.* 2012;7(12):e50545.

269. Hebert AS, Dittenhafer-Reed KE, Yu W, Bailey DJ, Selen ES, Boersma MD, Carson JJ, Tonelli M, Balloon AJ, Higbee AJ, et al. Calorie restriction and SIRT3 trigger global reprogramming of the mitochondrial protein acetylome. *Mol Cell.* 2013;49(1):186-99.

270. Rardin MJ, Newman JC, Held JM, Cusack MP, Sorensen DJ, Li B, Schilling B, Mooney SD, Kahn CR, Verdin E, et al. Label-free quantitative proteomics of the lysine acetylome in mitochondria identifies substrates of SIRT3 in metabolic pathways. *Proc Natl Acad Sci U S A.* 2013;110(16):6601-6.

271. Sondheimer N, Fang JK, Polyak E, Falk MJ, and Avadhani NG. Leucine-rich pentatricopeptide-repeat containing protein regulates mitochondrial transcription. *Biochemistry.* 2010;49(35):7467-73.

272. Matsumura T, and Thurman RG. Measuring rates of O2 uptake in periportal and pericentral regions of liver lobule: stop-flow experiments with perfused liver. *Am J Physiol.* 1983;244(6):G656-9.

273. Olson MJ, and Thurman RG. Quantitation of ketogenesis in periportal and pericentral regions of the liver lobule. *Arch Biochem Biophys.* 1987;253(1):26-37.

274. Yang Y, Cimen H, Han MJ, Shi T, Deng JH, Koc H, Palacios OM, Montier L, Bai Y, Tong Q, et al. NAD+-dependent deacetylase SIRT3 regulates mitochondrial protein synthesis by deacetylation of the ribosomal protein MRPL10. *J Biol Chem.* 2010;285(10):7417-29.

275. Dinardo MM, Musicco C, Fracasso F, Milella F, Gadaleta MN, Gadaleta G, and Cantatore P. Acetylation and level of mitochondrial transcription factor A in several organs of young and old rats. *Biochem Biophys Res Commun.* 2003;301(1):187-91.

276. Adams SH, Hoppel CL, Lok KH, Zhao L, Wong SW, Minkler PE, Hwang DH, Newman JW, and Garvey WT. Plasma acylcarnitine profiles suggest incomplete long-chain fatty acid beta-oxidation and altered tricarboxylic acid cycle activity in type 2 diabetic African-American women. *J Nutr.* 2009;139(6):1073-81.

277. Mihalik SJ, Goodpaster BH, Kelley DE, Chace DH, Vockley J, Toledo FG, and DeLany JP. Increased levels of plasma acylcarnitines in obesity and type 2 diabetes and identification of a marker of glucolipotoxicity. *Obesity (Silver Spring).* 2010;18(9):1695-700.

278. Kendrick AA, Choudhury M, Rahman SM, McCurdy CE, Friederich M, Van Hove JL, Watson PA, Birdsey N, Bao J, Gius D, et al. Fatty liver is associated with reduced SIRT3 activity and mitochondrial protein hyperacetylation. *Biochem J.* 2011;433(3):505-14.